Spatial and Temporal Particulate Variability at an Integrated Multi – Trophic Aquaculture (IMTA) Site in Kyuquot Sound, British Columbia, Using Bio-Optical Methods

by

Justin Del Bel Belluz
BSc, University of Victoria, 2010

A Thesis Submitted in Partial Fulfillment
of the Requirements for the Degree of

MASTER OF SCIENCE

in the Department of Geography

Supervisory Committee

Spatial and Temporal Particulate Variability at an Integrated Multi – Trophic Aquaculture (IMTA) Site in Kyuquot Sound, British Columbia, Using Bio-Optical Methods

by

Justin Del Bel Belluz
BSc, University of Victoria, 2010

Supervisory Committee

Dr. Maycira Costa (Department of Geography)
Supervisor

Dr. Stephen Cross (Department of Geography)
Co-Supervisor

Dr. Gregor Reid (Fisheries and Oceans Canada)
Additional Member

Abstract

Supervisory Committee
Dr. Maycira Costa (Department of Geography)
Supervisor
Dr. Stephen Cross (Department of Geography)
Co-Supervisor
Dr. Gregor Reid (Fisheries and Oceans Canada)
Additional Member

The goal of this thesis was to detail spatial and temporal organic particulate dynamics at an integrated multi-trophic aquaculture (IMTA) site on the west coast of Vancouver Island, Canada. To accomplish this goal, *in-situ* optical measurements of particulate scattering (b_p), particulate backscattering (b_{bp}) and the particulate backscattering ratio ($\tilde{b}_{bp}$) were collected in conjunction with discrete sampling for particulate organic carbon (POC) and chlorophyll *a* (chl *a*) concentrations. These measurements were performed over three seasons (autumn, winter and summer) at reference sites and at sites within and directly adjacent to the fish component of the IMTA system.

Chapter 2 of this thesis focused on the examination of bio-optical relationships over various timescales (seasonally, daily and within-day) to describe temporal and vertical particulate variability and to assess the effectiveness of bio-optical methods for environmental monitoring. Autumn showed low bio-optical magnitudes with distinct lower cage increases possibly attributable to aquaculture derived wastes. In spring, sampling was performed over diatom bloom conditions, dominating the bio-optical measurements. During summer, an *Emiliania Huxleyi* bloom likely occurred, strongly enhancing b_{bp} and $\tilde{b}_{bp}$ magnitudes in the thermally stratified upper water column.

Throughout these conditions, b_p was predominantly influenced by chl *a* suggesting sensitivity to phytoplankton concentrations. While b_{bp} was conditioned by chl *a* during the diatom bloom, it was also highly sensitive to the presence of inorganic and likely detrital materials. Finally, $\tilde{b}_{bp}$ was sensitive to particulate compositions, showing low values (< 0.010) in diatom dominated waters and high values when refractive coccoliths were likely present. Notably, in autumn, $\tilde{b}_{bp}$ was conditioned by detrital particles and along with b_{bp}, showed post-feeding lower cage increases suggesting that these parameters could be useful candidates for particulate waste tracking during low ambient particle conditions.

In chapter 3, the temporal, vertical and horizontal dispersion of the aquaculture derived particulate wastes are detailed. Autumn was the only period to show waste signals, likely due to their quick dilution into the particulate rich fields in spring/summer. During this period, post-feeding particulate waste increases were focused at the bottom of the cage with possible vertical sinking towards the seafloor. Minimal horizontal dispersion towards the scallop portion of the system was observed; however, more comprehensive sampling over differing hydrographic regimes is necessary to characterize waste dispersion. Based on our temporally limited autumn results, the most appropriate placement of uptake species for waste assimilation would be directly below the studied cage.

Our results highlight the need for high spatial and temporal resolution methods for particulate monitoring within IMTA settings as discrete sampling may miss “patchy” waste dispersal streams. The bio-optical measurements performed during this study

could fill this need as they can provide high resolution information on particulate concentrations and compositions not achievable solely through the use of discrete water sampling. With further research, optical instrumentation could be incorporated into IMTA systems allowing for the near real time and continuous collection of data on particulate dynamics. This knowledge could greatly aid in the design and implementation of systems optimized for waste removal by uptake species.

Table of Contents

List of Tables

List of Figures

List of Abbreviations and Symbols

Abbreviation/ Symbol	Full Name	Units
19HF	19' – hexonoyloxyfucoxanthin	µg l^{-1}
ac-s	Absorption and attenuation meter	
a_{pg}	Absorption by particulate and dissolved matter	m^{-1}
[chl]	Absorption estimated chlorophyll *a*	µg l^{-1}
c_{pg}	Attenuation by particulate and dissolved matter	m^{-1}
A	August	
BF	Before feeding	
BC	Beside-cage	
chl *a*	Chlorophyll *a*	µg l^{-1}
CTD	Conductivity, temperature and Depth sensor	
DFO	Department of Fisheries and Oceans, Canada	
z	Depth	m^{-1}
D.C.D	Dominant Current Direction	
E	Ebb tide	
E. huxleyi	Emiliania huxleyi	
F	Flood tide	
FAO	Food and Agriculture Organization of the United Nations	
Fuco	Fucoxanthin	µg l^{-1}
HPLC	High performance liquid chromatography	
IC	In-cage	
IOPs	Inherent optical properties	
IMTA	Integrated multi-trophic aquaculture	
M	May	
NDIR	Non-dispersive infrared	
N	November	
b_{bp}	Particulate backscattering coefficient	m^{-1}
$\tilde{b}_{bp}$	Particulate backscattering ratio	
POC	Particulate organic carbon (non – elemental)	mg l^{-1}
POC:chl *a*	Particulate organic carbon:Chlorophyll *a* ratio	
b_p	Particulate scattering coefficient	m^{-1}
PF	Post feeding	
PSU	Practical Salinity Unit	
REF	Reference site	
X	Scaling factor (backscattering corrections)	
SSM	Solid sample module	
a_{ph}*	Specific chlorophyll absorption value	m^2 mg^{-1}
SML	Surface Mixed Layer	
TSM	Total Suspended Matter	mg l^{-1}
β	Total volume scattering coefficient	m^{-1} sr^{-1}

β_{p}	Volume scattering of particles	$m^{-1} sr^{-1}$
β_w	Volume scattering of pure water	$m^{-1} sr^{-1}$
Λ	Wavelength	nm

Acknowledgments

First and foremost, I would like to thank my committee members who guided me through every step of this process. Specifically, I would like to thank Dr. Maycira Costa for the opportunity to be part of the CIMTAN project and for her continued support over the past three years. Dr. Stephen Cross allowed me nearly free rein of the Kyuquot SEAfoods site and imparted a breadth of aquaculture experience, which were invaluable to this research. While a late addition to the committee, Dr. Gregor Reid brought needed clarity and perspective to the project and was always available for expert advice and words of encouragement.

I am also extremely grateful for the help of Genevieve Berard, Nathan Blasco, Tyson Carswell, Michael Guindon, Felipe Lobo and Nicholas Sherrington, who all provided major support during field sampling. Additionally, I am thankful for the training provided by Eduardo Loos and Felipe Lobo for HPLC analysis and Ricardo Rossin for POC analysis. Furthermore, I would like to thank Chris Secord for constructing sampling systems which made my life in the field considerably less taxing.

Finally, I would like thank my partner, Kristen, for her love, encouragement and patience through this process. Without her support, I may never have finished.

Funding for this research was provided by the NSERC strategic Integrated Multi-Trophic Aquaculture Network and field work was conducted at the Kyuquot SEAfoods Inc. site.

Chapter 1 – Introduction

Worldwide, the aquaculture industry has rapidly expanded to offset global fisheries declines and to meet demand from a growing population (FAO, 2014). Canada has seen similar industry expansion with aquaculture production experiencing a four-fold increase over the past 20 years (DFO, 2013). Atlantic salmon is the country's top export making up 68 % of total aquaculture production. Canada is now the 4th largest producer of Atlantic salmon in the world (8 % of world production), with British Columbia, on Canada's west coast, being the country's principal producer of this species (DFO, 2012).

The expansion of the finfish industry, both worldwide and in Canada, has led to concern over its environmental impacts (Amberg & Hall, 2008; Schlag, 2010; FAO, 2014). One particular concern is the release of particulate organic materials, which are dominantly made up of wasted feed and feces, to the waters surrounding finfish aquaculture farms (Brooks & Mahnken, 2003). Recent improvements in feeding techniques have reduced the percentage of feed lost (~ 3 – 5 %) to the environment (Brooks & Mahnken, 2003; Mente et al., 2006; Reid et al., 2009) and thus, feces now constitute the greatest output of particulate wastes from finfish farms with as much as 15% of the feed consumed by salmon extruded as fecal pellets (Reid et al., 2009). Under peak production, large Atlantic salmon farms can release upwards of 1000 kg of feces to the coastal environment each day (Kutti et al., 2007b). With exception to unsettleable feed fines, which originate from feed pellets (Cranford et al., 2013), these particulate wastes ultimately settle to the seafloor where they can result in the organic

loading of seafloor sediments (Carroll et al., 2003; Brooks & Mahnken, 2003). While the extent of the dispersion of these particles is dependent on a variety of hydrographic (i.e. current speeds, depth/bathymetry, stratification) and husbandry practices (feeding regimes, fish size, particle sizes) their effects are localized with accumulation generally limited to within 25 – 50 m of the farm (Brooks & Mahnken, 2003; Carroll et al., 2003; Mente et al., 2006; Lander et al., 2013); however, this distance can be considerably greater (~ 250 m) for deep water sites (Kutti et al., 2007a). If this accumulation is excessive, these wastes can result in the development of enriched or even anaerobic sediments and consequently, conditions favourable for the replacement of macro-benthos with highly opportunistic species (Brooks & Mahnken, 2003; Carroll et al., 2003; Kutti et al., 2007b).

Integrated multi-trophic aquaculture (IMTA) systems work to capture the wastes released from finfish cages through the use of strategically placed commercially valuable uptake species (Barrington et al., 2009; Chopin et al., 2012). In theory, growth of the uptake species is augmented by the presence of additional feed inputs (aquaculture wastes) resulting in faster and larger growth when compared to those cultured in monoculture settings. Thus, these systems may help to alleviate the negative environmental effects described above while also, increasing farm profits (Troell et al., 2003; Neori et al., 2004; Barrington et al., 2009; Chopin et al., 2012). Currently, operational IMTA systems primarily utilize seaweeds for inorganic dissolved waste removal, bivalves (i.e. mussels, oysters, scallops) for suspended particulate removal and to a lesser extent, deposit feeders (sea cucumbers) for the uptake of settled wastes below fish cages (Soto, 2009; Cranford et al., 2013; Hannah et al., 2013). Studies

dealing with the interception of particulate wastes at IMTA systems have largely focused on the bivalve components of these systems. While it has been shown that bivalves are able to utilize aquaculture wastes as feed (Soto & Mena, 1999; Lefebvre et al., 2000; Mazzola & Sarà, 2001; Gao et al., 2006; Reid et al., 2010; Redmond et al., 2010; MacDonald et al., 2011; Handå et al., 2012b), their efficiency for waste removal in real world settings is controversial. This controversy has arisen from the fact that some bivalves grown in close proximity to fish cages have shown augmented growth (Wallace, 1980; Jones & Iwama, 1991; Peharda et al., 2007; Sarà et al., 2009; Lander et al., 2012; Handå et al., 2012a; Jiang et al., 2013) while others have shown little or no increased growth when compared to reference bivalves (Taylor et al., 1992; Stirling, 1995; Parsons et al., 2002; Cheshuk et al., 2003; Irisarri et al., 2013a). To complicate matters further, difficulties have arisen when quantifying particulate waste dispersion with some studies measuring large increases in particulate concentrations adjacent to fish cages (Taylor et al., 1992; MacDonald et al., 2011; Lander et al., 2013) and others finding no increases (Cheshuk et al., 2003; Irisarri et al., 2013a,b). These inconsistencies appear to arise from site specific oceanographic and hydrographic conditions (i.e. ambient particle concentrations, current directions and velocities) and husbandry practices (i.e. feeding regimes), resulting in high spatial and temporal variability in particulate dispersion (Troell & Norberg, 1998; Cheshuk et al., 2003; Irisarri et al., 2013a). Additionally, large differences in sampling designs between these studies make their results difficult to compare and may contribute to their highly contrasting results (Cranford et al., 2013).

In general, effective utilization by filter feeders within IMTA systems requires particulate wastes to (1) travel through the bivalve component of the system; (2) move at velocities that are slow enough for waste capture, but fast enough to limit quick vertical transport and; (3) be present in concentrations that are high enough to limit dilution into ambient particulate assemblages while remaining below bivalve pseudofeces thresholds (Troell & Norberg, 1998; Cheshuk et al., 2003; Cranford et al., 2013). Appropriately, augmented bivalve growth has typically been observed under low ambient seston conditions, such as those experienced in winter, and in bivalves reared within or directly adjacent to fish cages (Wallace, 1980; Stirling, 1995; Lander et al., 2012; Handå et al., 2012a; Cranford et al., 2013).

Considering these factors, it is apparent that extensive site specific knowledge is needed regarding ambient particulate dynamics, as well as, the timing and dispersal of particulate wastes for the appropriate selection and placement of uptake species at IMTA systems (Troell & Norberg, 1998; Reid et al., 2009; Irisarri et al., 2013a). A limitation of the aforementioned studies dealing with these wastes is their reliance on sampling at discrete depths and (or) at timescales that were not sufficient to characterize dispersal. This limitation could be addressed by the use of *in-situ* optical measurements, which can provide proxies for both particle concentrations and compositions (organic/inorganic) (Twardowski et al., 2001; Boss et al., 2004; Loisel et al., 2007). In comparison to discrete water sampling methods, which are laborious and time consuming, the sampling frequencies of optical parameters allow for the instantaneous collection of high spatial and temporal resolution data (Grizzle et al., 2006; Chang et al., 2006; Woźniak et al., 2010). While commonly used for particulate characterization

in the coastal environment, relatively few studies have utilized optical methods for aquaculture research (Millie et al., 1995; Grizzle et al., 2006; Ibarra et al., 2012; Brager, 2013). The use of these methods within IMTA settings may provide valuable knowledge on particulate dynamics that could be used to optimize the uptake species portions of IMTA systems for maximum waste removal.

1.1 Objectives

The goal of this research was to spatially and temporally detail ambient and aquaculture derived organic particulate dynamics at an IMTA site on the west coast of Vancouver Island, Canada. To accomplish this goal, *in-situ* optical measurements of the particulate scattering (b_{p}) and backscattering (b_{bp}) coefficients and the particulate backscattering ratio ($\tilde{b}_{bp}$) were collected in conjunction with discrete sampling for particulate organic carbon (POC) and chlorophyll *a* (chl *a*) concentrations over three seasons (autumn, spring and summer) at reference sites and sites directly within and adjacent to the fish component of the IMTA system. Specifically, chapter 2 of this thesis examines bio-optical relationships found at the study site over various timescales (seasonally, daily and within-day) with the purpose of describing temporal and vertical particulate variability and assessing the effectiveness of bio-optical methods for future environmental monitoring in coastal aquaculture settings. Chapter 3 builds on the knowledge gained in Chapter 2, focusing on the temporal, vertical and horizontal dispersal of particulate aquaculture wastes and the potential implications for the future placement of uptake species at the study site. Together, these chapters provide novel information on bio-optical relationships and particulate variability within a unique coastal environment, waste dispersion from the fish component of an IMTA site and the

use of bio-optical parameters within an aquaculture setting. With further research, this knowledge could guide future IMTA site management decisions.

1.2 Optical Theory

The optical parameters utilized in this study, the particulate scattering (b_p) and particulate backscattering (b_{bp}) coefficients, are commonly used as proxies for particulate concentrations in both oceanic and coastal environments (Boss et al., 2004; Chang et al., 2006; Loisel et al., 2007; Woźniak et al., 2010). These parameters are considered inherent optical properties (IOPs) in that they are independent of the effects of the ambient light field; thus, being entirely dependent upon the characteristics of water constituents (Mobley, 1994). The particulate scattering coefficient is the integration of light scattered by particles (excluding the effects of pure water and dissolved materials) over the entire hemisphere (all directions) of the volume scattering function (VSF), whereas the particulate backscattering coefficient includes only the light scattered by particles in the backwards direction taking into account the angle of light propagation (Mobley, 1994; Twardowski et al., 2001; Antoine et al., 2011). To the first order, both b_p and b_{bp} are sensitive to particulate concentrations followed by second order influences by particle size distributions, compositions (refractive index) and shapes (Antoine et al., 2011; Neukermans et al., 2012). These second order influences have variable effects on each scattering parameter with b_p generally considered to be most sensitive to relatively large (0.5 – 20 μm), low density organic particles (phytoplankton) (Babin et al., 2003; Behrenfeld & Boss, 2006; Martinez-Vicente et al., 2010; Neukermans et al., 2012). While theoretical modelling of b_{bp} variability shows high sensitivity to submicron particles, these computations, which are

based on Mie theory, are inappropriate for modelling natural particulate assemblages (Stramski et al., 2004; Antoine et al., 2011; Neukermans et al., 2012). This factor, coupled with a lack of *in-situ* b_{bp} measurements across a diverse range of conditions has led to controversy over the drivers of b_{bp} variability (Stramski et al., 2004; Antoine et al., 2011). Current studies have shown that relatively large sized (> 3 µm) particles may have a greater influence on b_{bp} than originally thought (Dall'Olmo et al., 2009) and also, this parameter appears to be sensitive to refractive inorganic and possibly detrital materials, notably in coastal waters (Martinez-Vicente et al., 2010; Neukermans et al., 2012). As a result of the differences in sensitivities, the ratio of b_{bp} to b_p, referred to as the backscattering ratio ($\tilde{b}_{bp}$), removes the first order effect of concentration and is commonly used as a measure of bulk particulate composition (Twardowski et al., 2001; Boss et al., 2004; Loisel et al., 2007; Neukermans et al., 2012). Generally, phytoplankton dominated waters show low $\tilde{b}_{bp}$ (< 0.010) magnitudes while mineral dominated coastal waters show high (> 0.015) values (Sullivan et al., 2005; Chang et al., 2006; Loisel et al., 2007). The use of these optical parameters (b_p, b_{bp} and $\tilde{b}_{bp}$), in conjunction with the collection of biophysical concentrations via discrete water sampling, have provided valuable information on particulate dynamics in coastal waters and thus, may be useful for particulate characterization and environmental monitoring within an aquaculture setting.

Chapter 2 – Assessment of Bio-Optical Data for Environmental Monitoring at a Vancouver Island Aquaculture Site

2.1 Abstract

Temporal and vertical particulate scattering (b_p) and backscattering (b_{bp}) variability were investigated over three seasons at an integrated multi-trophic aquaculture (IMTA) site on the west coast of Vancouver Island, Canada. Optical measurements were collected in conjunction with particulate organic carbon (POC) and chlorophyll *a* (chl *a*) concentrations to investigate ambient particulate dynamics and assess the potential of bio-optical measures for environmental monitoring. Large variability was observed over the three data collection periods indicating a diverse range of particulate assemblages. Autumn/winter conditions showed high stratification, low bio-optical magnitudes and possible influences on b_{bp} and the particulate backscattering ratio ($\tilde{b}_{bp}$) by aquaculture derived wastes. Spring was characterized by a developing diatom bloom, which dominated b_p variability. In summer, an *Emiliania huxley* bloom likely occurred, strongly enhancing b_{bp} and $\tilde{b}_{bp}$ magnitudes in the thermally stratified upper water column. Definitive optical signals from aquaculture wastes were not found during the bloom events, possibly indicating a masking effect and (or) quick dilution into ambient particle fields. Throughout the study, b_p was heavily influenced by phytoplankton, whereas b_{bp} showed greater sensitivity to non-algal particles, which could make it a useful candidate as a tracer of aquaculture derived wastes during low ambient particle conditions. The use of the bio-optical properties provided valuable information on both particle concentrations and compositions over the course of the study which is required for environmental monitoring and management decisions.

2.2 Introduction

Bio - optical properties such as, particulate scattering (b_p) and backscattering (b_{bp}), are routinely used for particulate characterization within the coastal domain (e.g. Boss et al., 2004; Sullivan et al., 2005; Chang et al., 2006; Loisel et al., 2007; Snyder et al., 2008; Martinez-Vicente et al., 2010; Neukermans et al., 2012). These parameters can be

collected at relatively high temporal and spatial resolutions making them effective tools for studying dynamic coastal waters (Chang et al., 2006; DaII'OImo et al., 2009; Woźniak et al., 2010). To the first order, b_p and b_{bp} are driven by particle concentration (Neukermans et al., 2012). In addition, these parameters are influenced by different particle size distributions, shapes and compositions (index of refraction) (Antoine et al., 2011). In general, b_p is considered to be most sensitive to relatively large (0.5 – 20 µm), low density organic particles (phytoplankton) (Babin et al., 2003; Behrenfeld & Boss, 2006; Martinez-Vicente et al., 2010; Neukermans et al., 2012) and b_{bp} to submicron and also, refractive inorganic materials (Martinez-Vicente et al., 2010; Neukermans et al., 2012). The ratio of the two parameters, referred to as the backscattering ratio ($\tilde{b}_{bp}$), removes the first order effect of concentration and as such, is used as a measure of bulk particulate composition (Twardowski et al., 2001; Boss et al., 2004; Loisel et al., 2007; Antoine et al., 2011). Generally, phytoplankton dominated waters show low $\tilde{b}_{bp}$ (<0.010) magnitudes while mineral dominated coastal waters show high (>0.015) values (Sullivan et al., 2005). Yet, the relationships between b_p, b_{bp} and $\tilde{b}_{bp}$ and the highly diverse particle assemblages present in coastal waters is complex and is often not straightforward (Snyder et al., 2008; Woźniak et al., 2010). For example, *in-situ* measurements of b_{bp} in dynamic coastal environments are limited, and as a result, much of the knowledge of the sources of b_{bp} variability comes from Mie theory computations, which are inappropriate for modelling natural particle assemblages (Antoine et al., 2011; Neukermans et al., 2012). Therefore, the sources of b_{bp} variability are not yet fully understood and are controversial (Stramski et al., 2004) with current studies showing greater influences by relatively large sized particles (> 3 µm) than originally

thought (Dall'Olmo et al., 2009) and also, high sensitivities to particle compositions (Neukermans et al., 2012). Nonetheless, these optical parameters are valuable tools for coastal monitoring and management as they provide high resolution data on particulate dynamics and can be used for the detection and tracking of contaminants and pollutants (e.g. Krasakopoulou & Karageorgis, 2005; Chang et al., 2006; Woźniak et al., 2010; Le et al., 2013). Specifically, bio-optical data could be of key importance for the coastal aquaculture industry where cultured species rely on high water quality, but also add particulate matter to the coastal environment (Barrington et al., 2009).

On the west coast of Canada, the environmental effects of the finfish aquaculture industry have led to high concern over its environmental sustainability. One, of many issues associated with this form of aquaculture is that it has the potential to add considerable amounts of organic particulate wastes to the waters surrounding the farm (Brooks & Mahnken, 2003). If these wastes accumulate excessively on the seafloor, the sediment may become enriched or even anaerobic, ultimately reducing localized biodiversity, creating conditions for more opportunistic species (Brooks & Mahnken, 2003; Kutti et al., 2007b). As a result of this and other concerns over finfish aquaculture, interest in the development of sustainable alternatives and practices has grown (Ridler et al., 2007). One method that has shown potential is integrated multi-trophic aquaculture (IMTA). These systems integrate the fed species (e.g. fish/shrimp) with commercially valuable extractive species (bivalves, algae/seaweed) which can utilize the nutrient waste from the fed species and ideally remove portions of this waste upon their harvest (Troell et al., 2003; Neori et al., 2004; Barrington et al., 2009).

However, substantial research is required before these systems can be implemented for effective waste uptake. In particular, additional knowledge is needed on the open-water dispersal of fish derived particulates so that adjacent co-cultured species can be maximized for waste removal (Troell & Norberg, 1998; Reid et al., 2009). In addition, an understanding of background environmental conditions is essential for assessing the effectiveness of open-water IMTA systems as certain species of bivalves are selective feeders and will become satiated during periods of high ambient phytoplankton concentrations. This satiation can greatly reduce their efficiency at filtering particulate wastes from the fed portions of IMTA systems (Troell & Norberg, 1998; Cheshuk et al., 2003). Furthermore, pollution and harmful algal blooms (HABs) can result in species being considered unfit for consumption (Lewitus et al., 2012; Martell et al., 2013). Thus, it is essential that background environmental variability is understood when developing IMTA systems and that environmental monitoring is continued at operational sites to ensure efficiency and to maintain species and ecosystem health (Barrington et al., 2009). In many cases, environmental monitoring at these sites is performed through the use of laborious, expensive and time consuming discrete sampling methods which do not allow for the collection of high temporal or spatial resolution data (Millie et al., 1995; Lander et al., 2013). Considering these factors, *in-situ* bio-optical methods could be a valuable tool for monitoring aquaculture systems and also, for the management of the coastal ecosystems that they are located within.

The aim of this paper was to assess the use of short term continuous sampling of b_{p}, b_{bp} and $\tilde{b}_{bp}$ for measuring particulates at an active IMTA site and to thereby evaluate the effectiveness of these optical parameters for temporal and vertical particulate

characterization and environmental monitoring over various timescales. Effectively, these measurements could guide future management decisions in coastal aquaculture settings and contribute to the greater knowledge of coastal particulate dynamics and optical responses to varying particle assemblages.

2.3 Methods

2.3.1 Study Site

Data collections for this research were conducted at the Kyuquot SEAfoods Inc. IMTA site, which is located in Kyuquot Sound, British Columbia, on the northwest coast of Vancouver Island at: 50° 02' 45.85" N and 127° 17'; 53.66" W. Over the data collection period approximately 15 000 adult sablefish (*Anoplopoma fimbria*), and 50 000 scallops (*Patinopectin yessoensis*) were in culture in the southwestern portion of the system. Rows of macrophytes (*Saccharina lattisima*) were also extended from the site during spring and summer of 2012 (Figure 2.1).

The studied IMTA system is located at the deepest part (25 m) of a shallow protected embayment between Vancouver Island and Surprise Island. The small channel to the southwest of the embayment connects to the much larger Crowthier channel which opens to the Pacific Ocean. To the east the embayment opens into Kyuquot Sound which is a deep coastal fjord. During flood tide, the water generally flows in from the southwestern channel and out towards Kyuquot Sound. The opposite occurs on ebb tide. The unique bathymetry of the embayment creates a gyre which reduces current velocities, causes unidirectional flow and recirculates water in the western sector of the embayment (Personal communication, Cross, 2011; unpublished data, Foreman, 2011).

The exposed coastline to the west of the IMTA site is one of the most intense wind and wave environments in the province of British Columbia. While the site is sheltered from waves, it is exposed to strong southeasterly winds during the winter months (Coast and Marine Planning Branch, 2003). Additionally, the area is characterized by high rainfall with the annual mean total precipitation being greater than 4000 mm. The majority of this precipitation occurs in late fall and winter with total precipitation for January usually being greater than 400 mm (Natural Resources Canada, 2009). This precipitation results in runoff which can lead to the development of a highly stratified water column with fresh water surface layers laden with suspended materials (Coast and Marine Planning Branch, 2003; Del Bel Belluz, 2010). Yet, during strong wind and tidal events considerable mixing can occur, de-stratifying the water column. In general, stratification develops during the calm summer months due to thermal heating of the surface waters (Blyth et al., 2004).

The coastal areas of Kyuquot Sound are located within the North American Coastal Upwelling Domain, characterized by the upwelling of nutrient rich waters during the summer and downwelling during the winter months (Hay et al., 2003). In spring and summer, phytoplankton production within the coastal inlets on the west coast of the island can be limited due to low water exchange, stratification and reduced nutrient availability (Hay et al., 2003). Yet, during these seasons, offshore diatom blooms (*Skeletonema costatum*) are commonly advected into the inlets via wind forcing. Similarly, *Emiliania huxleyi* (*E. huxleyi*), an opportunistic and cosmopolitan coccolithophore species, can also be advected into these inlets where they can form isolated blooms over periods of high thermal stratification (Taylor & Haigh, 1996).

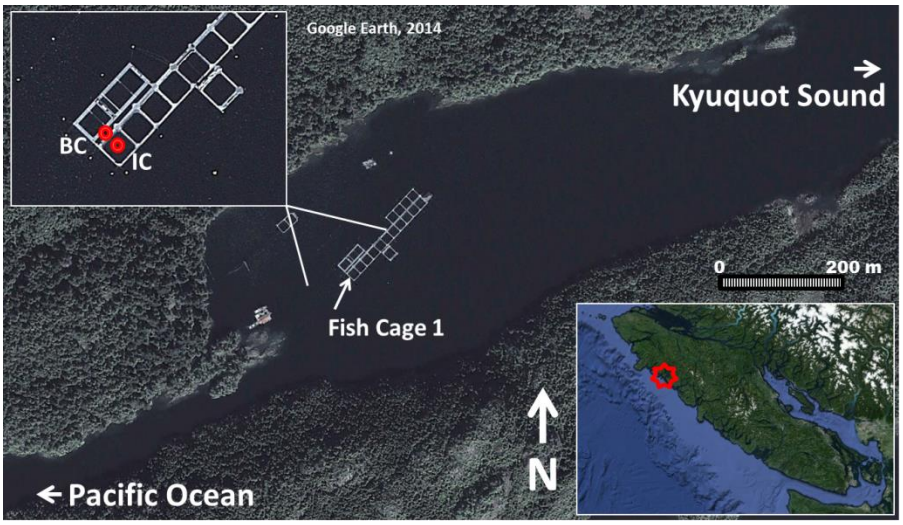

Figure 2.1 – Kyuquot SEAfoods IMTA site within Kyuquot Sound on the northwest coast of Vancouver Island. In-cage (IC) and beside cage (BC) sample site locations shown on inset.

2.3.2 Data Collection Regime

Data for this research was collected in November 2011, May 2012, and August 2012 representing autumn, spring and summer conditions, respectively. The specific sampling dates, sample site locations and other metadata are presented in Table 2.1. Sample site locations within the IMTA system are shown in Figure 2.1.

Table 2.1 – Data collection dates, sample locations and details of optical profile/water sampling depths and frequencies. The first letter in the acronym for the individual sampling day represents the month (November (N), May (M), August (A)), followed by the day and then sampling location where: In-Cage is (IC), Beside-Cage is (BC).

Collection Days	Water Sampling Depths (m)	Water Sampling Method	Water Sampling	Optical Profiles	Profile Depth (m)
N14-IC	1, 5, 13	Niskin	Hourly	Hourly	14
N15-BC	1, 5, 13				20
M19-21-IC	1, 7, 13	Niskin	Hourly*	Continuous	14
A16-18-IC	1, 7, 13				14
A20-23-BC	1, 7, 17	Pumped	Hourly	Continuous	21

*Pigment samples in May were collected bi-hourly

On each sampling day, data was either collected at in-cage (IC) or beside-cage (BC) sites (Figure 2.1). In-cage profiles were limited to 14 m, due to the bottom of the fish cage at 15 m depth. Beside cage profiles extended to 21 m, with the total depth of the

water column being approximately 25 m. In November, profiles and water sampling were performed before the fish were fed (BF), post-feeding (PF) and then at one hour intervals for a five hour period. More intensive approaches were taken in May and August when profiles were performed nearly continuously from BF to 8 hours PF; however, water sampling followed the same hourly regime as in November. Continuous profiling was performed during these periods so that high resolution data with depth and time were collected.

Total suspended matter (TSM), particulate organic carbon (POC) (non-elemental) and phytoplankton pigment analysis were collected via water sampling at three discrete depths (Table 2.1) to characterize surface, mid and lower cage/water column particulates. In November and May, a 5 L Niskin bottle was used for water sample collection. In August, a pumping system was used enabling the collection of water samples directly beside the profiler while inside the cage. The pump hose was purged before each new sample collection.

Water samples were collected into pre-washed 1 L Nalgene bottles and then placed into a cooler. They were then transferred to the onsite lab for immediate filtration. All samples were filtered at low vacuum through pre – weighed, washed and combusted 0.7 µm Whatman GF/F filters for further lab analysis of TSM, phytoplankton pigments and POC. After filtration, 300 mL of Deionized (DI) water was passed through the filters to minimize salt accumulation (Stavn et al., 2009). The filters were frozen on-site until they were transferred to the University of Victoria where they were stored at - 80 °C until analysis was performed.

An optical profiler containing a Wetlabs hyperspectral absorption and attenuation meter (ac-s), ECO-BB3 sensor and a Seabird CTD was used for the optical data collection. The ac-s measured total absorption and attenuation at 86 channels between 400 and 737 nm. This instrument has a 4 nm resolution, samples at 4 Hz and has 25 cm pathlengths. Deionized water calibrations were performed on the ac-s instrument before, during and after each data collection period to characterize instrument drift that occurred during sampling. These calibrations were conducted following the procedures set out by Twardowski et al. (1999). The ECO-BB3 was used to derive particulate backscattering (b_{bp}) at a fixed angle (117˚) for three wavelengths; 470, 530 and 660 nm.

2.3.3 Water Sample Analysis

Total suspended matter filters were dried at 60°C for six hours, desiccated, weighed and then the process was repeated until the weights had stabilized. Total suspended matter concentrations of the water (mg l^{-1}) were then determined by subtracting the pre-filtered weights from the post filtered weights (Clesceri et al., 1998).

Reverse-phase high performance liquid chromatography (HPLC) analysis was performed for the determination of phytoplankton pigments (Arar, 1997). Sample filters were extracted in 10 ml of 90% HPLC grade acetone, sonicated for 30s and then placed into a dark refrigerator to steep overnight (< 24 hrs.). Once steeped, the samples were centrifuged in a dark room at 1000 m/s^2 for 10 minutes. The separated solution was then filtered (0.45 µm) into vials which were immediately placed into the autosampler of a Dionex HPLC system. This system was pre-calibrated using DHI reference standards for the determination of chlorophyll c_1, c_2, *a* and *b*, Peridinin, 19'-but and

hex-anoyloxyfucoxanthin, Fucoxanthin, Diadinoxanthin, Alloxanthin, Zeaxanthin and b-carotene concentrations to indicate dominant phytoplankton groups.

Particulate organic carbon (POC) (non-elemental) was determined using a Shimadzu Solid Sample Module (SSM-5000) in line with a TOC-V carbon analyzer. Dry combustion of the filters at 900°C was performed within the combustion tube of the SSM-5000. The CO_2 created by the high temperature oxidation of the carbon was carried to a non-dispersive infrared (NDIR) detector within the TOC-V module via 99.9% O_2 carrier gas flowing at 500 ml/min (Obernosterer et al., 2005). Particulate organic carbon was estimated by comparison with calibration curves from lake sediment samples (LKSD – 2) with certified carbon concentrations (Natural Resources Canada, 2013). These samples were collected to quantify the total organic particulate pool including both autotrophic and detrital particles. In this study, the detrital pool may have included aquaculture derived wastes such as wasted feed and fish feces. The POC:chl *a* ratio was used as a further indicator of the composition of the total organic particulate pool as values that are < 200 generally indicate phytoplankton dominated waters, while values that are > 200 indicate waters dominated by detrital materials (Cifuentes et al., 1988; Savoye et al., 2012).

2.3.4 Optical Data Analysis

The optical and CTD data were merged using the WET Labs WAP software. This software subtracted the pure water attenuation and absorption coefficient values derived by Pope and Fry (1997) from the raw ac-s data. A customized script was then used on these data to subtract the pure water offsets from the DI calibrations, to perform temperature and salinity corrections (Sullivan et al., 2006) and to correct for unwanted

scattered light using the proportional method (Zaneveld et al., 1994) resulting in the derivation of the absorption (a_{pg}) and attenuation (c_{pg}) (m^{-1}) coefficients of particulate and dissolved matter minus the effects of pure water at each depth (z) and wavelength (λ). Once these corrections were performed, all of the merged profiler data were binned into 0.5 m increments and the particulate scattering coefficient (b_p) (m^{-1}) was calculated (Equation 2.1).

$$b_p(z,\lambda) = c_{pg}(z,\lambda) - a_{pg}(z,\lambda) \quad (2.1)$$

Following this step, the raw ECO-BB3 volume scattering measurements were corrected for absorption over the scattered light path length following Equation 2.2 (WETLabs, 2011);

$$\beta\ corr\left(117°, a_{pg}=0\right) = \beta\ meas\ (117°, a_{pg})^{(0.0391 a_{pg})} \quad (2.2)$$

where absorption (a_{pg}) values were derived from the ac-s at corresponding wavelengths to those of the ECO-BB3 sensor. Subsequently, the volume scattering coefficient of particles $\beta_p(117^\circ)$ was calculated by subtracting the volume scattering of pure water (β_w) from total volume scattering (β).

$$\beta_p\ (117°, \lambda) = \beta\ (117°, \lambda) - \beta_w\ (117°, \lambda) \quad (2.3)$$

Next, the particulate backscattering coefficient (b_{bp}) (z, λ) was determined through Equation 2.4, which used a scaling factor (X) derived by Boss and Pegau (2001). These authors determined X to be 1.1 based on measurements of the volume scattering function with high angular resolution in a diverse set of water types.

$$b_{\mathrm{bp}}(z,\lambda) = 2\pi\, X\, \beta_p\,(117°,\lambda) \quad (2.4)$$

Finally, the backscattering ratio ($\tilde{b}_{bp}$) was calculated using:

$$\tilde{b}_{bp}(z,\lambda) = \frac{b_{bp}(z,\lambda)}{b_p(z,\lambda)} \quad (2.5)$$

Similar to Boss et al. (2004) and Sullivan et al. (2005), chlorophyll *a* concentrations (µg l^{-1}) were estimated using a baseline subtraction method where the chlorophyll absorption peak ($a_t\,(676\,nm)$) from the ac-s data was divided by a specific chlorophyll absorption value (a_{ph}* (676 nm)) of 0.014 m^2 mg^{-1} through the use of equation 2.6.

$$[\mathrm{chl}] = \frac{(a_{pg}(676nm) - a_{pg}(650nm))}{0.014} \quad (2.6)$$

In other coastal studies, absorption estimated chlorophyll *a* has been found to be highly correlated with both chlorophyll fluorescence and extracted chlorophyll (Boss et al., 2004; Sullivan et al., 2005). Similarly, a strong linear relationship was found between HPLC derived and absorption estimated chlorophyll *a* for the combined May and August datasets (r^2 = 0.86, n = 234). Based on these results, we used absorption estimated chlorophyll *a* for these periods so that trends could be seen through the water column as opposed to at only 3 discrete depths where samples for HPLC chl *a* analysis were collected. In November, the chlorophyll absorption peak at 676 nm was not clearly observed and absorption at this wavelength was often less than at 650 nm resulting in negative absorption estimated chl *a* concentrations. As such, only HPLC derived chl *a* data were used during the November period. Care should be taken when

interpreting the absorption estimated chl *a* results as a_{ph}*(676) is variable through diverse phytoplankton populations (Boss et al., 2004; Sullivan et al., 2005). Sullivan et al. (2005) calculated that expected errors using this method should not exceed ± 50%, but would likely be less in waters showing a large dynamic range in chl *a* magnitudes.

2.3.5 Statistical Analysis

All statistical analysis and interpolations for colour-map plots were performed with the OriginPro software package. Optical relationships with biophysical parameters were assessed using Pearson's correlations, which were considered statistically significant at the 95% confidence level, unless otherwise stated.

2.4 Results

2.4.1 Hydrographic and Weather Conditions

A summary of the hydrographic and weather conditions for each sampling period is shown in Table 2.2. Large vertical variability in temperature and salinity was observed in autumn due to surface intrusions of fresh water. These intrusions were a result of residual runoff from a large storm event that occurred prior to sampling (November 9th – 105 mm of rain). In comparison, May exhibited low temperature/salinity variability, but the water column was still stratified showing distinct thermo/haloclines. This period began with calm conditions; however, heavy rain and strong winds occurred the night before M21. In August, a well-defined thermocline and a weak halocline were present throughout the sampling period. A few light rain events occurred between A19 and A22, but they were relatively unsubstantial in comparison to the previous data collection periods.

A mixed tidal regime was observed at the study site, regardless of the sampling month, with the maximum tidal range being 0.5 to 3.7 m. At this regime, current velocities were generally the greatest directly before high tide. The dominant current direction was to the South-West, with very little deviation.

Table 2.2 – Depth integrated ranges of temperature (°C) and salinity (PSU), modelled surface current velocities (cm s^{-1}) and tidal range (m). Total rainfall was recorded at the nearest weather station (Zeballos, B.C.) for each data collection period. Dominant current directions (D.C.D) were modelled.

	Temp. (˚C)	**Salinity (PSU)**	**Currents (cm s^{-1})**	**D.C.D**	**Max Tidal Range (m)**	**Rainfall (mm)**
November	5.42 – 12.07	5.12 – 31.31	1.4 – 4.4	SW	0.6 – 3.6	1.4
May	8.34 – 9.78	30.00 - 32.22	0.5 – 6.0	SW	0.5 – 3.6	29.2
August	10.13 – 16.58	29.51 – 32.96	1.1 – 4.7	SW	0.5 – 3.7	5.2

2.4.2 Seasonal Biophysical and Optical Dynamics

This section first presents the large scale seasonal trends and relationships in the biophysical and optical data. Then, daily and within-day biophysical and optical trends and relationships are explored within each sampling period (section 2.4.3).

Biophysical Trends

Table 2.3 shows the range and means of the biophysical variables (POC, chl *a*, and POC:chl *a*) for the entire study and for each specific sampling period. A large range in biophysical values was measured over the three periods. November exhibited the lowest mean POC (0.16 mg l^{-1}) and chl *a* (0.12 µg l^{-1}) concentrations, but the highest and most variable POC:chl *a* values (382 – 13 400). In May and August, the mean POC (0.53 and 0.59 mg l^{-1}, respectively) and chl *a* (2.31 and 2.90 µg l^{-1}, respectively) values increased considerably from those seen in November and the mean POC:Chl *a* values (334 and 469, respectively) decreased.

Unfortunately, the TSM data exhibited inconsistent concentrations, and analytical error could not be ruled out. Therefore, these data were excluded from the results.

Table 2.3 – Ranges and means (in brackets) of the biophysical variables (POC, chl *a*, and POC:chl *a*) and optical variables (b_p, b_{bp} and $\tilde{b}_{bp}$).

	POC (mg l^{-1})	**chl *a* (µg l^{-1})**	**POC:chl *a***	**b_p (660nm) (m^{-1})**	**b_{bp} (660nm) (m^{-1})**	**$\tilde{b}_{bp}$(660nm)**
Entire	0.09 – 1.54 **(0.47)**	0.00 – 13.34 **(2.31)**	61 – 13 400 **(929)**	0.03 – 3.08 **(0.77)**	0.001 – 0.047 **(0.015)**	0.002 – 0.078 **(0.020)**
Nov.	0.09 – 0.30 **(0.16)**	0.01 – 0.42 **(0.12)**	382 – 13 400 **(3026)**	0.05 – 1.26 **(0.14)**	0.001 – 0.009 **(0.003)**	0.002 – 0.065 **(0.022)**
May	0.16 – 1.54 **(0.59)**	0.01 – 13.34 **(2.31)**	73 – 1051 **(334)**	0.15 – 2.20 **(0.70)**	0.002 – 0.019 **(0.005)**	0.002 – 0.047 **(0.010)**
August	0.17 – 1.32 **(0.53)**	0.00 – 11.45 **(2.90)**	61 – 7537 **(469)**	0.15 – 3.08 **(0.88)**	0.003 – 0.047 **(0.019)**	0.003 – 0.078 **(0.022)**

Hyperspectral Trends

Figure 2.2 (a, b and c) summarizes the main trends in the mean inherent optical properties (IOPs) ($c_{pg}(\lambda)$, $a_{pg}(\lambda)$, $b_p(\lambda)$ and $b_{bp}(\lambda)$) for each sampling month. In May and August, both $c_{pg}(\lambda)$ and $b_p(\lambda)$ were nearly an order of magnitude higher than in November. In addition, the November $a_{pg}(\lambda)$ data did not exhibit a chlorophyll absorption peak at 676 nm. Notably, August showed considerably higher mean $b_{bp}(\lambda)$ values when compared to the other sampling periods. For further analysis we selected a specific wavelength, 660 nm, due to the quasi-wavelength independent behavior of $b_p(\lambda)$ (Figure 2.2 a, b and c) and for comparison with other coastal studies (Loisel et al., 2007; Garcia et al., 2011). From this point on $b_p\,(660\,nm)$, $b_{bp}(\lambda)\,(660\,nm)$ and $\tilde{b}_{bp}\,(660\,nm)$ will be denoted as b_p, b_{bp} and $\tilde{b}_{bp}$, respectively.

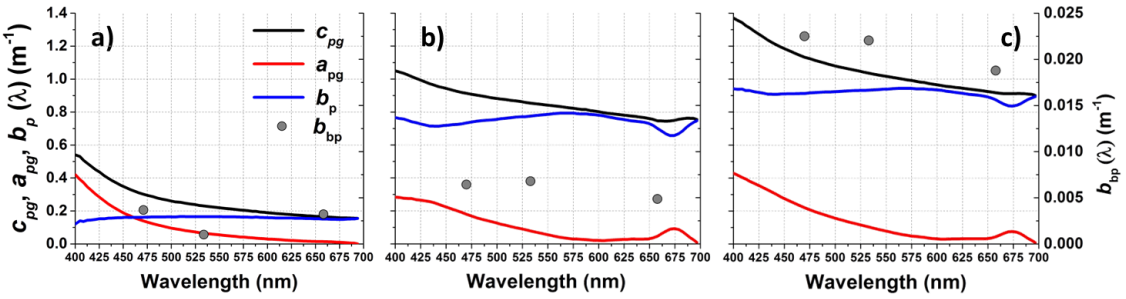

Figure 2.2 – Mean IOPs (c_{pg} (λ) (black), a_{pg} (λ) (red), b_p (λ) (blue) and b_{bp} (λ) (grey dots)) for the a) November, b) May and c) August data collection periods.

b_p, b_{bp} and $\tilde{b}_{bp}$ Trends

When separated by data collection period, November exhibited the lowest mean values for b_p and b_{bp} (0.14 and 0.003 m^{-1}, respectively), but showed a high mean $\tilde{b}_{bp}$ value (0.022) (Table 2.1). Comparatively, the mean b_p (0.70 m^{-1}) value for May increased by a factor of 5 when compared to November; however, b_{bp} only increased by a factor of 1.3 (0.005 m^{-1}) resulting in a low mean $\tilde{b}_{bp}$ value (0.010). Despite similar mean biophysical concentrations as the May data collection, August's mean b_{bp} value (0.019 m^{-1}) was an order of magnitude higher than in May. This increase led to a high mean $\tilde{b}_{bp}$ value (0.022), which was comparable to the one measured for the November data collection period when the biophysical state of the water was considerably different.

Optical – Biophysical Relationships

Due to the large measured variability in both the biophysical and optical data, statistical trends were examined for each individual sampling period. Exclusively for November, b_p and b_{bp} relationships with POC and chl *a* were separated by the surface/mid (surface and 5 m) and lower water column (13.0 m) as different relationships were found at the bottom of the fish cage (Table 2.4). In the surface/mid waters, both b_p and b_{bp} were

conditioned by chl *a* (r^2 = 0.82 and 0.69, respectively); however, their corresponding relationships with POC were considerably weaker (r^2 = 0.44 and 0.29, respectively). In comparison, the lower water column showed stronger b_p and b_{bp} relationships with POC (r^2 = 0.42 and 0.35, respectively) than with chl *a* (r^2 = 0.27 and 0.20, respectively).

May showed the strongest positive b_p and b_{bp} – chl *a* relationships (r^2 = 0.89 and 0.74), but relatively lower positive b_p and b_{bp} – POC relationships (r^2 = 0.64 and 0.46). In August, b_p was positively correlated with both POC and chl *a* (r^2 = 0.77 and 0.64, respectively); however, the corresponding b_{bp} relationships were highly scattered (r^2 = 0.33 and 0.12, respectively). Notably, b_p and b_{bp} showed positive correlations (r^2 = 0.68 and 0.33) with 19' – hexonoyloxyfucoxanthin (19HF) concentrations, the marker pigment for prymnesiophytes to which the coccolithophorid *E. Huxleyi* belong (Jeffrey & Vesk, 1997; Ras et al., 2008). Similar trends were not experienced in November and May when 19HF concentrations were either non-detectable or low.

Table 2.4 - Coefficient of Determination (r^2) values between the optical and biophysical variables. All presented relationships are significant ($p < 0.05$) unless marked not significant (*ns*). A power-law fit was applied to the $\tilde{b}_{bp}$ - chl *a* relationship for each period. The variability in sample sizes (n) was due to different sampling procedures (i.e. absorption estimated chl *a* *vs.* discrete chl *a* and POC samples). The November data was separated into surf./mid. and lower water column. May relationships with POC are presented for the surf./mid. depths only. All other May/August relationships were performed for the entire water column.

Relationship	Month/Depths	r^2	*n*	Equation
b_p (m^{-1}) – POC (mg l^{-1})	Nov. Surf/Mid	0.44	*28*	b_p = 6.05 (POC) - 0.59
	Nov. Bottom	0.42	*14*	b_p = 0.35 (POC) + 0.10
	May Surf/Mid	0.64	*98*	b_p = 1.49 (POC) + 0.05
	August	0.77	*203*	b_p = 1.74 (POC) - 0.02
b_p (m^{-1}) – chl *a* (µg l^{-1})	Nov. Surf/Mid	0.82	*27*	b_p = 2.08 (chl *a*) - 0.01
	Nov. Bottom	0.27	*11*	b_p = 2.71 (chl *a*) + 0.10
	May	0.89	*2897*	b_p = 0.11 (chl *a*) + 0.22
	August	0.64	*12 469*	b_p = 0.14 (chl *a*) + 0.41
b_p (m^{-1}) – 19HF (µg l^{-1})	May	*ns*	*47*	-
	August	0.68	*187*	b_p = 3.86 (19HF) + 0.24
b_{bp} (m^{-1}) – POC (mg l^{-1})	Nov. Surf/Mid	0.29	*28*	b_{bp} = 0.025 (POC) - 0.001
	Nov. Bottom	0.35	*13*	b_{bp} = 0.013 (POC) + 0.002
	May Surf/Mid	0.46	*98*	b_{bp} = 0.005 (POC) + 0.002
	August	0.33	*175*	b_{bp} = 0.019 (POC) + 0.001
b_{bp} (m^{-1}) – chl *a* (µg l^{-1})	Nov. Surf/Mid	0.69	*27*	b_{bp} = 0.011 (chl *a*) + 0.001
	Nov. Bottom	0.20	*10*	b_{bp} = 0.147 (chl *a*) + 0.002
	May	0.74	*2897*	b_{bp} = 0.001 (chl *a*) + 0.003
	August	0.12	*10 691*	b_{bp} = 0.001 (chl *a*) + 0.015
b_{bp} (m^{-1}) – 19HF (µg l^{-1})	May	*ns*	*47*	-
	August	0.33	*160*	b_{bp} = 0.044 (19HF) + 0.011
$\tilde{b}_{bp}$ (m^{-1}) – chl *a* (µg l^{-1}) Power Law	November	0.73	*38*	$\tilde{b}_{bp} = 0.003\ (\text{chl } a)^{-0.559}$
	May	0.74	*2897*	$\tilde{b}_{bp} = 0.010\ (\text{chl } a)^{-0.267}$
	August	0.15	*10 691*	$\tilde{b}_{bp} = 0.020\ (\text{chl } a)^{-0.094}$
$\tilde{b}_{bp}$ (m^{-1}) – POC:chl *a*	November	0.66	*37*	$\tilde{b}_{bp}$ = 0.6 (POC:chl *a*) - 3.6
	May	0.45	*30*	$\tilde{b}_{bp}$ = 0.3 (POC:chl *a*) - 2.9
	August	0.20	*164*	$\tilde{b}_{bp}$ = 0.2 (POC:chl *a*) - 2.1

Both November and May showed relatively strong negative power law $\tilde{b}_{bp}$ - chl *a* relationships (Figure 2.3, Table 2.4), with low $\tilde{b}_{bp}$ (<0.010) values in the surface waters

where chl *a* was the greatest. Comparatively, the August relationship was considerably weaker (r^2 = 0.15), with more scattered and very few values below 0.010 even at high chl *a* (Figure 2.3 c). November was the only period to show a relatively strong positive linear trend between $\tilde{b}_{bp}$ and POC:chl *a* (r^2 = 0.66).

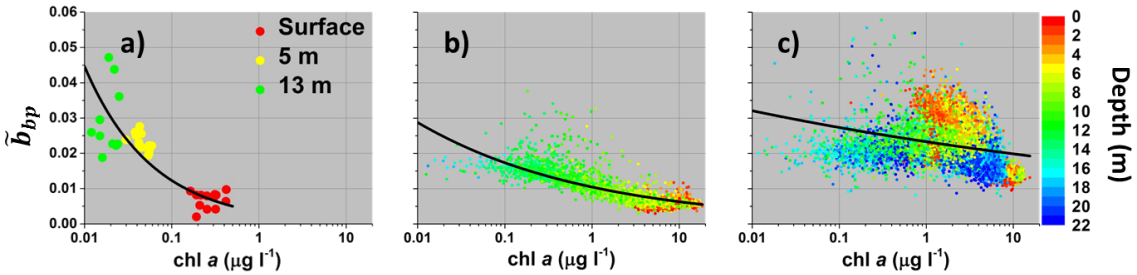

Figure 2.3 – Relationships between a) chl *a* and $\tilde{b}_{bp}$ for November and chl *a* and $\tilde{b}_{bp}$ for b) May and c) August. Discrete sampling depths are denoted by colour for the November relationship: Surface (red), 5 m (yellow), and 13 m (green). Colour – mapping was used for depths in the May and August relationships. Red denotes surface waters and blue denotes deep waters.

2.4.3 November Daily Trends in Biophysical and Optical Properties

November Biophysical Trends

Daily mean November biophysical concentrations separated by sampling depth are shown in Figure 2.4. Vertically, N14 and N15 showed relatively similar mean POC, chl *a* and POC:chl *a* values, with the highest mean chl *a* (0.28 µg l^{-1}) and POC (0.18 mg l^{-1}) magnitudes found at the surface. While chl *a* decreased with depth, POC increased slightly from 5.0 (0.13 mg l^{-1}) to 13.0 m (0.16 mg l^{-1}) resulting in high mean POC:chl *a* magnitudes (> 6000).

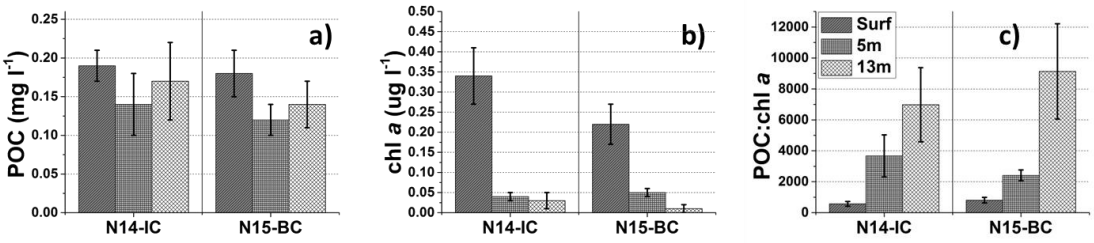

Figure 2.4 – Daily mean a) POC, b) chl *a* and c) POC:chl *a* values at discrete sampling depths for N14-IC and N15-BC. Error bars represent one standard deviation from the mean.

Over the November period, Fucoxanthin (Fuco), the marker pigment for diatoms, was the dominant pigment present in the water column with relative contributions ranging from 39 to 71 % (Figure 2.5).

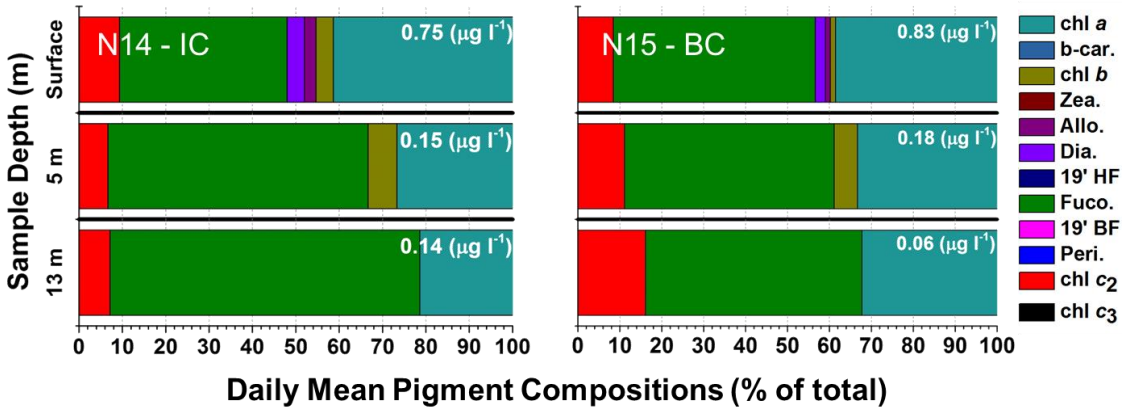

Figure 2.5 – Daily mean pigment compositions separated by discrete sampling depths (surface, 5.0 and 13.0 m) for each November sampling day. Total pigment concentrations are plotted in the upper right corner of each bar. Pigment compositions are a percent of each of individual pigment concentration to the total.

November Optical Trends

The daily range and means of the optical data for the November dataset are presented in Table 2.5. Colour-map plots of daily b_p, b_{bp}, $\tilde{b}_{bp}$ and salinity with depth and time are shown in Figure 2.6. Both November days showed relatively similar mean optical values. Vertically, the highest b_p values (0.07 – 1.26 m^{-1}) and relatively high b_{bp}

magnitudes (0.002 – 0.007 m^{-1}) were observed above the halocline within the surface layer (< 2 m) (Figure 2.6). This layer also exhibited variable, but generally low $\tilde{b}_{bp}$ magnitudes (< 2 m, 0.004 – 0.030) with the lowest values concentrated directly at the surface (0.5 m, 0.004 – 0.010).

Table 2.5 – Ranges and mean values (in brackets) of the optical variables (b_p, b_{bp} and $\tilde{b}_{bp}$) for each data collection day. Data collection periods are separated by black rows.

	b_p (m^{-1})	b_{bp} (m^{-1})	$\tilde{b}_{bp}$
N14-IC	0.03 – 0.99 (0.13)	0.001 – 0.013 (0.003)	0.003 – 0.73 (0.024)
N15-BC	0.05 – 1.35 (0.15)	0.001 – 0.009 (0.003)	0.002 – 0.72 (0.022)
M19-IC	0.15 – 1.39 (0.57)	0.002 – 0.011 (0.004)	0.003 – 0.045 (0.009)
M20-IC	0.16 – 2.20 (0.76)	0.002 – 0.019 (0.005)	0.004 – 0.032 (0.009)
M21-IC	0.16 – 2.09 (0.79)	0.002 – 0.017 (0.006)	0.002 – 0.047 (0.01)
A16-IC	0.11 – 1.17 (0.56)	0.004 – 0.030 (0.017)	0.013 – 0.035 (0.021)
A17-IC	0.12 – 1.98 (0.71)	0.008 – 0.045 (0.020)	0.013 – 0.032 (0.020)
A18-IC	0.20 – 3.78 (1.88)	0.016 – 0.040 (0.029)	0.010 – 0.018 (0.014)
A20-BC	0.35 – 2.10 (1.04)	0.006 – 0.047 (0.023)	0.009 – 0.038 (0.021)
A21-BC	0.41 – 1.76 (0.84)	0.009 – 0.045 (0.021)	0.008 – 0.043 (0.024)
A22-BC	0.21 – 1.52 (0.57)	0.005 – 0.042 (0.014)	0.008 – 0.069 (0.024)
A23-BC	0.15 – 1.08 (0.45)	0.003 – 0.040 (0.012)	0.008 – 0.078 (0.024)

Below the surface layer (2.0 – 9.5 m), b_p and b_{bp} decreased to the lowest values of the water column (0.05 – 0.18 m^{-1} and 0.001 – 0.004 m^{-1}, respectively) and $\tilde{b}_{bp}$ increased considerably (0.015 – 0.065). In the lower water column (> 9.5 m), b_p and b_{bp} magnitudes increased with depth on both days. Notably, the highest b_{bp} (0.003 – 0.009 m^{-1}) and $\tilde{b}_{bp}$ (0.018 – 0.063) magnitudes were measured near the bottom of the cage (14 m) on N14. These values were considerably higher than those observed at the same depth beside the cage on the following day (N15) (0.003 – 0.004 m^{-1} and 0.021 – 0.028 respectively); however, b_p magnitudes were comparable at this depth between N14 (0.14 – 0.18 m^{-1}) and N15 (0.14 – 0.17 m^{-1}).

Below the cage (> 15.0 m) on N15, increased b_p and b_{bp} magnitudes were observed towards the end of the day with values at 19.0 m depth ranging from 0.16 – 0.27 and 0.003 – 0.006 m^{-1}, respectively. No corresponding trends were seen in $\tilde{b}_{bp}$ which was relatively invariant at this depth (0.018 – 0.026).

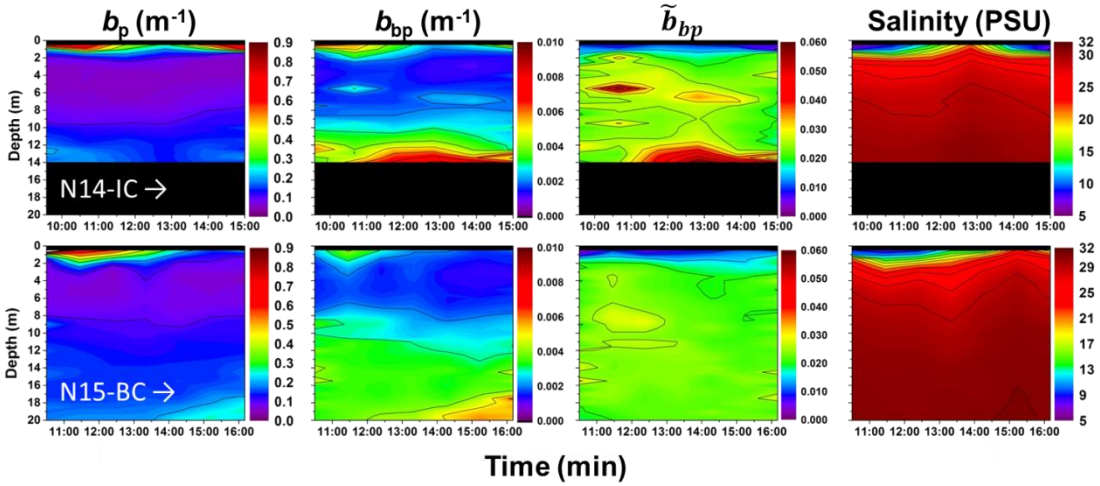

Figure 2.6 – N14-IC and N15-BC daily time-series of b_p (m^{-1}), b_{bp} (m^{-1}), $\tilde{b}_{bp}$ and salinity (PSU). Time is plotted on the x-axis, depth is plotted on the primary y-axis and the colours represent the magnitudes of each variable. Red denotes high values and purple denotes low values. Black areas indicate where no data was collected.

November Bio-Optical Relationships

On both November sampling days, significant positive b_p and b_{bp} relationships with chl *a* were present in the surface/mid water column with the strongest of these relationships (r^2 = 0.88 and 0.78, respectively) observed on N14 (Table 2.6). Particulate scattering was also related to POC at these depths; however these relationships were considerably weaker than those with chl *a*. The only significant positive b_{bp} – POC relationship was observed in the surface/mid water column on N15 (r^2 = 0.42). Daily regressions from the lower water column were not included due to small sample sizes. On both days, the

backscattering ratio was highly influenced by chl *a* and POC:chl *a*, showing negative power law and positive linear relationships, respectively.

Table 2.6 – Coefficient of Determination (r^2) values for the daily depth separated November relationships between the optical and biophysical variables. All presented relationships are significant ($p < 0.05$) unless indicated with *ns*. Power-law fits were applied to the $\tilde{b}_{bp}$ - chl *a* relationships.

	Depths	**N14-IC (r^2)**	***n***	**N15-BC (r^2)**	***n***
b_p - POC	Integrated	*ns*	23	**0.45**	21
	Surf/mid	**0.33**	15	**0.56**	14
b_p - chl *a*	Integrated	**0.85**	21	**0.51**	18
	Surf/mid	**0.88**	14	**0.72**	14
b_{bp} - POC	Integrated	*ns*	12	*ns*	21
	Surf/mid	*ns*	15	**0.42**	14
b_{bp} - chl *a*	Integrated	*ns*	21	*ns*	18
	Surf/mid	**0.78**	14	**0.48**	14
$\tilde{b}_{bp}$ - chl *a*	Integrated	**0.81**	23	**0.71**	18
$\tilde{b}_{bp}$ - POC/chl *a*	Integrated	**0.76**	22	**0.62**	16

2.4.4 May Daily Trends in Bio-Optical Properties

May Biophysical Trends

Depth separated mean values for each May sampling day are shown in Figure 2.7. Vertically, the surface waters showed both the highest mean POC (0.59 – 0.90 mg l^{-1}) and chl *a* concentrations (3.61 – 13.34 µg l^{-1}) and showed daily trends suggesting the development of a phytoplankton bloom. While mean surface chl *a* concentrations increased with each sampling day, mean surface POC magnitudes peaked on M20-IC and then stabilized on M21-IC. The high surface chl *a* values on each day resulted in low mean surface POC:chl *a* magnitudes (< 200). The mid-depth waters showed relatively similar daily POC (0.37 – 0.42 mg l^{-1}) and chl *a* (0.76 - 1.55 µg l^{-1}) concentrations; however, at this depth, POC:chl *a* magnitudes decreased with the development of the bloom.

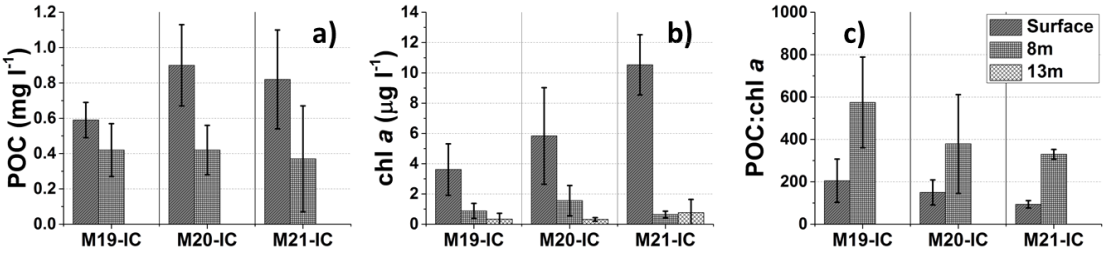

Figure 2.7 – Daily mean a) POC, b) chl *a* and c) POC:chl *a* values at discrete sampling depths (surface, 8.0 and 13.0 m (13.0 m only available for chl *a*) for M19-IC, M20-IC and M21-IC. Error bars represent one standard deviation from the mean.

During the May period, Fuco (diatom marker pigment) was the dominant pigment throughout the water column (Figure 2.8). Mean relative contributions of Fuco to the total pigment suite ranged from 51 – 73 % with the lowest contributions in the surface waters. Relative contributions of 19HF were low (0 – 4 %) on each day with the highest contributions measured at 13.0 m depth.

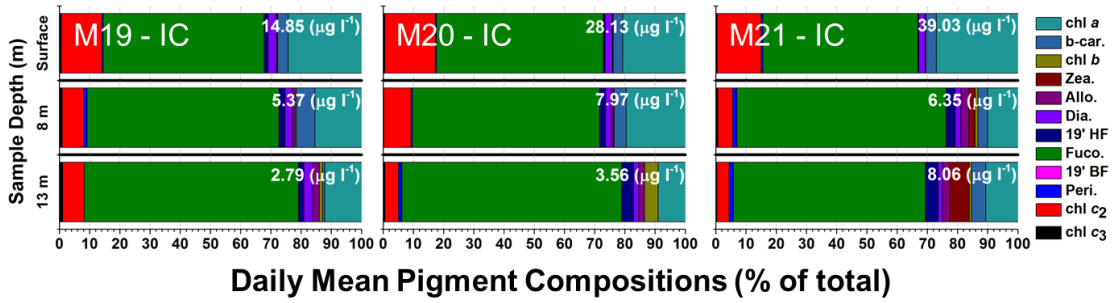

Figure 2.8 – Daily mean pigment compositions separated by discrete sampling depths (surface, 8.0 and 13.0 m) for each May sampling day. Total pigment concentrations are plotted in the upper right corner of each bar. Pigment compositions are a percent of each individual pigment concentration to the total.

May Optical Trends

Daily mean optical values for the May data collection period are shown in Table 2.5 and colour-map plots of daily chl *a*, b_p, b_{bp}, $\tilde{b}_{bp}$ and salinity with depth and time are shown in Figure 2.9. Daily mean b_p (0.57 – 0.79 m^{-1}) and b_{bp} (0.004 – 0.006 m^{-1}) values increased from M19 to M21 and followed similar vertical and temporal patterns as the chl *a* concentrations. On each day, the maxima of these variables were located within the surface mixed layer (SML) with decreased values below. Some spiking in the b_{bp} magnitudes was observed below the SML on each day. Despite the b_p, b_{bp} and chl *a* increases, daily mean $\tilde{b}_{bp}$ values (0.009 – 0.010) were stable throughout the sampling period and showed an inverse trend to that of chl *a* with low values (< 0.010) within the SML and increased values with depth.

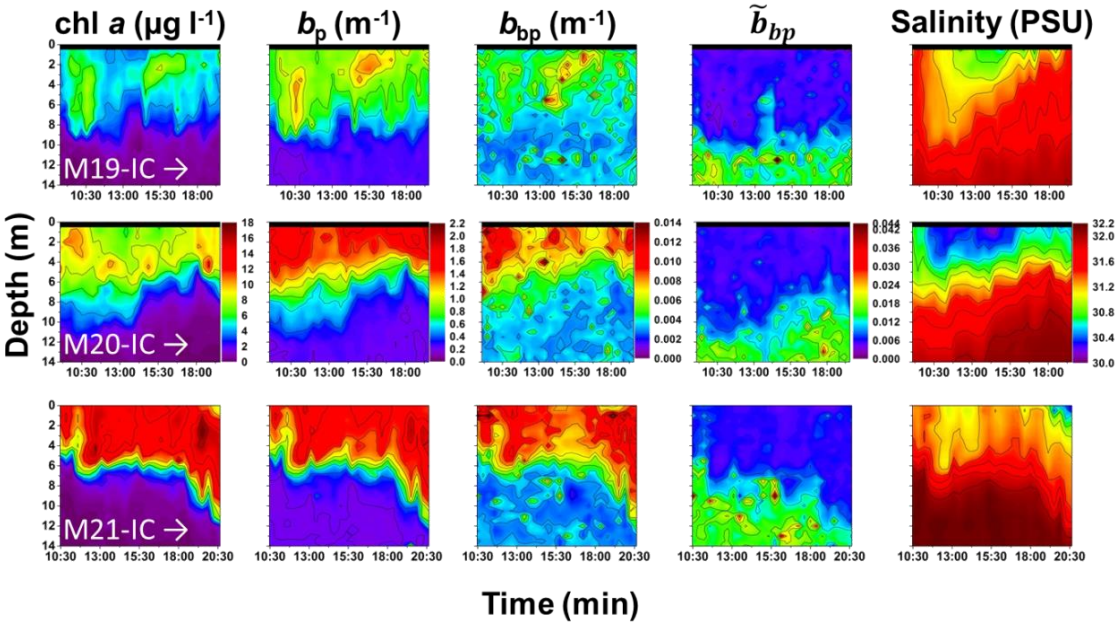

Figure 2.9 – May daily time-series of chl *a* (µg l^{-1}), b_p (m^{-1}), b_{bp} (m^{-1}), $\tilde{b}_{bp}$ and salinity (PSU). Time is plotted on the x-axis, depth is plotted on the primary y-axis and the colours represent the magnitudes of each variable. Red denotes high values and purple denotes low values.

May Bio-Optical Relationships

Coefficient of determination values for the daily relationships between the optical and biophysical parameters are shown in Table 2.7. Both of the daily b_p and b_{bp} – POC relationships strengthened with the development of bloom. In addition, b_p showed remarkably strong linear relationships with chl a on each day (r^2 = 0.95, 0.89 and 0.97, respectively), which can also be visualized in Figure 2.9. In comparison, the b_{bp} – chl *a* relationship (r^2 = 0.32) was weak and scattered on the M19-IC, but increased with the bloom conditions. Relatively strong negative power-law $\tilde{b}_{bp}$ – chl *a* and positive linear $\tilde{b}_{bp}$ – POC/chl *a* relationships were observed on each sampling day.

Table 2.7 – Coefficient of Determination (r^2) values for the daily May relationships between the optical and biophysical variables ($p < 0.05$). A power-law fit was applied to the $\tilde{b}_{bp}$ - chl *a* relationships

	M19-IC (r^2)	***n***	**M20-IC (r^2)**	***n***	**M21-IC (r^2)**	***n***
b_p **- POC**	**0.26**	*25*	**0.67**	*25*	**0.69**	*17*
b_p **- chl *a***	**0.95**	*1059*	**0.89**	*953*	**0.97**	*887*
b_p **- 19HF**	**0.74**	*15*	*ns*	*18*	*ns*	*16*
b_{bp} **- POC**	**0.24**	*25*	**0.38**	*25*	**0.57**	*17*
b_{bp} **- chl *a***	**0.32**	*1059*	**0.68**	*953*	**0.86**	*887*
b_{bp} **- 19HF**	**0.81**	*15*	ns	*18*	ns	*16*
$\tilde{b}_{bp}$ **- chl *a***	**0.79**	*1059*	**0.83**	*953*	**0.77**	*887*
$\tilde{b}_{bp}$ **- POC/chl *a***	**0.53**	*13*	**0.**74	*12*	**0.80**	*8*

2.4.5 August Daily Trends in Bio-Optical Properties

August Biophysical Trends

Figure 2.10 shows that temporally, mean POC and chl *a* increased from A16 to A18 and then declined each subsequent sampling day. Vertically, the mid-depth waters (8 m) showed the highest mean POC concentrations throughout the period; however, mean surface concentrations were often nearly as high (A16, A17, A23). In contrast, mean chl

a concentrations were occasionally the highest in the lower water column, notably on A20-BC and A21-BC. With exception to A18-IC, mean surface chl *a* concentrations were low (< 1.0 ug l^{-1}) and POC:chl *a* values were relatively high (> 600). On A18-IC, high POC (~ 1.0 mg l^{-1}) and chl *a* (> 6.0 µg l^{-1}) concentrations led to low POC:chl *a* (< 200) at each sampling depth.

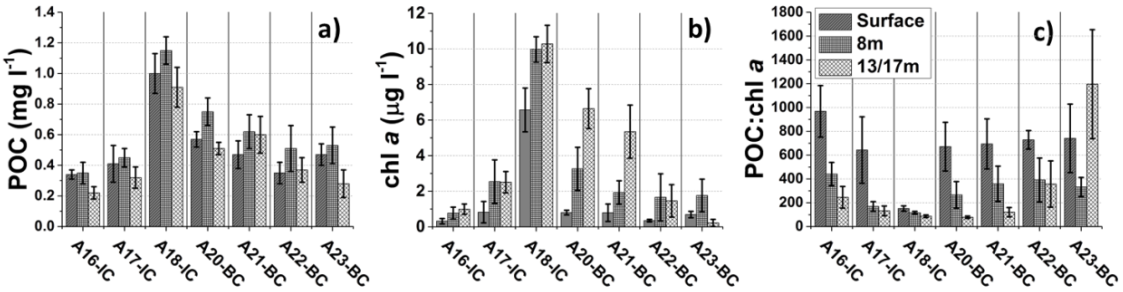

Figure 2.10 – Daily mean a) POC, b) chl *a* and c) POC:chl *a* values at discrete sampling depths (surface, 8.0, 13.0 (IC), and 17.0 m (BC)) for the August period. On the IC days the lower water column was sampled at 13 m and on the BC days at 17 m. Error bars represent one standard deviation from the mean.

During August, high relative contributions of 19HF were found in the surface waters, notably on A16-IC (15 %) and A17-IC (9 %), possibly indicating the presence of *E. huxleyi* cells (Figure 2.11). Furthermore, with exception to A18-IC, the range of surface contributions of fuco in August (15 – 32 %) was noticeably lower than those seen in May (surface, 51 – 55 %). August 18th showed high total pigment concentrations (21.54 – 35.45 µg l^{-1}), high contributions of Fuco (45 – 51 %), low contributions of 19HF (1 – 2 %) and similar pigment compositions throughout the water column, likely indicating the intrusion of a diatom bloom. After A18-IC, the contribution of Fuco in the surface waters declined (15 – 19 %) and the influence of 19HF increased (5 – 6 %). The pigment signatures in the lower water column on A20-BC, which were similar to those on A18, suggest the downward movement of diatoms on this day. At the same depth on

A21-BC, chl *b*, the marker pigment for green algae (Ras et al., 2008) had a large influence (25 %) on the total pigment suite. Towards the end of the sampling period (A22 and A23-BC), the relative contributions of Peridinin (15 – 38 %) and Zeaxanthin (2 – 10 %) increased. These pigments are diagnostic markers for dinoflagellates and cyanobacteria, respectively (Ras et al., 2008).

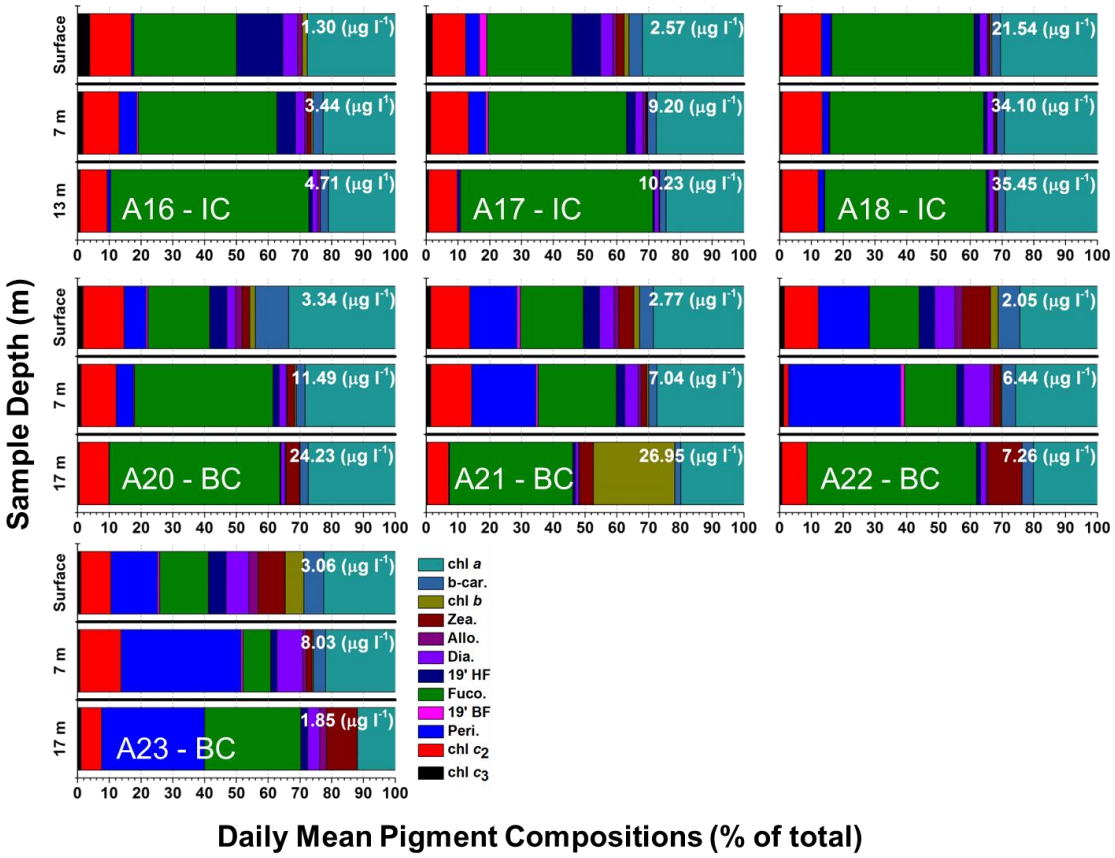

Figure 2.11 – Daily mean pigment compositions separated by discrete sampling depths (surface, 8.0, 13.0 (IC), 17.0 m (BC)) for each August sampling day. Total pigment concentrations are plotted in the upper right corner of each bar. Pigment compositions are a percent of each individual pigment concentration to these totals.

August Optical Trends

The August daily optical ranges and their means are shown in Table 2.5. Mean b_p followed a similar trend as POC and chl *a* with values peaking (1.88 m^{-1}) on A18-IC

and then decreasing every subsequent day. Mean b_{bp} also followed a similar trend; however, some of the highest values (0.047 m^{-1}) were measured from A20-BC to A22-BC. The particulate backscattering ratio showed the lowest mean (0.014) and range (0.010 – 0.018) in values on A18-IC. Yet, the mean value on this day was high in comparison to those seen during the May period (< 0.010) despite comparable chl *a* magnitudes.

Daily vertical-temporal distributions of chl *a*, b_p, b_{bp}, $\tilde{b}_{bp}$, and temperature are shown in Figure 2.12. Both A16-IC and A17-IC showed relatively high b_p (0.69 – 1.98 m^{-1}), b_{bp} (0.12 – 0.34 m^{-1}) and $\tilde{b}_{bp}$ (0.015 – 0.031) magnitudes within the surface mixed layer (SML) (< 2 m) of the highly stratified waters. While A16-IC showed low chl *a* (0.11 – 3.62 µg l^{-1}), A17-IC exhibited increasing chl *a* magnitudes below the thermocline, which were matched by increased b_p and b_{bp} magnitudes. On A18-IC, mixing resulted in a cooler (1.0 m, 14.2 – 15.3 °C) and deeper (~ 8.0 m) SML. Both chl *a* and b_p were high within the SML and followed a similar trend with depth and time until approximately 3:00pm. At this point a surface intrusion of warm water (15.3 °C) was observed which was matched by increases in b_p and b_{bp} magnitudes, but not chl a .

After A18-IC, thermal stratification intensified with the re-development of warm (15.29 – 16.42 °C) and relatively shallow SMLs. On A20 and A21, distinct regions of high b_p (0.015 – 0.043 m^{-1}) and $\tilde{b}_{bp}$ (0.018 – 0.043) were confined within these surface layers (< 2.0 m) where chl *a* magnitudes were generally low (0.14 – 3.31 µg l^{-1}). On these days, the chl *a* maximum was observed below or at the base of the SML. By A23, chl *a* concentrations were low throughout the water column (0.01 – 5.30 µg l^{-1}), but b_p, b_{bp}

and $\tilde{b}_{bp}$ remained elevated within the SML. Relatively high $\tilde{b}_{bp}$ magnitudes (0.008 – 0.078) were measured through the water column on this day.

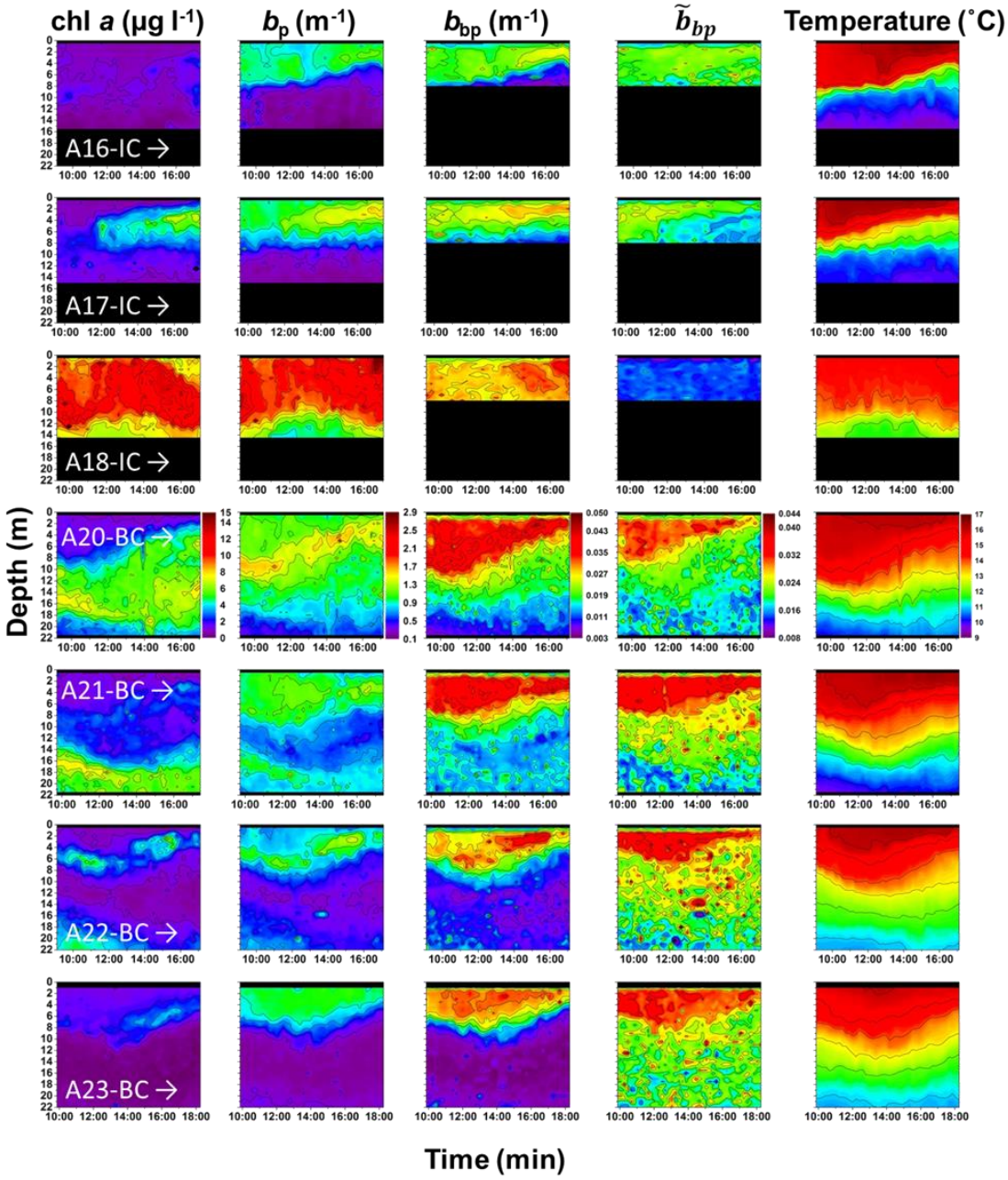

Figure 2.12 – August daily time-series of chl *a* (µg l^{-1}), b_p (m^{-1}), b_{bp} (m^{-1}), $\tilde{b}_{bp}$ and temperature (°C). Time is plotted on the x-axis, depth is plotted on the primary y-axis and the colours represent the magnitudes of each variable. Red denotes high values and purple denotes low values. Black areas on A16 – A18 indicate where no data was collected. The b_{bp} data on these days were cut to 8 m depth due to cage interference. Unlike November and May, Temperature was plotted to illustrate thermal stratification that occurred during this time frame.

August Bio-Optical Relationships

Daily bio-optical relationships for the August sampling period are shown in Table 2.8. Significant positive b_p – POC relationships (r^2 = 0.28 – 0.65) were measured on each August data collection day; however the variability in the daily strength of these relationships did not seem to follow a trend. In comparison, b_{bp} and POC were only correlated on days when the b_p – POC relationships were the strongest (A16, A20, A22, A23).

Unlike May, high b_p and b_{bp} magnitudes were measured in the upper water column where chl *a* concentrations were low (Figure 2.12), resulting in either negative linear relationships (b_{bp} – chl a, A17, A21 and A22) or no significant relationships. Yet, positive linear relationships were defined between b_p and chl *a* outside of the SML. For instance, a relatively strong correlation was found between the two variables within the chlorophyll maximum on A21-BC (14.0 – 22.0 m) (r^2 = 0.75).

On each day, higher statistical relationships were generally found between b_p, b_{bp} and 19 HF than with chl *a*; however, it should be noted that on A21-BC, no significant correlation was found between the optical parameters and 19HF. In general, the strongest b_p – 19HF relationships were found during the beginning of the sampling period (A16 and A17) while the strongest b_{bp} – 19HF relationship occurred on A20. The highest values within these relationships occurred within the surface waters.

While a weak negative trend was found between $\tilde{b}_{bp}$ and chl *a* for the August period, some individual days showed significant relationships between the parameters. In particular, A20-BC and A21-BC showed scattered, but significant negative linear $\tilde{b}_{bp}$ –

chl *a* relationships (r^2 = 0.54). In addition, these days showed significant positive $\tilde{b}_{bp}$ – POC:chl *a* relationships.

Table 2.8 – Coefficient of determination (r^2) values for the daily August relationships between the optical and biophysical variables ($p < 0.05$). A power-law fit was applied to the $\tilde{b}_{bp}$ - chl *a* relationship for each day. The sample size for each correlation is provided in brackets.

	A16-IC (r^2)	**A17-IC (r^2)**	**A18-IC (r^2)**	**A20-BC (r^2)**	**A21-BC (r^2)**	**A22-BC (r^2)**	**A23-SC (r^2)**
b_p - POC	**0.65** (n = 30)	**0.28** (n = 30)	**0.42** (n = 27)	**0.61** (n = 31)	**0.22** (n = 31)	**0.38** (n = 30)	**0.41** (n = 30)
b_p - chl *a*	*ns* (n = 1174)	**0.26** (n = 1403)	**0.29** (n = 1551)	*ns* (n = 2264)	*ns* (n = 2026)	**0.43** (n = 2067)	**0.57** (n = 1990)
b_p - 19HF	**0.63** (n = 26)	**0.74** (n = 29)	**0.42** (n = 30)	**0.57** (n = 31)	*ns* (n = 31)	**0.56** (n = 25)	**0.35** (n = 21)
b_{bp} - POC	**0.46** (n = 20)	*ns* (n = 20)	*ns* (n = 19)	**0.44** (n = 31)	*ns* (n = 31)	**0.21** (n = 30)	**0.43** (n = 30)
b_{bp} - chl *a*	*ns* (n = 645)	*ns* (n = 792)	*ns* (n = 913)	**(-) 0.31** (n = 2264)	**(-) 0.25** (n = 2026)	**0.18** (n = 2067)	**0.49** (n = 1990)
b_{bp} - 19HF	**0.28** (n = 13)	**0.23** (n = 19)	**0.16** (n = 21)	**0.71** (n = 31)	*ns* (n = 31)	**0.44** (n = 25)	**0.36** (n = 21)
$\tilde{b}_{bp}$ - chl *a*	*ns* (n = 645)	**(-) 0.45** (n = 792)	*ns* (n = 913)	**(-) 0.54** (n = 2264)	**(-) 0.54** (n = 2026)	*ns* (n = 2067)	**0.16** (n = 1990)
$\tilde{b}_{bp}$ - POC/chl *a*	*ns* (n = 17)	*ns* (n = 19)	**(-) 0.36** (n = 19)	**0.45** (n = 31)	**0.29** (n = 31)	*ns* (n = 26)	**(-) 0.25** (n = 27)

2.5. Discussion

The variability in the bio-optical relationships (Table 2.4) observed during this study are indicative of a diverse range of particulate assemblages, each with distinct influences on the optical properties. This variability limited the use of global relationships for particulate characterization and highlights the complexities of using optical parameters in dynamic coastal environments; however, short timescale temporal bio-optical analysis provided valuable insight into the biogeochemical make-up of the particle assemblages over each sampling period. During autumn (November), b_p and b_{bp} were conditioned by phytoplankton (surface), resuspended materials (lower water column) and possible aquaculture derived particles such as wasted fish feed and feces.

This period was the only time that increases in the optical and biophysical magnitudes could be associated with aquaculture derived particles, likely due to low ambient seston concentrations. In spring (May), a developing diatom bloom had a dominant effect on both of the scattering parameters. Aquaculture derived wastes, if existing at the sampling locations, were likely masked and (or) quickly diluted into the rich ambient particulate fields experienced during the bloom development conditions. Finally, in late summer (August), a hypothesized *E. huxleyi* bloom had strong influences, notably on b_{bp} variability. The co-presence of high concentrations of non-coccolithophore species during this period had notable effects on b_p, which was sensitive to both the refractive surface materials and the lower refractivity phytoplankton species. Again, bloom conditions likely masked a unique optical signal from aquaculture derived wastes during this period. Other authors employing different methods (i.e. water sampling) for defining aquaculture particulate concentrations have also had difficulties during periods of high ambient seston concentrations (Lander et al., 2013).

Specifically in November, the observed bio-optical magnitudes were a result of low organic particulate concentrations, typical of winter downwelling conditions in the study area (Riche et al., 2013). Chlorophyll *a* concentrations were notably lower than during the subsequent sampling periods. Runoff particulate material inputs were low as evidenced by the high water clarity (> 10.0 m) and the low b_{bp} magnitudes (0.001 – 0.009 m^{-1}), which were not suggestive of high inorganic loads (Snyder et al., 2008; Martinez-Vicente et al., 2010)

At this time of the year, the water was highly stratified and four distinct bio-optical layers were observed: (1) a surface layer (< 2.0 m) which was characterized by variable

but, low salinity, relatively high and variable b_p (0.07 – 1.26 m^{-1}) and b_{bp} (0.001 – 0.007 m^{-1}) magnitudes and the highest mean POC and chl *a* concentrations; (2) the mid-depth layer (2.0 – 9.5 m), which had the lowest b_p (0.05 – 0.18 m^{-1}), b_{bp} (0.001 – 0.004 m^{-1}) magnitudes and was associated with low POC and chl *a*; (3) the bottom of the cage layer (10.0 – 14.0 m), which showed the highest b_{bp} magnitudes (0.002 – 0.009 m^{-1}), some of the highest POC concentrations and low chl *a* and; (4) the beside-cage lower water column (10.0 – 20.0 m) where b_p (0.11 – 0.31 m^{-1}) and b_{bp} (0.002 – 0.006 m^{-1}) increased towards the seafloor, POC concentrations were near surface values and chl *a* concentrations were the lowest of the study.

Through the water column, $\tilde{b}_{bp}$ was influenced by both chl *a* and POC:chl *a*, thus suggesting sensitivity to both phytoplankton concentrations and the relative contribution of detritus to the total organic particle pool (Loisel et al., 2007). While strong, the slope of the $\tilde{b}_{bp}$ - chl *a* relationship was steep, which was a result of low $\tilde{b}_{bp}$ magnitudes at relatively low chl *a* concentrations within the surface waters. Considering the conditions, low phytoplankton biomass likely dominated the particulate assemblages in the surface waters. In turn, the $\tilde{b}_{bp}$ – POC:chl *a* relationship showed comparable coefficients to those found by Loisel et al. (2007) (Table 2.4). Refractive index increases from mineral/detrital aggregation and (or) the transition to small particle sizes with increasing detrital concentrations may have played a role in the higher $\tilde{b}_{bp}$ during this study (Loisel et al., 2007). These processes may have been at play, notably in the lower water column (beside the cage) where a mix of seafloor sediments and settled aquaculture wastes would have interacted and possibly been resuspended together. While the size and refractivity of the farm derived particles at the

study site are largely unknown, they appear to have had compositions favoring high $\tilde{b}_{bp}$ signatures.

At the surface/mid-depths, the b_p – chl *a* relationship (r^2 = 0.82) suggests the conditioning of b_p by phytoplankton concentrations. Particulate scattering is most sensitive to organic particles with low apparent densities, such as phytoplankton (Babin et al., 2003; Martinez-Vicente et al., 2010; Neukermans et al., 2012) and similarly strong relationships have been reported for open ocean waters where phytoplankton plays a dominant role in optical variability (Behrenfeld & Boss, 2006; Huot et al., 2008). Yet, the slope of our relationship was an order of magnitude steeper than those found in oceanic waters and also May/August of this study suggesting an increased number of cells in the surface waters at comparable chl *a* concentrations (i.e. higher b_p per unit chl *a*). Alternatively, due to the nature of the surface layer (runoff – derived, aquaculture setting), it is possible that other particle types (minerogenic) co-varied with phytoplankton concentrations and enhanced the b_p magnitudes. Evidence of the former is that directly at the surface (0.5 m), $\tilde{b}_{bp}$ magnitudes (0.002 – 0.010) were indicative of phytoplankton dominated waters (Sullivan et al., 2005). While the surface POC:chl *a* magnitudes (692 $\pm$ 193) were higher than those usually found for phytoplankton dominated particle assemblages (>200), they were generally an order of magnitude lower than those found deeper in the water column (> 6000). Phytoplankton responses to the ambient growth conditions (i.e. larger cells, intracellular pigment changes) may have been responsible for the relatively higher b_p (Behrenfeld & Boss, 2006) and POC:chl *a* magnitudes. Yet, it must be considered that throughout the rest of the surface layer (1.0 – 1.5 m), $\tilde{b}_{bp}$ magnitudes were considerably more variable (0.003 – 0.030)

suggesting the presence of non – algal particles. As such, aquaculture and (or) runoff derived wastes may have had a greater influence within the surface layer than suggested by the b_p - chl *a* relationship, which was based on samples collected directly at the surface.

The higher scatter in the b_{bp} – chl *a* relationship (r^2 = 0.69) at the surface/mid-depths indicates greater sensitivity to non-algal particles and (or) changes in phytoplankton morphology when compared to b_p (Martinez-Vicente et al., 2010; Antoine et al., 2011). Of particular note, after the fish were fed on both N14-IC and N15-BC, b_{bp} magnitudes at 1.5 m depth increased from 0.002 to 0.004 m^{-1}, which corresponded with the highest $\tilde{b}_{bp}$ magnitudes of the surface layer. This increase may have been a result of wasted feed, post feeding feed "fines" and (or) fish waste. Other authors sampling in close proximity to salmon cages have found increased particulate organic matter concentrations during and after feeding cycles (Taylor et al., 1992; Lander et al., 2013).

The scattered surface/mid-depth b_p and b_{bp} relationships with POC (r^2 = 0.43 and 0.18, respectively) suggest high variability in organic particle compositions (Woźniak et al., 2010). The disparity between the strength of the bio-optical relationships with chl *a* (strong) and those with POC (weak) indicates that at these sample depths, the optical parameters were most sensitive to phytoplankton carbon. We hypothesize that scatter in the bio-optical POC relationships were introduced by the high spatial variability of POC in a finfish aquaculture setting. Specifically, the POC samples (collected near the side of the net pen) may have been exposed to aquaculture derived particles that were not seen by the optical profiler located near the center of the net pen. Nevertheless, the

slope of the surface/mid-depth b_p – POC relationship was comparable to those found in other coastal waters (Gardner et al., 2001; Krasakopoulou & Karageorgis, 2005).

At the bottom of the cage, the timing of the distinct high b_{bp} signal (after feeding to mid – day maximum) suggests the detection of the release of wastes by the fish. Under conditions of low inorganic concentrations, b_{bp} variability by detrital particles has been proposed by other authors (Martinez-Vicente et al., 2010). No studies have been performed on b_{bp} responses to fish wastes; however, it is plausible that the contribution of these wastes to b_{bp} magnitudes could be significant. These increases were matched by the highest $\tilde{b}_{bp}$ magnitudes of the November period (0.050 ± 0.007) suggesting an increase in small and (or) highly refractive particles (Stramski et al., 2008). Appropriately, mean POC concentrations increased from the mid-depth waters towards the bottom of the cage (13.0 m) and the mean POC:chl *a* magnitude (6978 ± 2362) at this depth was indicative of a particle assemblage heavily dominated by detrital materials (Cifuentes et al., 1988). Furthermore, lower cage/water column b_p and b_{bp} were conditioned by POC ($r^2 = 0.42$ and 0.35, respectively) suggesting sensitivity to the aquaculture derived wastes at this depth.

Outside of the cage, the lower water column increases in b_p and b_{bp} may have been due to a combination of resuspended seafloor sediments (Gardner et al., 2001) and aquaculture wastes. Similar to the within the cage, increased POC and POC:chl *a* with depth indicate the dominance of detrital particles. The below cage optical increases observed towards the end of the day on N15 may have been a result of increased resuspension at this time of the day or aquaculture derived wastes sinking out of the bottom of the cage. The horizontal transport of aquaculture wastes out of the bottom of

fish cages has been documented by other authors (Sutherland et al., 2001; Kutti et al., 2007a). These below cage increases were not matched by enhanced $\tilde{b}_{bp}$ magnitudes suggesting relatively stable bulk particulate compositions through the lower water column. The outer cage wastes may have had differing properties to those inside the cage (i.e. lower refractivity, different sizes) due factors such as longer immersion times (water penetration), physical and biological breakdown and (or) aggregation possibly resulting in their comparatively lower $\tilde{b}_{bp}$ magnitudes.

In May, a developing diatom bloom characterized the ambient biogeochemical concentrations resulting in higher b_p (0.02 – 2.20 m^{-1}) and to a lesser extent b_{bp} (0.002 – 0.011 m^{-1}) magnitudes and also, lower $\tilde{b}_{bp}$ (0.002 – 0.038) when compared to November. Cell concentrations increased nearly 13 fold from May 15th ($0.53 * 10^{-6}$ cells l^{-1}) to May 22nd (6.28 – 7.76 $*$ cells l^{-1}) (Guindon, 2012) and the pigment suite was dominated by Fuco (51 – 73 %), the marker pigment for diatoms (Ras et al., 2008). This bloom was likely the first of the season and was made up of species from the genera *Chaetoceros* and *Skeletonema* (Guindon, 2012), which are commonly advected into the inlets along the west coast of Vancouver Island during the spring and summer seasons (Taylor & Haigh, 1996). While the waters in May were weakly stratified, a surface mixed layer was present throughout the period and the chl *a* maximum was consistently confined within this layer.

During this period, a relatively strong relationship was found between $\tilde{b}_{bp}$ and chl *a* (r^2 = 0.74), which had a comparable slope coefficient to others found in coastal waters (Twardowski et al., 2001; Sullivan et al., 2005; Loisel et al., 2007) (Table 2.4). Similar

to these authors, scatter was observed at low chl *a* magnitudes likely due to the increased influence of detrital and mineral particles at low phytoplankton concentrations (Twardowski et al., 2001). On each day, low $\tilde{b}_{bp}$ magnitudes within the SML (< 5.0 m, 0.006 $\pm$ 0.001) indicated that despite variable, but relatively high chl *a* concentrations (1.15 – 18.43 µg l^{-1}), phytoplankton dominated the particle assemblage at these depths. This is corroborated by the low POC:chl *a* magnitudes in the surface waters (162 $\pm$ 87), most of which fell below those expected for phytoplankton bloom conditions. Below the SML (> 10.0 m), where chl *a* magnitudes were the lowest (0.53 $\pm$ 0.81 µg l^{-1}), $\tilde{b}_{bp}$ magnitudes increased (0.015 $\pm$ 0.004) and were indicative of a mixed assemblage of algal and non-algal materials (Sullivan et al., 2005), possibly indicating the presence of aquaculture wastes. Samples were not available for POC:chl *a* determination at the bottom of the cage during this period; however, the range of magnitudes in the mid-depth waters, which sometimes fell outside of the SML, were highly variable (153 – 886) suggesting a move to mixed assemblages in the deeper waters. When compared to November, the $\tilde{b}_{bp}$ – POC:chl *a* relationship showed a shallower slope which was likely a result of the bloom conditions and the high influence of phytoplankton on the optical parameters. Nonetheless, the daily $\tilde{b}_{bp}$ – POC:chl *a* relationships were strong which further suggests that detrital materials played a role in $\tilde{b}_{bp}$ variability below the SML.

The strong global May (r^2 = 0.89) and daily b_p – chl *a* relationships suggest that b_p was highly conditioned by phytoplankton biomass throughout the development of the bloom. The slope of this relationship was comparable to those found in other coastal studies (Gardner et al., 2001; Sullivan et al., 2005) (Table 2.4). Sullivan et al. (2005),

who used the same chlorophyll *a* estimation method as in this study, found high variability in b_p below chl *a* concentrations of 5 mg m^{-3}, which the authors attributed to the influence of non – photosynthetic particles. As such, our high statistical relationship indicates that throughout the water column, and over a large range of chl *a* magnitudes (0.01 – 18.43 µg l^{-1}) the influence on b_p from non-autotrophic particles was minimal. In addition, photoacclimation does not appear to have occurred, likely due to the mixing experienced during this period (Behrenfeld & Boss, 2006).

In contrast, the strength of the b_{bp} – chl a relationship increased with the development of the bloom suggesting that at the beginning of the sampling period (M19), b_{bp} was conditioned by non-algal particulates and (or) differing phytoplankton species. As the bloom developed, phytoplankton concentrations within the SML likely masked the influence of other particle types possibly by the incorporation of small and (or) inorganic particles into large organic aggregates (Flory et al., 2004). The strongest b_{bp} – chl *a* relationship of the entire study ($r^2 = 0.86$) was observed at the height of the bloom (M20) suggesting relatively monospecific bloom conditions (Whitmire et al., 2010). Nonetheless, below 10.0 m depth, b_{bp} was not always related to chl *a*, possibly due to the influence of fish wastes. Unlike November, these increases were not confined to the bottom of the cage and were relatively random with depth and time.

The bio-optical relationships with POC were weaker than those with chl *a* and similar to the b_{bp} – chl *a* relationship, showed increasing strength with the development of the bloom. This trend indicates the increased influence of phytoplankton derived carbon on the total carbon pool as the bloom developed. Similar to November, scatter in the bio-optical – POC relationships may have been introduced by the contact of the sampling

bottle with the side of the fish cage. When compared to November, the May b_p – POC relationship was considerably shallower, likely due to the bloom conditions, and was comparable to one found in August and to those found by other authors in a variety of coastal and oceanic waters (Gundersen et al., 1998; Gardner et al., 2006; Stramski et al., 2008). In contrast, the May b_{bp} – POC relationship had a considerably shallower slope than in both November and August, likely due to the lower sensitivity of b_{bp} to the large diatoms.

In August, we hypothesize that the observed trends were due to the development of a coccolithophore bloom. Specifically, the coccolithophorid species, *Emiliania huxleyi*, are known to commonly form isolated inshore blooms in this region (Taylor & Haigh, 1996). With exception to A18-IC, the thermally stratified surface waters, which exhibited low chl *a* concentrations (1.5 m, 1.24 $\pm$ 0.61 µg l^{-1}) and high b_{bp} and $\tilde{b}_{bp}$ magnitudes (1.5 m, 0.015 – 0.043 m^{-1} and 0.018 – 0.043, respectively), were indicative of *E. huxleyi* bloom conditions (Balch et al., 1991; Tyrrell & Merico, 2004; Garcia et al., 2011). Similar b_{bp} and $\tilde{b}_{bp}$ have been reported in other regions where *E. huxleyi* blooms were occurring (Garcia et al., 2011). This species produce highly refractive calcite shells (coccoliths), which they shed into the water column during the late stages of a bloom. These coccoliths are efficient backscatters of light and are the reason why *E. huxleyi* blooms appear as highly reflective patches on satellite imagery (Balch et al., 1991). Further evidence of this type of bloom is that 19HF, the marker pigment for prymnesiophytes to which *E. huxleyi* belongs (Jeffrey & Vesk, 1997; Ras et al., 2008), showed high relative contributions within the surface waters (5 – 15 %) over this period. These contributions were considerably higher than those observed in the surface

waters in May (0 – 1 %) when diatoms dominated the phytoplankton assemblage. While 19HF is not unique to coccolithophores, it has been shown to correlate with *E. huxleyi* cell and coccolith concentrations in other coastal waters (Ediger et al., 2006; Siegel et al., 2007). Notably, our mean surface concentrations of Fuco and 19HF on A16-IC (0.43 and 0.19 µg l^{-1}, respectively) were comparable to those found by Siegel et al. (2007) within a coastal *E. huxleyi* bloom off of Namibia (0.53 and 0.15 µg l^{-1}, respectively).

Temporally, the moderately high b_p (0.70 – 1.98 m^{-1}), b_{bp} (0.01 – 0.034 m^{-1}) and $\tilde{b}_{bp}$ (0.015 – 0.031) magnitudes within the SML at the beginning of the sampling period (A16 and A17) suggest the presence of *E. huxleyi,* but at lower detached coccolith concentrations when compared to the days after A18. On A16 and A17, the high relative surface contributions of the 19HF pigment may be indicative of intact cells that had not begun releasing their coccoliths into the water column. While both scattering parameters were conditioned by 19HF on these days, the stronger b_p – 19HF relationships may have been due to the sensitivity of b_p to these intact cells. Even at low concentrations/biomass, *E. huxleyi* cells and coccoliths cause marked differences in the scattering properties of the water (Balch et al., 1991), which could explain why the surface b_{bp} magnitudes on A16 and A17 were still considerably higher than those seen in November and May.

On A18-IC, the differing hydrographic conditions (mixing), high chl *a* concentrations (6.78 – 18.52 µg l^{-1}) and disparate pigment compositions (reduced surface 19HF – 1 %, increased Fuco – 45%), suggest the intrusion of an offshore diatom bloom into the study area. During late summer, *Chaetoceros* blooms are commonly advected into the

region via wind forcing (Taylor & Haigh, 1996). The lowest $\tilde{b}_{bp}$ magnitudes of the period were found on this day (0.014 ± 0.001); however, these magnitudes were higher than those found under similar chl *a* conditions in May (< 0.010) suggesting the continued presence of *E. Huxleyi*.

After A18, the greatly enhanced SML b_{bp} and $\tilde{b}_{bp}$ magnitudes suggest the detachment of coccoliths into the water column. Both of these parameters showed their strongest positive relationships with 19HF on A20 ($r^2 = 0.71$ and 0.51, respectively), likely due to the influence of the detached coccoliths on this day. However, these relationships were not found on A21 (day with the highest b_{bp} magnitudes), which was a result of increasing 19HF concentrations with depth. This trend was unique to A21 and may have been due to the presence of complex phytoplankton assemblages located beneath the SML. Nonetheless, high relative 19HF concentrations were found within the SML on A21 and the mean b_p, b_{bp} and $\tilde{b}_{bp}$ magnitudes at 1.5 m depth on this day (1.00 m^{-1}, 0.034 m^{-1} and 0.035, respectively) were comparable to those found by Garcia et al. (2011) near the center of an intense *E. huxleyi* bloom over the Patagonian Shelf (~ 1.00 m^{-1}, > 0.035 m^{-1} and 0.03, respectively). Furthermore, using the method derived by Twardowski et al. (2001), the modelled mean bulk refractive index value at this depth (1.24 ± 0.01) was the same as the value found for calcite (Lide, 2004). On both A20 and A21, the chlorophyll maximum and likely the bulk of the non – coccolithophore biomass were found in the lower water column. This is evidenced by the relatively strong linear b_p – chl *a* relationships that were observed below the SML on these days. For instance, within the chlorophyll maximum on A21-BC (14.0 – 22.0 m), b_p was highly influenced by chl *a* ($r^2 = 0.75$) and exhibited a shallower slope (0.08) than those

observed during the May period. At these depths, $\tilde{b}_{bp}$ magnitudes generally decreased suggesting an increased influence by less refractive non-coccolithphorid species.

The decrease in SML b_{bp} magnitudes towards the end of the sampling period (A22, A23) suggests reduced coccolith concentrations; however, $\tilde{b}_{bp}$ magnitudes remained high indicating that coccoliths continued to dominate the optical signal in the surface waters. The increase of $\tilde{b}_{bp}$ with depth on these days may have represented the sinking of the coccoliths out of the SML.

In August, $\tilde{b}_{bp}$ had a weak dependence on chl *a* (r^2 = 0.15) and showed a similar slope coefficient to Sun et al. (2009), who sampled in waters where the scattering properties were dominated by inorganic materials. While these authors found decreased $\tilde{b}_{bp}$ magnitudes with increasing inorganic suspended materials (ISM), we postulate that in our study, $\tilde{b}_{bp}$ increased with detached calcite coccolith concentrations. Additionally, the weak August $\tilde{b}_{bp}$ – POC:chl *a* relationship (r^2 = 0.21) had a shallow slope when compared to the other sampling periods due to relatively high $\tilde{b}_{bp}$ at low POC:chl *a* magnitudes. The scattered daily $\tilde{b}_{bp}$ – POC:chl *a* relationships found through August suggests that detrital materials had less of an influence on $\tilde{b}_{bp}$ variability when compared to the other sampling periods, which was likely a result of the presence of coccoliths.

The global August b_p – chl *a* and b_p - POC relationships (r^2 = 0.64 and 0.77, respectively) were relatively strong considering the influence of the refractive surface materials on the scattering parameters. Our b_p – chl a relationship was remarkably

similar to the one found by Sullivan et al. (2005) who sampled through a wide variety of environments (inorganic dominated coastal waters to organic dominated bloom conditions) and our b_p – POC relationship was comparable to the one found during the diatom bloom in May of this study. In contrast, Garcia et al. (2011) did not find a relationship between b_p and these biogeochemical parameters when sampling through a coccolithophore bloom on the Patagonian Shelf. Rather, they found correlations with particulate inorganic carbon (PIC), which was a result of high concentrations of the detached calcite coccoliths. Yet, these authors observed a relatively small dynamic range in chl *a* (0.29 – 1.48 µg l^{-1}) (POC range not provided) concentrations due to the oceanic nature of their study area. We suggest that the strength of our global August relationships were a result of our comparatively large range in chl *a* (0.01 – 17.56 µg l^{-1}) and POC (0.17 – 1.32 mg l^{-1}) concentrations and the sensitivity of b_p to the presence of high concentrations (bloom magnitudes) of non - coccolithophore phytoplankton species which likely existed during this period. In comparison, b_{bp} was highly influenced by the refractive surface materials and showed scattered or no correlation with chl *a* or POC on a global or daily basis. Unfortunately, PIC measurements were lacking; however, if coccoliths were in fact present, inorganic carbon would likely have influenced b_{bp} variability during this period (Garcia et al., 2011).

2.6. Conclusion

Our results suggest large temporal and vertical variability in particulate concentrations and compositions at the Kyuquot SEAfoods IMTA site, which is located within a coastal fjord environment. These included winter conditions where organic concentrations and optical magnitudes were low, but highly variable with depth,

possibly due to the presence of aquaculture derived wastes; spring diatom bloom conditions where organic concentrations and b_p magnitudes increased considerably and were confined within the SML and; late summer conditions where a hypothesized *E. huxleyi* bloom resulted in increases in b_{bp} magnitudes within the surface layer of the thermally stratified water column. During this period, the coexistence of the highly refractive materials (possibly coccoliths) and bloom conditions of non-coccolithophorid species led to interesting trends in the optical data. In particular, b_p showed sensitivity to both the surface materials and the lower refractivity organic materials lower in the water column.

While it is difficult to derive direct conclusions due to the dynamic biogeochemical conditions, our results suggest that b_p variability was dominantly driven by changes in phytoplankton concentrations. Even during a possible *E. huxleyi* bloom, the global August b_p relationships with chl *a* and POC were comparable to those seen during the diatom bloom in May. As such, this parameter could be a valid tool for describing spatial and temporal variations in phytoplankton biomass at the study site, especially during bloom conditions. Yet, care must be taken when using b_p for this purpose as this parameter showed variable biogeochemical relationships on seasonal (November) and daily scales (August) and with depth (lower water column, November) suggesting additional influences by non-algal particle types (coccoliths, detritus).

While b_{bp} appears to have been related to phytoplankton concentrations under low ambient particle regimes (November) and intense spring diatom bloom conditions (May), our results suggest that when present, detrital and inorganic materials had strong influences on b_{bp} variability. For instance, the b_{bp} – biogeochemical relationships during

August were weak or not significant on global or daily scales, likely as a result of highly refractive coccoliths. Additionally, b_{bp} showed promise as a proxy for aquaculture derived waste concentrations when ambient particle concentrations were low, such as the conditions experienced in November. In this case, b_{bp} increases could have been associated with the composition (refractivity) and (or) particulate size distribution (PSD) changes of the fish waste and more research is needed to elucidate on this finding.

When used in conjunction, b_p and b_{pp} provided insight into the bulk compositions of the particulate assemblages through the water column (vertically) over short temporal timescales. Notably, the use of $\tilde{b}_{bp}$ aided in the determination of the phytoplankton dominated waters during the November and May sampling periods and suggested an *E. huxleyi* bloom in August. Furthermore, $\tilde{b}_{bp}$ increased with presumed aquaculture derived wastes during the November period, which is an important finding as it suggests that $\tilde{b}_{bp}$ could be used as a tracer for these wastes. As such, we recommend the collection of both b_p and b_{bp} for future coastal aquaculture studies as the determination of bulk particulate compositions would be important for management (i.e. food availability for bivalves) and environmental monitoring (i.e. bloom conditions, waste dispersal, resuspension). These future efforts should include measurements of inorganic materials and *in-situ* PSDs, so that greater knowledge can be gained on the sources of b_{bp} and $\tilde{b}_{bp}$ variability.

Chapter 3 – Spatial and Temporal Particulate Dynamics and their Influence on Uptake Species Placement at an IMTA Site on the Northwest Coast of Vancouver Island, British Columbia

3.1. Abstract

Spatial and temporal organic particulate dynamics were investigated over three seasons (autumn, spring, and summer) at a reference site and sites within and directly adjacent to a Sablefish (*Anoplopoma fimbria*) cage at an integrated multi-trophic aquaculture (IMTA) site on the west coast of Vancouver Island, Canada. High resolution (vertical and temporal) bio-optical measurements of the particulate backscattering coefficient (b_{bp}) and the particulate backscattering ratio ($\tilde{b}_{bp}$) were collected in conjunction with discrete sampling of particulate organic carbon (POC) and chlorophyll *a* (chl *a*) for the characterization of organic particulate concentrations and compositions. During autumn/winter conditions, when ambient reference seston concentrations were low, distinct bio-optical and POC enhancements were measured with time after feeding at the bottom of the studied cage, likely due to the presence of fish wastes. In contrast, reference and cage influenced bio-optical and biophysical variability during spring/summer was driven by phytoplankton concentrations and compositions. During these periods, aquaculture derived wastes were likely quickly diluted into the particle rich environments. These results suggest that organic particulate wastes would be most available to uptake species (i.e. scallops) during periods of low ambient seston concentrations. Under these conditions, our results suggest the dominant vertical movement of particulate wastes outwards from the bottom of the studied cage. Therefore, the future placement of uptake species below this cage may be the most effective location for waste interception. With further research, bio-optical measurements could provide an efficient means of collecting high temporal and spatial resolution data on particulate dynamics within IMTA settings. These data could be used to develop highly optimized IMTA systems for waste removal by uptake species.

3.2. Introduction

Worldwide, the aquaculture industry has rapidly expanded to offset global fishery declines and to meet growing demand (FAO, 2014). This growth has been mirrored in Canada, where production has shown a four-fold increase from 1990 to 2010 (DFO, 2013). Atlantic salmon (*Salmo salar*) is the country's top aquaculture export (68 % of total production), with Canada being the 4th largest producer of this species in the world (8 % of world production) (DFO, 2012). The rapid expansion of the finfish aquaculture industry, both worldwide and in Canada, has led to concern over its environmental sustainability as it can add considerable particulate organic wastes, which are dominantly made up of wasted feed and feces, to the environments surrounding the farms (Brooks & Mahnken, 2003; Carroll et al., 2003; Kutti et al., 2007a). Integrated multi-trophic aquaculture (IMTA) systems work to capture some of these wastes through the use of strategically placed uptake species, which are also commercially valuable (Troell et al., 2003; Neori et al., 2004; Barrington et al., 2009). Commercial scale IMTA systems have already been established on the Atlantic coast of Canada where blue mussels (*Mytulis edulis*) and kelp (*Saccharina latissima* and *Alaria esculenta*) are cultured adjacent to pre-existing Atlantic salmon cages (Hannah et al., 2013). On the Pacific coast, more intensive methods are being tested using a variety species grown in a specialized system adjacent to (Pacific scallops – *Patinopectin yessoensis*) and underneath (sea cucumbers – *Parastichopus californianus*) sablefish (*Anoplopoma fimbria*) cages (SEAVison Group, 2011; Reid, 2011; Hannah et al., 2013).

While it is has been shown that bivalves are capable of consuming aquaculture wastes (Soto & Mena, 1999; Lefebvre et al., 2000; Mazzola & Sarà, 2001; Gao et al., 2006; Reid et al., 2010; Redmond et al., 2010; MacDonald et al., 2011; Handå et al., 2012b), their effectiveness at capturing these wastes within IMTA systems is highly debated. Some studies have found growth enhancements (Jones & Iwama, 1991; Peharda et al., 2007; Sarà et al., 2009; Lander et al., 2012; Handå et al., 2012a; Jiang et al., 2013), while others have found minimal or no increased growth (Taylor et al., 1992; Stirling, 1995; Parsons et al., 2002; Cheshuk et al., 2003; Navarrete-Mier et al., 2010; Irisarri et al., 2013a) in bivalves reared in close proximity to fish cages. Conflicting results have also been found when quantifying particulate dispersion out of fish cages with some authors observing particulate organic matter increases that were 2 – 4 times greater than ambient levels (Taylor et al., 1992; MacDonald et al., 2011; Lander et al., 2013) and others finding no increased concentrations (Cheshuk et al., 2003; Irisarri et al., 2013a). These differences indicate high variability in the production and dispersion of particles at IMTA systems, as well as their quick dilution into ambient particulate assemblages, all of which influence their availability to uptake species (Troell & Norberg, 1998; Cheshuk et al., 2003; Lander et al., 2013; Brager, 2013). Thus, at each IMTA site, it is imperative that in-depth knowledge of the timing and dispersal of these wastes, as well as ambient particulate dynamics, is gained so that uptake species can be effectively placed for maximum waste uptake (Reid et al., 2009; Irisarri et al., 2013a). Unfortunately, this knowledge is site specific, dependent on a host of environmental factors, and is hard to measure in real world settings (Reid et al., 2009) as evidenced by the mixed results shown in the literature cited above.

As such, the objectives of this study were to determine spatial differences (reference vs. cage influenced) and to detail vertical and temporal particulate characteristics within and beside a sablefish cage at an active IMTA site in Kyuquot Sound, British Columbia, in order to aid in the placement of uptake species for maximum waste removal. To address these objectives, this research applied a combination of discrete water sampling (POC and chl *a*) and *in-situ* optical measurements of particulate backscattering (b_{bp}) and the backscattering ratio ($\tilde{b}_{bp}$) for particulate quantification and characterization at the studied IMTA site. In previous studies, the characterization of particulates in aquaculture settings has generally been done through the use of discrete water sampling followed by laboratory analysis (Taylor et al., 1992; Sutherland et al., 2001; Cheshuk et al., 2003; Macdonald et al., 2011; Lander et al., 2013). Relatively few studies have utilized optical variables as proxies for the direct in-situ quantification of aquaculture particulates (Grizzle et al., 2006; Ibarra et al., 2012; Brager, 2013). However, these methods are commonly used for particulate characterization in coastal waters as they allow for the collection of high spatial and temporal resolution data (Boss et al., 2004; Sullivan et al., 2005; Chang et al., 2006; Woźniak et al., 2010). In particular, the backscattering (b_{bp}) coefficient and the backscattering ratio ($\tilde{b}_{bp}$) are routinely used as proxies for particulate concentrations and compositions (mineral/inorganic), respectively (Boss et al., 2004; Loisel et al., 2007; Neukermans et al., 2012), and have shown promise for detecting aquaculture derived particulate wastes and characterizing ambient particulate dynamics within an IMTA setting (chapter 2 of this thesis).

3.3. Methods

3.3.1 Study Site

The Kyuquot SEAfoods IMTA site is located in Kyuquot Sound, British Columbia on the northwest coast of Vancouver Island (50° 02' 45.85" N and 127° 17’ 53.66" W). Data collections were entirely focused on cage 1 (Southwestern most cage – Figure 3.1 a) of the system as this cage was populated with approximately 10 000 adult Sablefish (*Anoplopoma fimbria*) throughout the duration of the study (Table 3.1).

Table 3.1 – Approximate fish population, average weights and daily feed for cage 1 over the sampling periods. For consistency, fish were fed 75 kg on sampling days, but following a different feeding regime before and after sampling periods.

Sampling Month	Cage 1 Fish Population	Fish Weight (kg)	Feed/Day (kg)
November	10 000	1.15	75
May	9 950	1.25	75
August	9 939	1.35	75

This cage is 15 x 15 x 15 m (L × W × D) and is located in waters that were approximately 25 m deep. On the morning of each data collection day, the fish within cage 1 were consistently hand fed 75 kg of Black Cod (Sablefish) feed, produced by Taplow Feeds in Vancouver, BC. The composition of this feed is presented in Table 3.2. Each feeding cycle took approximately 10 – 20 minutes to complete. The scallop culture component of the system was located adjacent to cage 1 and held 50 000 scallops (*Patinopectin yessoensis*) contained in lantern nets which extended from 5 to 15 m depth and were spaced 1 m apart. During the summer season, macrophytes (*Saccharina lattisma*) were extended on 50 m lines outwards from the scallop component.

Table 3.2 – Black cod (Sablefish) feed composition directly taken from a 25 kg feed bag during the November, 2011 sampling period. Feed produced by Taplow Feeds in Vancouver, British Columbia, Canada. Feed ingredients were not provided on the feed-bag.

Composition	Concentration
Crude Protein (minimum)	44%
Crude Fat (minimum)	15%
Crude Fibre (maximum)	2%
Vitamin A (minimum)	6000 IU/kg
Vitamin D (minimum)	3000 IU/kg
Vitamin E (minimum)	135 IU/kg
Calcium (actual)	1%
Sodium (actual)	1%
Phosphorus (actual)	1.1%

The study site is situated within a dynamic coastal area. During flood tide, water flows into the study site embayment through the western channel (Figure 3.1 b) with an opposite trend occurring during ebb tides where water flows in from Kyuquot Sound (Figure 3.1 c). Unique bathymetry at the IMTA site results in the development of a gyre, which slows currents and generally causes unidirectional westerly flow through the various components of the system (Figure 3.1 a and b) (Personal Communication, Cross, 2011).

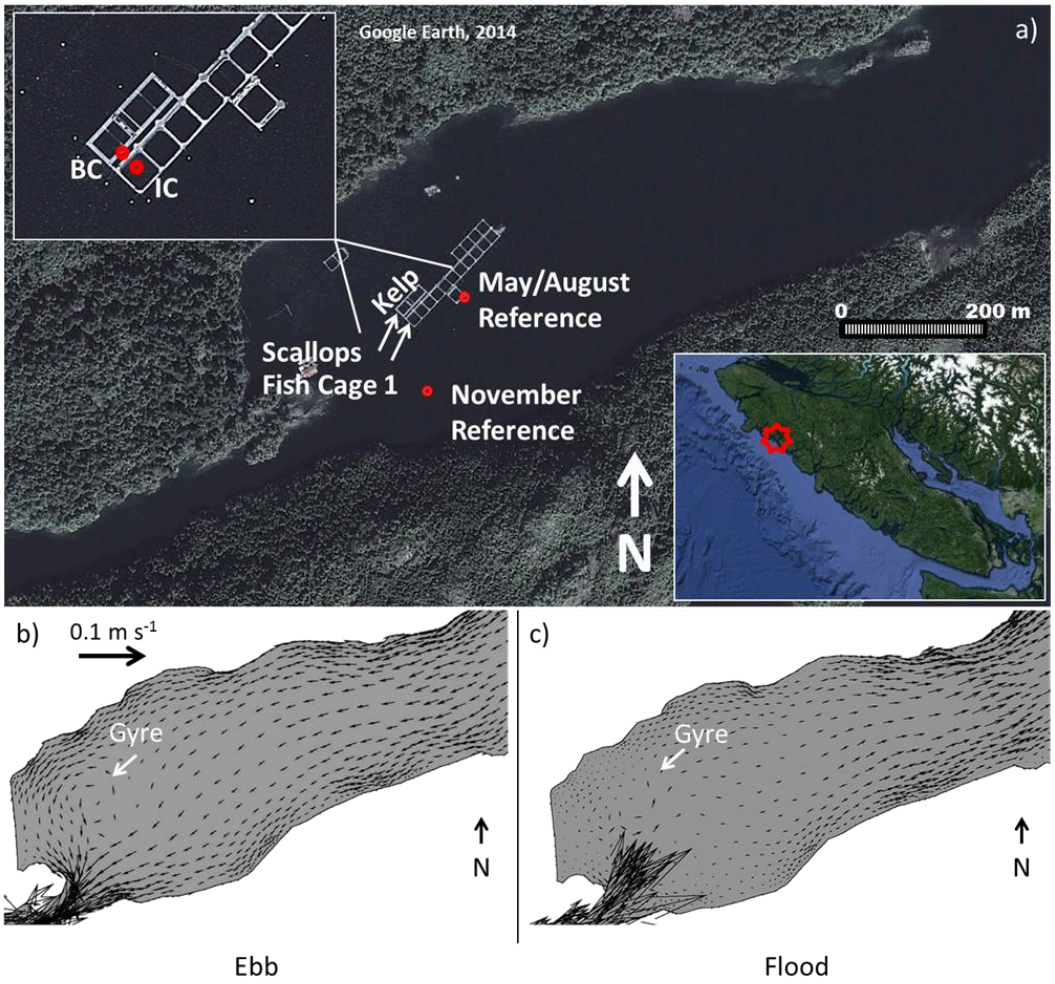

Figure 3.1– Kyuquot SEAfood IMTA site within Kyuquot Sound on the northwest coast of Vancouver Island (a) and modelled surface currents for ebb (b) and flood (c) tides showing a distinct gyre in the western sector of the embayment. The in-cage and beside cage sampling sites are denoted by IC and BC, respectively. Note the different locations for the reference sites between the November and May/August data collection periods. Modelled currents were provided by Foreman, unpublished data, 2011. The length of the arrows on the surface current plots are representative of current speeds and a scale arrow is provided (b).

During winter, large storms move through the region bringing high rainfall (> 4000 mm annually, > 400 mm January) and strong southeasterly winds (> 100 km h^{-1}) (Coast and Marine Planning Branch, 2003; Natural Resources Canada, 2009). This rainfall results in runoff originating from local streams and the surrounding landmasses, which are heavily vegetated. In the calm intermittent periods between storms, this runoff can

cause stratification, due to the presence of a strong freshwater surface lens (Hannah et al., 2013). Additionally, the region is located within the North American Coastal Upwelling Domain and thus, is exposed to nutrient rich upwelled waters during the summer months and downwelling conditions during the winter months (Hay et al., 2003). A lack of biological productivity during downwelling can result in low turbidity conditions with Secchi depths up to 16 m having previously been observed at the study site (Hannah et al., 2013). In the spring and summer, offshore diatom blooms (*Skeletonema costatum*) are commonly advected in the inlets on the west coast of Vancouver Island via wind forcing; however when this is not occurring, nutrient depletion and stratification can limit phytoplankton growth (Taylor & Haigh, 1996; Hay et al., 2003). During summer periods of high thermal stratification, the cosmopolitan and opportunistic coccolithophore species *Emiliania huxleyi* can also form isolated blooms within these inlets (Taylor & Haigh, 1996). Generally, high productivity experienced during the spring and summer months results in high turbidity (Secchi depths $\sim$ 2 – 3 m) (Hannah et al., 2013) with high and variable surface total suspended matter concentrations (> 5 mg l^{-1}) (Brager, 2013).

3.3.2 Experimental Design

Sampling was performed in November 2011, May 2012 and August 2012 representing autumn, spring and summer conditions, respectively. The specific sampling dates and sample site locations (e.g. N14-IC), reference site and before feeding (BF) sampling times and other metadata are presented in Table 3.3.

Table 3.3 – Data collection dates, sample locations, reference site (REF) and BF data collection start times and tidal stage (Ebb (E), Flood (F)), and details of optical profile/water sampling depths and frequencies. The first letter in the acronym for the individual sampling day represents the month (November (N), May (M), and August (A)), followed by the day and then sampling location. Variability in the number of sampling days arose from logistical complications.

Collection Days	REF/BF Times (Tide E/F)	Water Sampling Depths (m)	Water Sampling Method	Water Sampling Frequency	Optical Profile Frequency	Profile Depth (m) Ref/IC-BC
N14-IC	8:40/9:30 (F)	1, 5, 13	Niskin	Hourly	Hourly	20/14
N15-BC	9:10/10:30 (F)	1, 5, 13	Niskin	Hourly	Hourly	20/20
M19-IC	7:45/8:45 (F)	1, 7, 13	Niskin	Hourly*	Continuous	20/14
M20-IC	8:25/9:05 (F)	1, 7, 13	Niskin	Hourly*	Continuous	20/14
M21-IC	9:20/10:30 (F)	1, 7, 13	Niskin	Hourly*	Continuous	20/14
A16-IC	8:00/9:05 (F)	1, 7, 13	Pumped	Hourly	Continuous	20/14
A17-IC	8:10/9:35 (F)	1, 7, 13	Pumped	Hourly	Continuous	20/14
A18-IC	8:15/9:20 (F)	1, 7, 13	Pumped	Hourly	Continuous	20/14
A20-BC	8:05/9:10 (F)	1, 7, 17	Pumped	Hourly	Continuous	20/20
A21-BC	8:30/9:45 (F)	1, 7, 17	Pumped	Hourly	Continuous	20/20
A22-BC	8:10/9:05 (E)	1, 7, 17	Pumped	Hourly	Continuous	20/20

*Pigment samples in May were collected bi-hourly

On the morning of each data collection day, optical profiles and water sampling were performed at an up-current reference site, which in November was located approximately 100 m to the south of cage 1 and in May/August, was approximately 50 m east of cage 1, off of the central portion of the IMTA system (Figure 3.1 a). The reference location was moved in May/August as it was more efficient to collect data off of the stable harvesting platform and also, no fish were present in the central cages during these periods, eliminating the likelihood of fish derived waste influences. According to the known current directions, both reference site locations were representative of incoming waters, which should not have previously passed through the system. Water sampling depths at the reference sites were done at comparable depths to the subsequent samples taken at the IMTA site. All of the optical profiles performed at the reference sites extended to 20.0 m depth to characterize ambient lower water column conditions.

After sampling at the reference site, the sampling equipment was moved to a site either within or directly adjacent to cage 1 (Figure 3.1 a and 3.2, Table 3.3). This transfer was done as quickly as possible, and over the same tide regime, so that the initial profiles performed at the IMTA site could be compared to those at the reference site (Table 3.3). Once at the IMTA site location, optical profiles were performed before feeding (BF), post feeding (PF) and then at one hour intervals (November) or continuously (May/August) from 5 – 8 hours PF. Continuous profiling was performed during May and August so that high resolution vertical and temporal data were collected. In-cage optical profiles extended to 14.0 m depth as they were limited by the cage bottom (15 m) whereas the BC profiles extended to 20.0 m with the water column depth being approximately 25.0 m at this location. For each sampling day/time, water sampling for the derivation of chlorophyll *a* (chl *a*) and particulate organic carbon (POC) concentrations was performed at the reference site, BF, PF and then at one hour intervals through the day. Samples were collected at three depths (Table 3.3) to characterize surface, mid-depth and lower cage/water column particulates. In November and May, a 5 L Niskin bottle was used for water sample collection. In August, a pumping system was used enabling the collection of water samples directly beside the profiler while inside the cage. The pump hose was purged before each new sample collection.

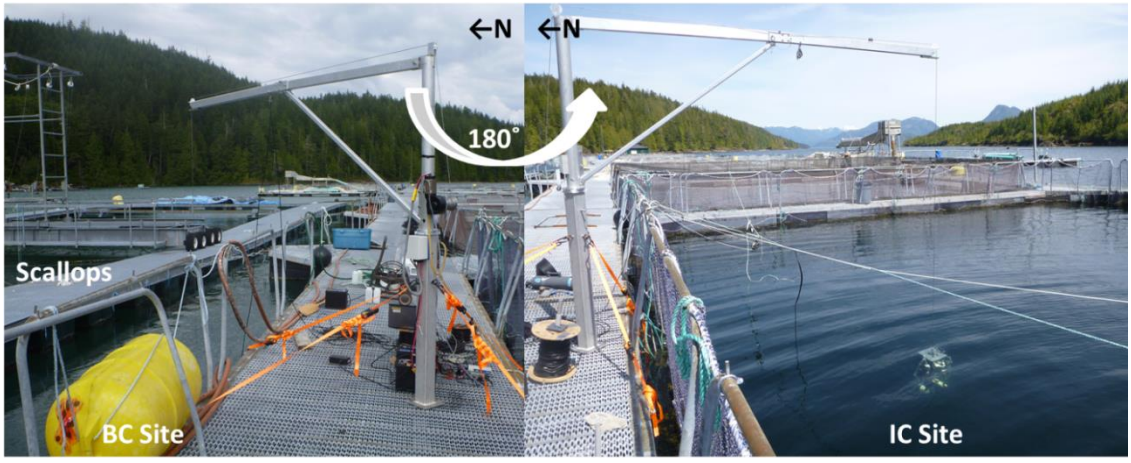

Figure 3.2 – Sampling images showing locations of IC and BC sites. For perspective, the crane structure is approximately in the same position in both pictures; however, the crane arm was rotated 180˚ from the BC to the IC site. The walkway between the IC and the BC site was approximately 2 m wide.

Water samples were collected into pre-washed 1 L Nalgene bottles, which were placed into a cooler and transferred to the onsite lab for immediate filtration. All samples were filtered at low vacuum through pre-washed and combusted 0.7 µm Whatman GF/F filters for further lab analysis of POC and chl *a*. After filtration, 300 mL of Deionized (DI) water was passed through the filters to remove salt accumulation (Stavn et al., 2009). The filters were frozen on-site until they were transferred to the University of Victoria where they were stored at - 80 °C until analysis was performed.

Optical data were collected with a profiler containing a Wetlabs hyperspectral absorption and attenuation meter (ac-s), ECO-BB3 sensor and a Seabird CTD. The ac-s measured total absorption and attenuation at 86 channels between 400 and 737 nm. This instrument has a 4 nm resolution, samples at 4 Hz and has a 25 cm pathlength. Deionized water calibrations were performed on the ac-s instrument before, during and after each data collection period to characterize instrument drift that occurred during sampling (Twardowski et al., 1999). The ECO-BB3 was used to derive particulate

backscattering (b_{bp}) at a fixed angle (117˚) for three wavelengths - 470, 530 and 660 nm.

3.3.3 Water Sample Analysis

Reverse-phase high performance liquid chromatography (HPLC) analysis was performed for the determination of chl *a* (Arar, 1997). Sample filters were extracted in 10 ml of 90% HPLC grade acetone, sonicated for 30s and then placed into a dark refrigerator to steep overnight (< 24 hrs.). Once steeped, the samples were centrifuged in a dark room at 1000 m/s^2 for 10 minutes. The separated solution was then filtered (0.45 µm) into vials which were immediately placed into the autosampler of a Dionex HPLC system. This system was pre-calibrated using DHI reference chl *a* standards.

Non elemental particulate organic carbon (POC) was determined using a Shimadzu solid sample module (SSM-5000) in line with a TOC-V carbon analyzer. Dry combustion of the filters at 900°C was performed within the combustion tube of the SSM-5000. The CO_2 created by the high temperature oxidation of the carbon was carried to a non-dispersive infrared (NDIR) detector within the TOC-V module via 99.9% O_2 carrier gas flowing at 500 ml/min (Obernosterer et al., 2005). Particulate organic carbon was estimated by comparison with calibration curves from lake sediment samples (LKSD – 2) with certified carbon concentrations (Natural Resources Canada, 2013). The POC:chl *a* ratio was used as an indicator of the composition of the total organic particulate pool as values that are < 200 generally indicate phytoplankton dominated waters, while values that are > 200 indicate waters dominated by detrital materials (Cifuentes et al., 1988; Savoye et al., 2012).

3.3.4 Optical Data Analysis

The optical and CTD data were merged and absorption and attenuation by pure water were subtracted from the raw ac-s data through the use of the Wetlabs host software. All other optical corrections and binning of the data into 0.5 m increments were done through the use of a customized script. These corrections are detailed in chapter 2 and resulted in the determination of the attenuation (c_{pg}) and absorption (a_{pg}) coefficients of particulate and dissolved matter, and particulate backscattering (b_{bp}) at each depth (z) and wavelength (λ). The particulate scattering coefficient (b_p) was calculated following equation (1).

$$b_p(z,\lambda) = c_{pg}(z,\lambda) - a_{pg}(z,\lambda) \quad (1)$$

Then, the backscattering ratio ($\tilde{b}_{bp}$) was calculated using:

$$\tilde{b}_{bp}(z,\lambda) = \frac{b_{bp}(z,\lambda)}{b_p(z,\lambda)} \quad (2)$$

Only the optical data at 660 nm were used for analysis as this wavelength is comparable to those used in other coastal studies.

3.3.5 Statistical Analysis

All statistical analysis and interpolations for colour-map plots were performed with the OriginPro software package. Paired t-tests were employed on the optical data collected at the reference sites versus those collected BF at the IC/BC sites to assess statistical differences between mean ambient and mean aquaculture particulate concentrations and compositions. This analysis was done to determine if any pre-feeding spatial differences in particulate dynamics existed between the two sites. In addition, on each sampling day, the temporal IMTA site optical data (b_{bp} and $\tilde{b}_{bp}$) were separated into

depth bins. Optical values within each bin were averaged and their confidence intervals ($p < 0.05$) were calculated. The depth ranges of these bins (2.0 – 9.5 m, 10.0 – 14.0 m and 14.5 – 20.0 m) were selected based on the daily trends reported in chapter 2. In particular, the mid-water column bin (2.0 – 9.5 m) was generally characterized by high chlorophyll; the lower cage bin (10.0 – 14.0 m) exhibited distinct temporal increases from possible aquaculture derived wastes (November) and; the lower water column bin (14.5 – 20.0 m) defined below cage conditions. The surface waters (< 2.0 m) were removed from this analysis due to possible terrigenous influences during the November sampling period. This averaging was also done for the daily biophysical (chl *a*, POC) concentrations at each discrete sampling depth (Table 3.3).

3.4. Results

The results are comprised of three sections; one for each of the sampling periods. Within these sections spatial variability between the reference and IC/BC sites (t-tests) are assessed. Additionally, select days, which are representative of notable trends in the data, were chosen for a comparison of reference site and BF-IC/BC b_{bp}, POC, and chl *a* profiles and for the temporal analysis of within day IC/BC variability of b_{bp}. Finally, depth averaged b_{bp}, $\tilde{b}_{bp}$, and POC were compared for each data collection day within each sampling period.

3.4.1 November – Autumn Conditions

Reference site and BF depth profiles of b_{bp}, POC and chl *a* for N14-IC and N15-BC are shown in Figure 3.3. No statistical differences in b_{bp} and $\tilde{b}_{bp}$ magnitudes between the reference site and the IC and BC sites were observed, with exception to N15-BC, where

$\tilde{b}_{bp}$ showed slightly higher values beside the cage when compared to the reference site (Table 3.4). Both sampling days exhibited similar trends, with b_{bp} and POC increasing from the mid to lower water column (N15 – reference POC data missing) and chl *a* decreasing with depth. On N14, b_{bp} (~ 0.006 m^{-1}) and POC (0.17 mg l^{-1}) magnitudes were slightly higher at the bottom of the cage when compared to reference values (~ 0.004 m^{-1} and 0.14 mg l^{-1}, respectively), despite having comparable chl *a* concentrations (0.02 µg l^{-1}) (Figure 3.3 a).

Table 3.4 – Results of paired t-tests (*p > 0.05 and **p > 0.01) between reference site and BF - IC/BC optical profiles of b_{bp} (particulate concentration) and $\tilde{b}_{bp}$ (particulate composition) where *n* is the sample size of the statistical analysis. Particulate backscattering (m^{-1}) and $\tilde{b}_{bp}$ ranges for the reference and BF sites are provided in brackets.

Sampling Day	**(b_{bp}) Ref vs. BF**	***n***	**($\tilde{b}_{bp}$) Ref vs. BF**	***n***
N14-IC (t-test)	**ns**	*28*	**ns**	*28*
Range (Ref)	(0.002 – 0.006)		(0.006 – 0.028)	
Range (BF)	(0.001 – 0.007)		(0.010 – 0.030)	
N15-BC	**ns**	*38*	**Ref < BF***	*38*
Range (Ref)	(0.001 – 0.009)		(0.004 – 0.025)	
Range (BF)	(0.002 – 0.005)		(0.002 – 0.031)	
M19-IC	**ns**	*28*	**ns**	*28*
Range (Ref)	(0.003 – 0.006)		(0.004 – 0.018)	
Range (BF)	(0.003 – 0.005)		(0.005 – 0.020)	
M20-IC	**Ref > BF***	*26*	**ns**	*26*
Range (Ref)	(0.003 – 0.014)		(0.004 – 0.021)	
Range (BF)	(0.002 – 0.009)		(0.004 – 0.022)	
M21-IC	**ns**	*28*	**ns**	*28*
Range (Ref)	(0.003 – 0.009)		(0.005 – 0.019)	
Range (BF)	(0.002 – 0.012)		(0.006 – 0.027)	
A16-IC	**Ref > BF***	*15*	**ns**	*15*
Range (Ref)	(0.017 – 0.021)		(0.017 – 0.022)	
Range (BF)	(0.015 – 0.022)		(0.017 – 0.025)	
A17-IC	**Ref > BF****	*15*	**Ref > BF****	*15*
Range (Ref)	(0.016 – 0.027)		(0.015 – 0.024)	
Range (BF)	(0.014 – 0.023)		(0.018 – 0.024)	
A18-IC	**ns**	*15*	**Ref > BF***	*15*
Range (Ref)	(0.025 – 0.032)		(0.013 – 0.016)	
Range (BF)	(0.024 – 0.035)		(0.011 – 0.015)	
A20-BC	**Ref < BF***	*35*	**Ref < BF****	*35*
Range (Ref)	(0.010 – 0.039)		(0.014 – 0.027)	
Range (BF)	(0.012 – 0.041)		(0.016 – 0.031)	
A21-BC	**Ref < BF***	*35*	**Ref < BF****	*35*
Range (Ref)	(0.013 – 0.037)		(0.015 – 0.033)	
Range (BF)	(0.014 – 0.036)		(0.015 – 0.036)	
A22-BC	**ns**	*35*	**Ref < BF****	*35*
Range (Ref)	(0.007 – 0.038)		(0.015 – 0.040)	
Range (BF)	(0.007 – 0.029)		(0.017 – 0.036)	

Temporally, b_{bp} magnitudes on N14 were the highest near the cage bottom (13.5 – 14.0 m) showing a distinct increase directly PF (Figure 3.3b). The b_{bp} increases at 14.0 m depth (0.006 – 0.009 m^{-1}) peaked at approximately 2.5 hours PF (13:10), but remained elevated above the BF b_{bp} magnitude (0.003 m^{-1}) throughout the day. Particulate backscattering ratio values at this depth followed similar temporal trends with values ranging from 0.018 to 0.063. Comparatively, lower cage POC concentrations at 13.0 m depth ranged from 0.18 – 0.24 mg l^{-1} with the highest concentration collected directly PF. This PF concentration (0.24 mg l^{-1}) was 41% higher than the BF magnitude (0.17 mg l^{-1}). At this depth, chl *a* magnitudes were low and remained stable throughout the day (~ 0.02 µg l^{-1}) and consequently, high, but variable, POC:chl *a* magnitudes (5455 – 9988) were observed near the bottom of the cage.

On N15, the trend of increasing b_{bp} with depth observed at the reference site continued at the BC site throughout the day (Figure 3.3 d). While the BC lower water column b_{bp} magnitudes at 13.0 m depth (0.003 – 0.004 m^{-1}) were lower than those seen within the cage on the previous day (N14) (0.003 – 0.009 m^{-1}), the POC (0.18 – 0.21 mg l^{-1}) and chl *a* (0.01 – 0.02 µg l^{-1}) concentrations were comparable. Notably, below the cage (19.0 m), b_{bp} increased from BF with time through the day (0.003 – 0.006 m^{-1}). Yet, it should be noted that a similarly high magnitude (0.006 m^{-1}) was found in the morning at the reference site. Interestingly, $\tilde{b}_{bp}$ magnitudes at this depth on N15 were relatively stable throughout the day (0.018 – 0.030).

On both days, b_{bp} increases were also measured directly after feeding at the base of the surface layer (Figure 3.3 b and d). On N14-IC the post-feeding b_{bp} magnitude (0.003 m^{-}

^{1}) at 2 m depth was nearly double those found throughout the rest of the day (0.001 – 0.002 m^{-1}). A similar peak, but with a lower increase, was found in the post-feeding b_{bp} magnitude (0.002 m^{-1}) beside the cage on the following day (N15). Unlike the lower cage increases seen on N14, these b_{bp} increases returned to near BF levels within an hour of feeding.

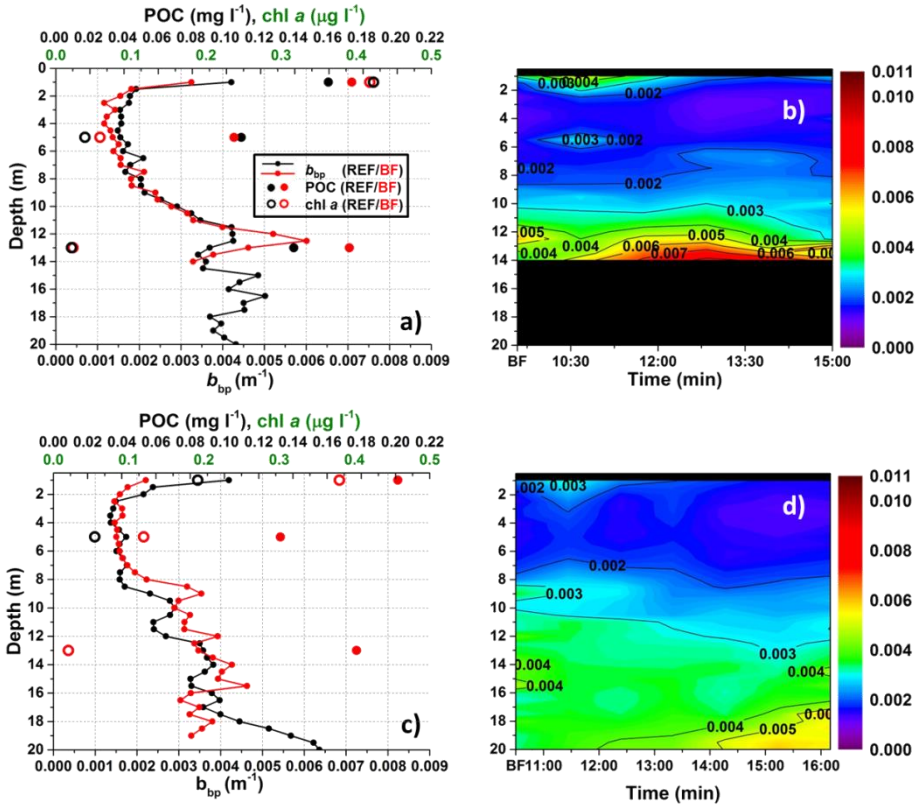

Figure 3.3 – Average fall/winter b_{bp} (m^{-1}) (lower x-axis) profiles at a reference and BF (closest temporally) site within cage 1 on N14 (a) and directly beside and down-current of cage 1 on N15 (c). Discrete POC (mg l^{-1}) and chl *a* (µg l^{-1}) values (upper x-axes) are plotted for both the reference and BF-IC/BC sites at the three sampling depths. Colour-map plots of b_{bp} profiles from BF to approximately 5 hours PF for both days are also shown (b and d). Time is plotted on the x-axis, depth on the y-axis and the colours represent b_{bp} (m^{-1}) magnitudes with purple showing low values and red showing high values.

When averaged into depth bins, the lower cage depth (10.0 – 14.0 m) showed the highest daily mean b_{bp}, $\tilde{b}_{bp}$, and POC and magnitudes of the sampling period (Figure

3.4). The next highest daily mean b_{bp} value (0.004 m^{-1}) was measured below the cage (14.5 – 20.0 m) on N15; however, the mean $\tilde{b}_{bp}$ magnitude at this depth was comparable to the ones found through the rest of the water column (0.023). While the daily mean POC concentrations were relatively similar between depths (Figure 3.4 c), chl *a* decreased with depth and high daily mean POC:chl *a* values (> 6000) occurred at the 13 m sampling depth on both N14 and N15 (Figure 3.4 d).

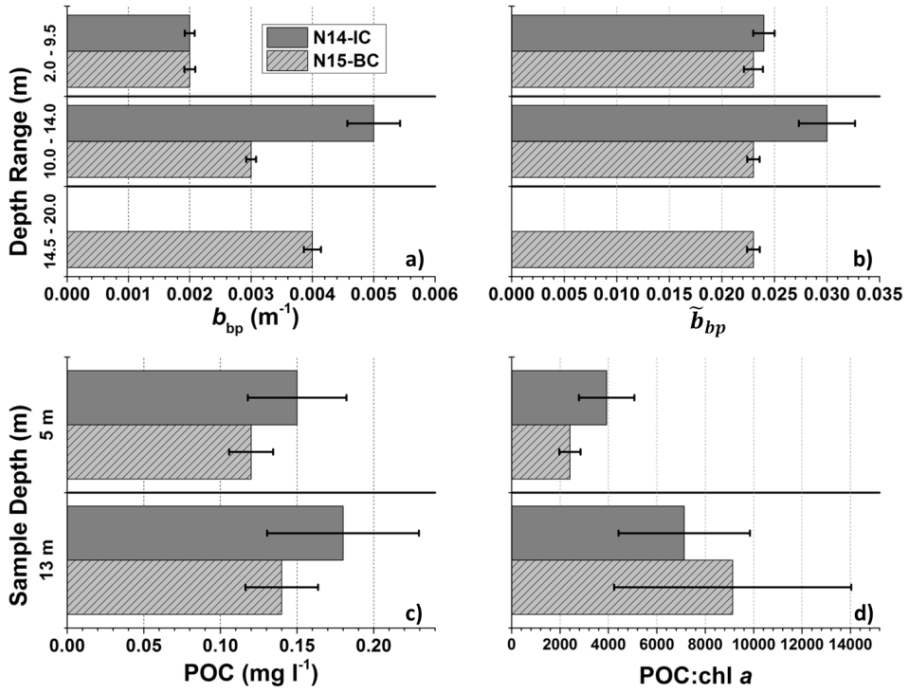

Figure 3.4 – Daily average fall/winter a) b_{bp} (m^{-1}) and b) $\tilde{b}_{bp}$ values at three depth bins and daily average c) POC (mg l^{-1}) and d) POC:chl *a* values at discrete sampling depths within and directly beside cage 1. Error bars represent confidence intervals for the data ($p < 0.05$).

3.4.2 May – Spring Conditions

Particulate backscattering profiles and a colour-map plot are only shown for M19-IC (Figure 3.5) as the statistical relationship between b_{bp} and chl *a* strengthened as a diatom bloom developed over this period (r^2 = 0.32, 0.68 and 0.86; for M19, M20 and

M21, respectively) (Chapter 2). Thus, as the bloom developed, phytoplankton had a greater influence on b_{bp} variability, which would have reduced the likelihood of measuring aquaculture wastes on M20 and M21. While slightly more variable, the M19 BF-IC b_{bp} profile showed similar trends and magnitudes with depth as the reference site (Figure 3.5 a) and no statistical differences were found between the two locations (Table 3.4). The surface POC measurements between the two sites were similar (0.64 and 0.61 mg l^{-1}, respectively); however, the IC POC sample at 8.0 m depth was ~ 117 % (0.35 mg l^{-1}) higher than at the reference site (0.16 mg l^{-1}) on this day. This higher POC magnitude was matched by a chl *a* concentration (1.11 µg l^{-1}) that was one order of magnitude higher than at the reference site (0.18 µg l^{-1}). The lower cage POC samples were not included in these analyses due to cage interference with the sampling bottle at this depth; however, the corresponding lower cage chl *a* concentration (0.25 µg l^{-1}) was higher than the one found at the reference site (0.08 µg l^{-1}).

Throughout the day, b_{bp} showed variability within the cage (Figure 3.5 b) with the highest values generally found in the upper-water column (< 8.0 m) where the chl *a* maximum was located. Unlike November, b_{bp} did not show distinct PF increases at the bottom of the cage and the range in values at 14.0 m depth was smaller and showed lower magnitudes (0.003 – 0.005 m^{-1}) than the one observed on N14-IC (0.003 – 0.009 m^{-1}). Unfortunately, lower cage POC concentrations were not available for this sampling period, however, chl *a* concentrations at this depth were higher and more variable (0.25 – 0.36 µg l^{-1}) when compared to November.

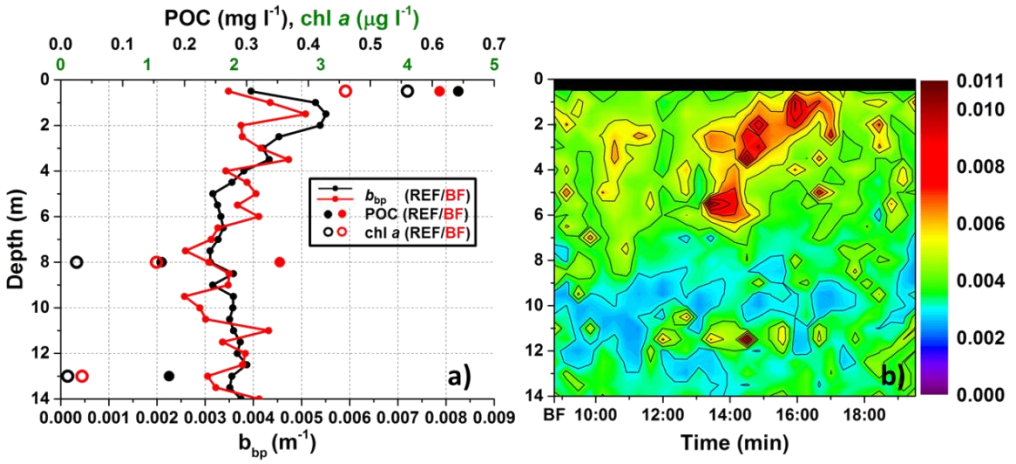

Figure 3.5 – Average spring b_{bp} (m^{-1}) (lower x-axis) profiles at the reference and BF (closest temporally) site within cage 1 on M19-IC. Discrete POC (mg l^{-1}) and chl *a* (µg l^{-1}) values (upper x-axes) are plotted for both the reference and BF-IC site at the three sampling depths (surface, 8m and 13m). A colour-map plot of b_{bp} from BF to approximately 8 hours PF is also shown (b). Time is plotted on the x-axis, depth on the y-axis and the colours represent b_{bp} (m^{-1}) magnitudes with purple showing low values and red showing high values.

Daily average optical and biophysical values for all of the May sampling days are shown in Figure 3.6. The mean b_{bp} values for the upper water column (2.0 – 9.5 m) increased on each consecutive May sampling day. In contrast, mean lower cage (10 – 14 m) b_{bp} values were the same on each day (0.003 m^{-1}) (Figure 3.6 a). These mean values were about 67% lower (0.003 m^{-1}) than the mean value observed at the bottom of the cage on N14-IC (0.005 m^{-1}) (Figure 3.4 a). Over the May period, mean $\tilde{b}_{bp}$ showed similar trends as the b_{bp} data in both the upper and lower water column. It should be noted that mean upper water column $\tilde{b}_{bp}$ values all fell below 0.010 and the mean lower cage $\tilde{b}_{bp}$ values (< 0.016) were considerably lower than the one found on N14-IC (0.030) (Figure 3.4 b). Mean daily POC concentrations at the 8.0 m sampling depth were over twice as high as those seen in November, and did not follow the b_{bp} trend of increasing magnitudes with each consecutive day. At this depth, mean POC:chl

a magnitudes were generally an order of magnitude lower (< 1000) than those seen in November, but were higher than those expected for phytoplankton dominated waters (< 200) (Cifuentes et al., 1988).

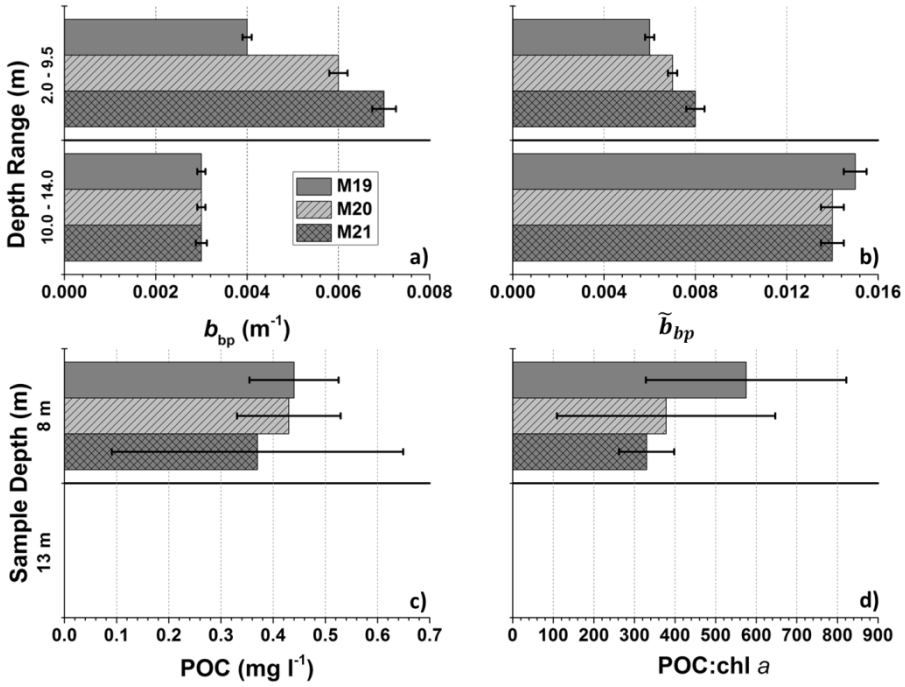

Figure 3.6 – Daily average springtime a) b_{bp} (m^{-1}) and b) $\tilde{b}_{bp}$ values at two depth bins and daily average c) POC (mg l^{-1}) and d) POC:chl *a* values at discrete sampling depths within cage 1. Discrete samples from 13 m are not shown due to sampling error. Error bars represent confidence intervals for the data ($p < 0.05$).

3.4.3 August – Summer Conditions

Reference site and BF b_{bp}, POC and chl *a* profiles are shown for A16-IC and A20-BC (Figure 3.7 a and c) as these two days represent distinct conditions in the water column at the time of sampling. The IC b_{bp} data from the August period was cut at 8.0 m depth due to contact of the instruments with the side of the net and as such, this data was likely compromised by the influence of net fouling. On both days the b_{bp} profiles showed similar trends between the reference and BF IC/BC sites; however, unlike the

other sampling periods, POC and chl *a* values were lower within/beside the cage than at the reference sites. While the differences between the b_{bp} and $\tilde{b}_{bp}$ magnitudes between these sites were statistically significant, these differences were slight (Table 4) and similarly minor differences were observed on the August sampling days not shown in Figure 7.

On both A16 and A20, b_{bp} values were elevated within the surface waters (< 8.0 m) throughout the day (Figure 3.7 b and d), and were nearly one order of magnitude higher than the majority of values measured in November and May. Chlorophyll *a* concentrations were generally low (< 1.0 µg l^{-1}) within these surface waters of high b_{bp} values. Furthermore, these waters were confined within the surface mixed layer of the thermally stratified water columns (Chapter 2).

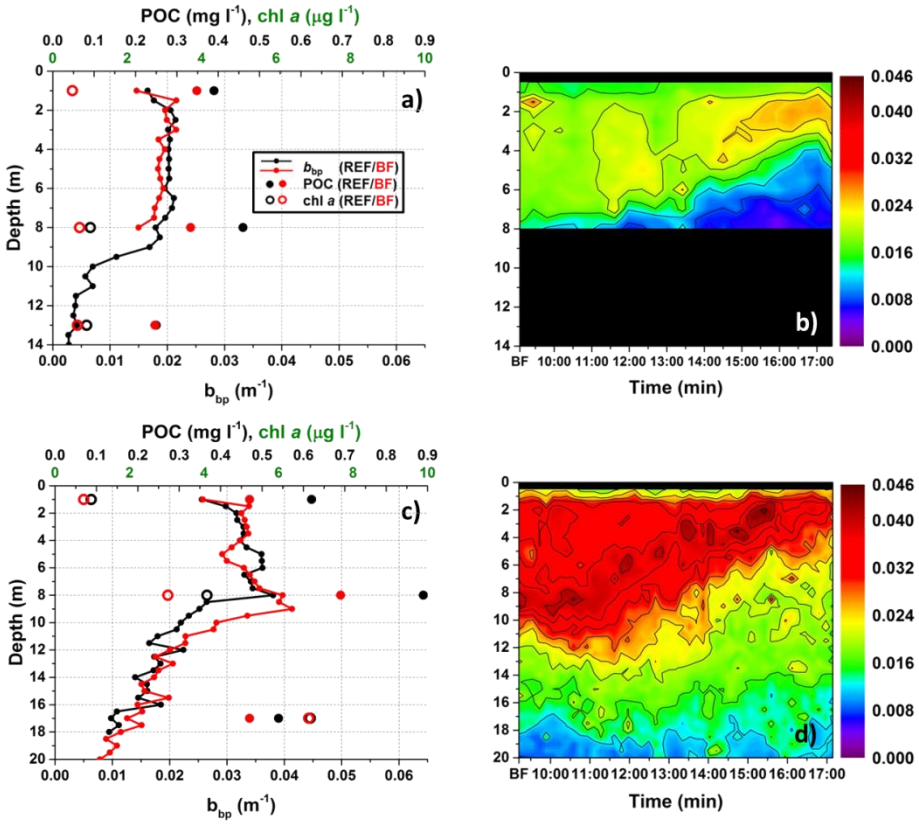

Figure 3.7 – Average summer b_{bp} (m^{-1}) (lower x-axis) profiles at a reference and BF (closest temporally) site within cage 1 on A16 (a) and directly beside and down-current of cage 1 on A20 (c). Discrete POC (mg l^{-1}) and chl *a* (µg l^{-1}) values (upper x-axes) are plotted for both the reference and BF-IC/BC sites at the three sampling depths (surface, 8 m, 13 m (IC), 17 m (BC)). Colour-map plots of b_{bp} from BF to approximately 8 hours PF for both days are also shown (b and d). Time is plotted on the x-axis, depth on the y-axis and the colours represent b_{bp} (m^{-1}) magnitudes with purple showing low values and red showing high values. Note that the colour-map b_{bp} scale is considerably higher than those for November and May.

Daily depth bin averaged b_{bp}, $\tilde{b}_{bp}$, POC and POC:chl *a* for the IC days (A16 – 18) and the BC days (A20 – 23) are shown in Figure 3.8. Within the cage, mean b_{bp} values for the sub-surface layer (2.0 – 8.0 m) and POC concentrations at both sampling depths (8 and 13 m) increased from A16 – A18 (Figure 3.8 a). In turn, average $\tilde{b}_{bp}$ magnitudes and POC:chl *a* values showed an inverse trend with decreasing values through the first three days of the study. Despite an average 8.0 m depth POC concentration (1.18 mg l^{-}

^{1}) nearly three times as high as those seen in May and a low POC:chl *a* value (< 200), A18-IC exhibited a relatively high mean $\tilde{b}_{bp}$ magnitude (0.014) when compared to May (< 0.010) (Figure 3.6 b).

The highest mean b_{bp} magnitude (> 0.030 m^{-1}) of the entire study was measured in the sub-surface waters on A20-BC (Figures 3.7 d and 3.8 a). This value was an order of magnitude higher than the mean b_{bp} magnitudes measured in both November and May. After A20-BC, daily mean b_{bp} values decreased at both the 2.0 – 9.5 and 10.0 – 14.0 m depth bins on each consecutive sampling day, but remained well above those measured during the other sampling periods. On A21-BC, the lower water column showed the highest daily mean b_{bp} magnitude (0.015 m^{-1}) and POC concentration (0.06 mg l^{-1}) for this depth bin, which was associated with presence of the chl *a* maximum (Chapter 2). Fittingly, these values were matched by a low mean POC:chl *a* value (80). The mean $\tilde{b}_{bp}$ data showed disparate trends to those seen in the b_{bp} and POC datasets (Figure 3.8 b) with the highest mean value (0.030) of the August period occurring on A21-BC. In the lower water column, daily average $\tilde{b}_{bp}$ values were lower than at the surface, but increased with each consecutive sampling day.

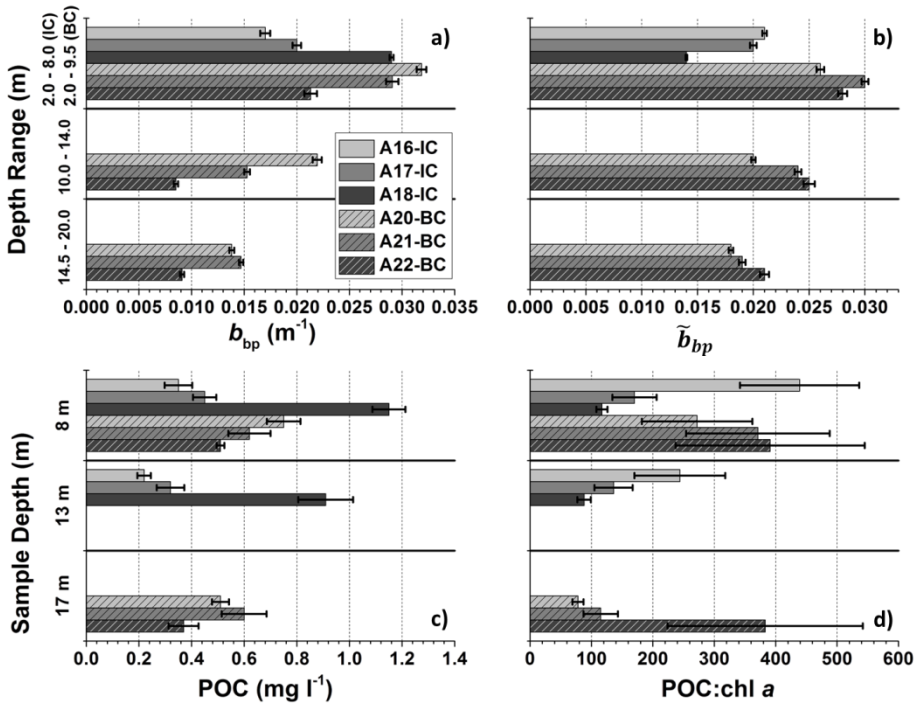

Figure 3.8 – Daily Average summer a) b_{bp} (m^{-1}) and b) $\tilde{b}_{bp}$ values at depth bins (IC bin was 2.0 – 8.0 m due to sampling error) and daily average c) POC (mg l^{-1}) and d) POC:chl *a* values at 8, 13 m (IC) and 17 m (BC) depths from within and directly beside cage 1. Error bars represent confidence intervals for the data ($p < 0.05$).

3.5. Discussion

The strategic placement of commercially viable bivalves for particulate assimilation within IMTA systems has been suggested as a possible approach for the minimization of the environmental effects of coastal finfish aquaculture (Barrington et al., 2009; MacDonald et al., 2011; Lander et al., 2012). Important considerations for the effective use of bivalves within IMTA systems include, but are not limited to, the spatial and temporal dispersion of particulate organic wastes, particulate characteristics such as size and organic content, particulate waste production/output in relation to ambient seston concentrations, site design and proximity of the bivalves to the fish cages and the extraction efficiency of the bivalve species (Troell & Norberg, 1998; Cheshuk et al.,

2003; Cranford et al., 2013). When considering the site specific variability of these factors, it is not surprising that disparate results have been observed in bivalve growth enhancement studies (i.e. Cheshuk et al., 2003; Lander et al., 2012) and when attempting to quantify organic particulate concentrations dispersing out of open water fish cages at IMTA systems. Yet, differences in results may also be partially explained by differing sampling methods, including those that were not of high enough resolution to capture spatial/temporal patterns in organic particulate dynamics (Lander et al., 2013).

Our study focused on near field (in-cage and beside-cage) and high temporal (hourly discrete water samples and nearly continuous optical data) and vertical (three discrete water sampling depths and nearly continuous optical data) resolution measurements within a small scale IMTA site. The sampled cage within this site contained nearly the same amount of fish and had comparable feeding regimes over the course of our three study periods. With this sampling strategy, our results suggest that during fall/winter, when ambient seston concentrations were low (POC < 0.25 mg l^{-1} and chl *a* < 0.12 µg l^{-1}), slightly enhanced particulate organic matter concentrations, which were likely due to aquaculture derived wastes, were present post-feeding near the bottom of the cage. In contrast, the spring and summer sampling periods showed high ambient seston concentrations (POC and chl *a* as high as 1.50 mg l^{-1} and 13.34 µg l^{-1}, respectively) with bio-optical variability being driven by changes in phytoplankton concentrations and compositions. The lack of distinct particulate aquaculture waste signals measured during these productive months was likely due to their quick dilution and masking by the particle rich environments, which has been observed by other authors sampling in

regions with high ambient seston concentrations (Cheshuk et al., 2003; Lander et al., 2013).

3.5.1 Particulate Dynamics and Bio-Optical Variability

The bio-optical data from the November period suggest the post-feeding release of feces at the bottom of the studied cage (N14-IC - Figure 3.3 b). Particulate backscattering magnitudes at 14.0 m depth peaked (0.009 m^{-1}) at approximately two hours post-feeding and were elevated above the BF magnitude (0.003 m^{-1}) throughout the day. This persistence may have been a result of the continued release of feces and (or) the accumulation of wastes at the bottom of the cage. In addition, the mean lower cage POC concentration (0.18 mg l^{-1}) was the highest of the period and was matched by low chl *a* (0.02 µg l^{-1}) and a high mean POC:chl *a* magnitude (7130) suggesting the dominance of detrital materials (Cifuentes et al., 1988; Savoye et al., 2012), likely due to the presence of feces. Furthermore, the high mean $\tilde{b}_{bp}$ value found at the bottom of the cage (~ 0.030) was suggestive of particulates with higher refractive indices and (or) smaller particulate size distributions than those found at the other depths (Loisel et al., 2007), which may have been a result of the dominance of fish feces. These feces may have had less time to absorb water and (or) break apart than those outside of the cage, possibly resulting in their higher refractivity.

The mid-water column trends observed on N14-IC and N15-BC did not indicate horizontal dispersion of wastes outwards from the side of the cage towards the scallop portion of the system. Rather, increases on N15-BC were found below the cage, with b_{bp} at 19.0 m depth peaking (0.006 m^{-1}) at four hours post-feeding (Figure 3.3 d).

Brager (2013) also observed a slight peak in calibrated transmissometer measurements at a comparable location (beside cage 1) and depth (20.0 m), which lasted for roughly 1 hour, occurred during current speeds that were < 0.5 m s^{-1} and represented a total suspended matter increase of 0.7 mg l^{-1}. These increases possibly represented the downwards precipitation of the wastes out of the cage. Sutherland et al. (2001) found similar trends with increased suspended particulate matter (SPM) concentrations, which were primarily made up of feces, within and directly below an Atlantic salmon cage on the east coast of Vancouver Island. At our study site, augmented sea cucumber growth was measured directly below the studied cage when compared to control individuals (Hannah et al., 2013) further suggesting the vertical precipitation of wastes from the bottom of the cage. While the b_{bp} trends observed at the bottom of cage (N14) were distinct, and thus likely indicate increased fish waste concentrations, the N15 below cage b_{bp} increases may have been due to resuspension as comparable magnitudes were found near the seafloor at the reference site on this day (Figure 3.3 c). Based on the reference b_{bp} profiles, it appears that an ambient nepheloid layer was present extending upwards to approximately 8.0 – 10.0 m depth, which is an important consideration for food availability to filter feeders if the resuspended materials contained previously settled particulate wastes. The relatively high BC lower water column POC (~ 0.14 mg l^{-1}) and POC:chl *a* (~ 9132) magnitudes indicate that either feces or resuspended detrital materials were likely present at these depths (Cifuentes et al., 1988).

On both days, b_{bp} increases were also measured directly after feeding at the base of the surface layer (Figure 3.3 b and d), which may have been a result of the addition of wasted feed and (or) feces in the upper water column and its horizontal dispersion

towards the scallop component of the system. Other authors have observed enhanced particulate concentrations beside salmon cages over the course of relatively long continuous feeding cycles (Taylor et al., 1992; MacDonald et al., 2011; Lander et al., 2013). Comparatively, the pulse feeding regime (~ 15 min.) conducted during our study appears to have resulted in the short residence time (< 1 hr.) and quick dilution of surface feed/feces particulates, which may reduce its availability to filter feeders (Troell & Norberg, 1998).

While the b_{bp} and POC increases measured during this period were relatively slight, these magnitudes were expected considering the amount of feed inputs on each sampling day (75 kg). In comparison, the Atlantic salmon sites sampled by Lander et al. (2013) were fed between 1144 – 8683 kg of feed over the course of their 24 hour sampling periods, which were focused on the synergistic effects of the entire system rather than a single cage. The only other comparable study which directly sampled within a cage (Sutherland et al., 2001) and also, during winter conditions, measured a mean in-cage feeding cycle SPM concentration of 0.61 mg l^{-1}. It should be noted that the POC measured in our study would make up only a percentage of total SPM and thus, our concentrations may be somewhat comparable to the mean SPM concentration found inside an Atlantic salmon cage on the east coast of Vancouver Island by Sutherland et al. (2001). Considering these magnitudes, it is not surprising that distinct increases in our study were only observed during autumn/winter conditions when ambient particulate concentrations were low.

In May and August, all of the measurements were highly influenced by phytoplankton concentrations and compositions. In particular, a diatom bloom developed (*Chaetoceros*

and *Skeletonema*) during the May sampling period with cell concentrations increasing from $0.53*10^6$ cells/L on May 15th to $6.28 – 7.76*10^6$ cells/L on May 22nd (Guindon, 2012). Increases in upper-water column b_{bp} measurements reflected the daily increases in phytoplankton biomass and low $\tilde{b}_{bp}$ magnitudes (<0.010) indicated a particulate assemblage dominated by large low refractivity phytoplankton cells (Sullivan et al., 2005). Unlike November, lower water column b_{bp} and $\tilde{b}_{bp}$ did not increase with depth and time after feeding suggesting either a lack of fish derived wastes or scattered and diluted waste assemblages (Figure 3.5 b). The lower cage $\tilde{b}_{bp}$ magnitudes ($\sim$ 0.014) were considerably lower than those observed in November ($\sim$ 0.030) and were indicative of a mixed assemblage of phytoplankton and more refractive materials (Sullivan et al., 2005). While the mean mid-water column POC:chl *a* magnitudes ($\sim$ 300 – 600) were considerably lower than in November, they were still higher than those expected for phytoplankton dominated waters (< 200) (Cifuentes et al., 1988), possibly indicating the presence of detrital particulates below the surface layer. Considering these factors, fish derived wastes may have been present, but in more scattered, diluted and mixed (with phytoplankton) assemblages when compared to November when distinct lower cage increases were observed. The presence of a surface mixed layer during this period (and August) may have influenced the dispersion and mixing of the particulate wastes partially resulting in the lack of distinct lower cage increases. Stratification has been found to decrease seafloor sedimentation rates below fish cages as it can cause increased mixing and dilution and wider dispersion due to longer suspension times (Tsutsumi et al., 2006).

In August, a possible bloom of the coccolithophore species, *Emiliania huxleyi* occurred in conjunction with other phytoplankton species. In-depth analysis of these trends and evidence of the presence of *E. huxleyi* are presented in detail in chapter 2. *E. huxleyi* blooms commonly occur off of the coast of Vancouver Island during the summer season (Taylor & Haigh, 1996; Irvine & Crawford, 2013). In general, this coccolithophore species produces calcium carbonate plates (coccoliths), which they release at high concentrations into the water column during the later stages of blooms (Balch et al., 1991). These refractive coccoliths are highly efficient at backscattering light, which would explain the higher surface b_{bp} and $\tilde{b}_{bp}$ (> 0.030 m^{-1} and > 0.030, respectively) when compared to the other sampling periods (Balch et al., 1991; Garcia et al., 2011). These trends were most notable on A20-BC and can be observed in Figure 3.7 d. In addition to *E. huxleyi*, the high POC and low POC:chl *a* on A18 were likely a result of the intrusion of an offshore diatom bloom. After A18, the chl *a* maximum, and likely the bulk of the diatom biomass, moved below the surface layer increasing both b_{bp} and POC in the lower water column (A21). While $\tilde{b}_{bp}$ was reduced on A18 and within the chl *a* maximum on the following days, values were higher than those expected for diatom bloom conditions, likely due to the co-presence of coccoliths. Under these conditions it is unlikely that distinct fish waste signals would be measured as the effect of the *E. huxleyi* cells, coccoliths and the high concentrations of other phytoplankton species would mask any aquaculture derived inputs.

3.5.2 Implications for IMTA

Studies assessing bivalve growth adjacent to fish farms have found that particulate wastes are most beneficial to bivalves during periods of low ambient seston

concentrations where they provide an added source of nutrient rich feed allowing for continued growth (Troell & Norberg, 1998; Lander et al., 2012; Handå et al., 2012a; Cranford et al., 2013). In contrast, bivalves lacking this food source experience no or even reduced growth during periods of low biological activity (Wallace, 1980; Stirling, 1995; Troell & Norberg, 1998). Our results suggest that the addition of aquaculture derived wastes would have been most available to the cultured scallops during November (autumn) as ambient organic particulate concentrations were low and possible fish wastes were detectable above background levels. Yet, it seems that during this sampling period, the majority of these wastes were dispersed below the scallop portion of the system (lantern nets < 15 m). Even resuspended materials, which likely contained aquaculture derived wastes, would only have been available to the scallops located in the lower water column (> 10.0 m). Under these conditions, uptake species placed deeper in the water column and (or) below the studied cage may be more appropriate for waste removal. As mentioned previously, sea cucumbers suspended in trays below the studied cage have already shown promise for assimilating fish wastes precipitating from the bottom of the cage (Hannah et al., 2013). Nevertheless, it should be noted that waste particulates may be horizontally advected toward the scallop component of the system under differing hydrographic conditions not encompassed by our sampling regime. Furthermore, horizontal advection may have occurred in directions not captured by our sampling sites. For instance, the modelled dominant current direction at the sampled cage over our study periods was in the southwest direction (Unpublished data, Foreman, 2011), due to its location in relation to the gyre. Appropriately, a study using kelp bio-essays to track dissolved waste dispersal showed

increased growth dominantly off of the southern and southwestern portions of the studied cage (Prussin, 2012). It is plausible that particulate wastes released from the more eastern cages of the system may have moved towards the scallops due to the current regimes at these locations. Thus, further sampling should be focused on particulate dynamics from the entire system, rather than at a single cage.

The quick dilution of the fish wastes into the particle rich assemblages experienced during the May and August periods would likely have reduced their availability to the uptake species. Even if these wastes were available to the scallops, ambient seston concentrations may have been high enough that additional inputs would not have spurred augmented growth. In fact, under high ambient seston concentrations, bivalves can reach their pseudofeces threshold and if this occurs, additional inputs are released as pseudofeces, which could concentrate and amplify waste deposition beneath the fish cages (Troell & Norberg, 1998; Cheshuk et al., 2003; Cranford et al., 2013). While our spring/summer sampling periods fell during bloom conditions, periods of nutrient depletion and limited phytoplankton growth would also occur in the study site embayment during these seasons (Taylor & Haigh, 1996; Hay et al., 2003). As such, fish wastes could provide an important food source to uptake species during these times and thus, more intensive summer sampling regimes should be conducted to fully characterize seston dynamics.

Our study highlights the high spatial (vertical and horizontal) and temporal variability and "patchiness" in fish waste dispersion, which has also been described by other authors (Brager, 2012; Irisarri et al., 2013; Lander et al., 2013). These findings indicate that care should be taken when employing discrete water sampling methods and (or)

sampling at coarse timescales as these regimes may not fully characterize or even completely miss the waste streams. For instance, during the November sampling period, waste signals from the optical data were concentrated at very narrow depth ranges (cage bottom) or at short timescales (PF surface), which were largely missed by the discrete sampling. Furthermore, care should be taken when averaging data over multiple depths and times, as this method may dilute waste signals and lead to unrepresentative results.

3.6. Conclusions

The objectives of this study were to detail spatial (vertical and horizontal) and temporal organic particulate concentrations at the studied IMTA site in order to aid in the placement of uptake species for maximum particulate waste uptake. Our study shows distinct signals, likely a result of particulate aquaculture wastes, during the November sampling period when ambient seston concentrations were low. Under spring and summer bloom conditions, these wastes, if present, were quickly diluted into the particle rich environments. The temporal and spatial bio-optical (b_{bp} and $\tilde{b}_{bp}$) and biophysical (POC and chl *a*) trends observed during the November sampling period suggest that particulate wastes would be most available to uptake species placed below the studied cage and appropriately, augmented sea cucumber growth has been measured in this location (Hannah et al., 2013). Based on our temporally limited results, mid-water column horizontal movements of particulate wastes towards the scallop portion of the system were slight, possibly limiting the effectiveness of this species for waste removal. Yet, further studies are needed over longer periods, differing hydrographic regimes and at more comprehensive sampling locations so that full system particulate dynamics can be assessed over variable conditions. Future studies should also include

simultaneous reference site measurements so that ambient conditions can be characterized over the entire day.

The optical measurements performed during this study showed promise as potential proxies for both aquaculture waste and ambient particulate concentrations and compositions. The high sampling frequencies of these measurements make them valuable tools for overcoming the issues introduced by discrete sampling methods and thus, further studies should include these measurements so that the optical effects of fish wastes can be fully characterized. With greater understanding, optical instrumentation could eventually be incorporated into IMTA monitoring systems for the near real time and continuous collection of data on particulate dynamics. This knowledge could greatly aid in the design and implementation of IMTA systems highly optimized for waste removal by uptake species.

Chapter 4 – Conclusions

The goal of this thesis was to spatially and temporally characterize ambient and aquaculture derived organic particulate dynamics at an active IMTA site on the west coast of Vancouver Island, Canada. To accomplish this goal, *in situ* optical measurements (b_p, b_{bp} and $\tilde{b}_{bp}$) and discrete sampling for biophysical concentrations (POC and chl *a*) were performed over three seasons (autumn, spring and summer) at reference sites and sites within and directly adjacent to a fully stocked sablefish cage.

Our results showed high temporal and vertical variability in particulate concentrations and compositions at the study site over the sampling periods. Autumn (November) showed low biophysical concentrations and optical magnitudes (high $\tilde{b}_{bp}$) with lower water column variability likely attributable to the influence of aquaculture derived wastes. In spring (May), a diatom bloom resulted in considerable increases in biophysical concentrations and notably, b_p magnitudes when compared to November. The summer period (August) showed similar biophysical concentrations and b_p magnitudes as May; however, distinctly high b_{bp} and $\tilde{b}_{bp}$ suggested the presence of an *E. huxleyi* bloom.

The highly dynamic nature of the study area, as described above, resulted in variable bio-optical relationships over the data collection periods highlighting the complexity of using optical parameters within coastal environments. Nonetheless, the use of the selected optical parameters provided valuable information on particulate concentrations and compositions at temporal and vertical scales that would not have been achievable solely through discrete water sampling. In particular, b_p was predominantly influenced

by changes in chl *a* suggesting a sensitivity to phytoplankton concentrations over a wide range of biogeochemical conditions. While b_{bp} was conditioned by phytoplankton during the height of the May diatom bloom and during low ambient conditions (surface waters – November), this parameter was highly influenced by the presence of inorganic (coccoliths) and likely detrital materials (aquaculture wastes). Finally, $\tilde{b}_{bp}$ appears to have been sensitive to particulate composition showing expectedly low values (< 0.010) under the spring diatom bloom conditions (May) when the particulate assemblage would have been dominated by large low refractivity particles. In November, this parameter was influenced by detrital materials, as shown by its relationship with POC:chl *a*, suggesting that the increased lower cage magnitudes may have been due to aquaculture wastes. Finally, the high $\tilde{b}_{bp}$ (> 0.040) observed within the surface mixed layer in August suggests the existence of refractive materials such as coccoliths. The unique sensitivities of each of these optical parameters would make them useful for environmental monitoring and possibly, waste dispersion studies within IMTA settings. While b_{bp} and $\tilde{b}_{bp}$ appear to have been sensitive to aquaculture derived wastes, further studies are required to elucidate on whether their distinct increases were due to particle size distribution changes and (or) the refractivity of the wastes.

Distinct particulate waste increases in the optical and biophysical data were only measureable during the November period when ambient seston concentrations were low. This finding is consistent with the results of other studies performed in coastal areas and was fitting considering the amount of feed inputs (75 kg) on each day. Waste output was likely not high enough to result in direct increases during the spring and summer sampling periods where particulate wastes would have been quickly diluted

into the particle rich environments. Furthermore, the influence of highly refractive materials (coccoliths) in August would likely have masked any signal from fish wastes, even if they were not quickly diluted. Based on the November dataset, waste release was focused at the bottom of the cage, where b_{bp} increased with time after feeding and remained elevated above before feeding magnitudes throughout the day. Below cage b_{bp} magnitudes on the following day increased towards the seafloor, which was likely due to sediment resuspension; however, temporal increases at these lower cage depths may have represented waste dispersal from the bottom of the cage. With exception to the temporally discrete post feeding surface layer b_{bp} and $\tilde{b}_{bp}$ increases measured on both November days, there was little evidence of horizontal particulate waste dispersal towards the scallop component of the system. This being said, horizontal dispersion may have been occurring in directions away from the scallop component of the system and also, could occur towards the scallops under differing hydrographic conditions not captured by our sampling regime. Furthermore, particulate wastes from the eastern cages of the IMTA system may disperse towards the scallops due to their more favourable location within the gyre. Nonetheless, our results suggest that uptake species placed below the studied cage would likely be most appropriate for waste uptake and fittingly, augmented sea cucumber growth has already been measured at this location (Hannah et al., 2013).

Our study highlights the need for high spatial and temporal resolution methods for particulate characterization within IMTA settings. Particulate waste dispersal has been shown to be highly variable and “patchy” and discrete methods may completely miss dispersion pathways. Additionally, ambient particulate dynamics are variable with time

and depth and this variability could influence waste dispersal, food availability and species health. Further bio-optical studies within IMTA settings should utilize multiple parameters, such as b_{p}, b_{p} and $\tilde{b}_{bp}$, as their synchronized collection can provide high resolution information on particulate concentrations, compositions (inorganic/organic) and possibly even particle size distributions (Twardowski et al., 2001). Discrete sampling of inorganic concentrations and particulate size distributions, in addition to POC and chl *a*, would provide a more comprehensive understanding of bio-optical variability including the influence of aquaculture derived wastes on b_{bp} and $\tilde{b}_{bp}$. Furthermore, simultaneous measurements could be made using multiple optical packages placed at both the reference site and at various locations within the IMTA system. This comprehensive approach would allow for direct temporal and spatial comparisons between IMTA influenced and ambient particulate assemblage dynamics. Waste monitoring studies should also be performed during periods of low ambient seston concentrations, whether this is during winter or summer nutrient depletion. While these studies would initially be labour and financially intensive (cost of optical instrumentation), they would allow for the determination of more focused methods (i.e. derivation of most important parameters and selection of pertinent sensors, focused placement of moored sensors, reduction in discrete sampling and laboratory analysis) that could ultimately reduce equipment and labour costs. Bio-optical methods could then be incorporated into IMTA monitoring systems allowing for the near real time and continuous collection of data on particulate dynamics. This knowledge could greatly aid in the design and implementation of systems highly optimized for waste removal by uptake species.

Bibliography

Amberg, S. M., & Hall, T. E. (2008). Communicating risks and benefits of aquaculture: A content analysis of US newsprint representations of farmed salmon. *Journal of the World Aquaculture Society, 39*(2), 143-157.

Antoine, D., Siegel, D. A., Kostadinov, T., Maritorena, S., Nelson, N. B., Gentili, B., Vellucci, V., & Guillocheau, N. (2011). Variability in optical particle backscattering in contrasting bio-optical oceanic regimes. *Limnology and Oceanography, 56*(3), 955.

Arar, E. J. (1997). *Method 447.0: Determination of chlorophylls a and B and identification of other pigments of interest in marine and freshwater algae using high performance liquid chromatography with visible wavelength detection*. United States Environmental Protection Agency, Office of Research and Development, National Exposure Research Laboratory.

Babin, M., Morel, A., Fournier-Sicre, V., Fell, F., & Stramski, D. (2003). Light scattering properties of marine particles in coastal and open ocean waters as related to the particle mass concentration. *Limnology and Oceanography, 48*(2), 843-859.

Balch, W. M., Holligan, P. M., Ackleson, S. G., & Voss, K. J. (1991). Biological and optical properties of mesoscale coccolithophore blooms in the Gulf of Maine. *Limnology and Oceanography, 36*(4), 629-643.

Barrington, K., Chopin, T., & Robinson, S. (2009). Integrated multi-trophic aquaculture (IMTA) in marine temperate waters. *Integrated Mariculture: A Global Review. FAO Fisheries and Aquaculture Technical Paper,* 529, 7-46.

Behrenfeld, M. J., & Boss, E. (2006). Beam attenuation and chlorophyll concentration as alternative optical indices of phytoplankton biomass. *Journal of Marine Research, 64*(3), 431-451.

Blyth, C. A., Cake, D. A., Bryden, C. A., Kingzett, B. C., & White, P. P. (2004). *Shellfish culture capability appraisal for the Checleset Bay region, British Columbia*. AXYS Environmental Consulting Ltd. and Kingzett Professional Services Ltd.

Boss, E., & Pegau, W. S. (2001). Relationship of light scattering at an angle in the backward direction to the backscattering coefficient. *Applied Optics, 40*(30), 5503-5507.

Boss, E., Pegau, W. S., Lee, M., Twardowski, M., Shybanov, E., Korotaev, G., & Baratange, F. (2004). Particulate backscattering ratio at LEO 15 and its use to study particle composition and distribution. *Journal of Geophysical.Researc., 109*, C01014. doi:10.1029/2002JC001514

Brager, L. M. (2013). *Spatial and temporal dynamics of suspended particulate matter surrounding finfish farms on the east and west coasts of Canada.* (Unpublished Master's Thesis). Dalhousie University, Halifax.

Brooks, K. M., & Mahnken, C. V. (2003). Interactions of Atlantic salmon in the Pacific Northwest environment: II. Organic wastes. *Fisheries Research, 62*(3), 255-293.

Carroll, M. L., Cochrane, S., Fieler, R., Velvin, R., & White, P. (2003). Organic enrichment of sediments from salmon farming in Norway: Environmental factors, management practices, and monitoring techniques. *Aquaculture, 226*(1), 165-180.

Chang, G. C., Barnard, A. H., McLean, S., Egli, P. J., Moore, C., Zaneveld, J. R. V., Dickey, T. D., & Hanson, A. (2006). In situ optical variability and relationships in the Santa Barbara channel: Implications for remote sensing. *Applied Optics, 45*(15), 3593-3604.

Cheshuk, B., Purser, G., & Quintana, R. (2003). Integrated open-water mussel (*mytilus planulatus*) and Atlantic salmon (*salmo salar*) culture in Tasmania, Australia. *Aquaculture, 218*(1), 357-378.

Chopin, T., Cooper, J. A., Reid, G., Cross, S., & Moore, C. (2012). Open-water integrated multi-trophic aquaculture: Environmental biomitigation and economic diversification of fed aquaculture by extractive aquaculture. *Reviews in Aquaculture, 4*(4), 209-220.

Cifuentes, L., Sharp, J., & Fogel, M. L. (1988). Stable carbon and nitrogen isotope biogeochemistry in the Delaware Estuary. *Limnology and Oceanography, 33*(5), 1102-1115.

Clesceri, L. S., Greenberg, A. E., & Eaton, A. D. (1998). Standard methods for the examination of water and wastewater. *American Public Health Association, Washington, DC, 20005*, 5.48-5.54.

Coast and Marine Planning Branch. (2003). *The Kyuquot Sound coastal plan*. British Columbia: Ministry of sustainable Resource Management, Government of BC.

Cranford, P. J., Reid, G. K., & Robinson, S. M. (2013). Open water integrated multi-trophic aquaculture: Constraints on the effectiveness of mussels as an organic extractive component. *Aquatic Environmental Interactions, 4*, 163-173.

Dall'Olmo, G., Westberry, T., Behrenfeld, M., Boss, E., & Slade, W. (2009). Significant contribution of large particles to optical backscattering in the open ocean. *Biogeosciences, 6*(6), 947-967.

Del Bel Belluz, J. (2010). *An optical study of the waters surrounding an integrated multi-trophic aquaculture site on the northwest coast of Vancouver Island.* (Unpublished Honours Thesis). University of Victoria, Victoria.

Department of Fisheries and Oceans Canada (DFO) (2012). Aquaculture in Canada 2012: A report of aquaculture sustainability.

Department of Fisheries and Oceans, Canada (DFO) (2013). Aquaculture statistics, facts and figures. Retrieved 06/01, 2014, from http://www.dfo-mpo.gc.ca/aquaculture/stats/index-eng.htm.

Ediger, D., Soydemir, N., & Kideys, A. (2006). Estimation of phytoplankton biomass using HPLC pigment analysis in the southwestern Black Sea. *Deep Sea Research Part II: Topical Studies in Oceanography, 53*(17), 1911-1922.

Food and Agriculture Organization of the United Nations (FAO) (2014). *The state of world fisheries and aquaculture*. Rome: FAO.

Flory, E., Hill, P., Milligan, T., & Grant, J. (2004). The relationship between floc area and backscatter during a spring phytoplankton bloom. *Deep Sea Research Part I: Oceanographic Research Papers, 51*(2), 213-223.

Gao, Q., Shin, P. K., Lin, G., Chen, S., & Cheung, S. G. (2006). Stable isotope and fatty acid evidence for uptake of organic waste by green-lipped mussels (*perna viridis*) in a polyculture fish farm system. *Marine Ecology-Progress Series-, 317,* 273.

Garcia, C. A. E., Garcia, V. M. T., Dogliotti, A. I., Ferreira, A., Romero, S. I., Mannino, A., Souza, M. S., & Mata, M. M. (2011). Environmental conditions and bio-optical signature of a coccolithophorid bloom in the Patagonian shelf. *Journal of Geophysical Research: Oceans (1978–2012), 116*(C3)

Gardner, W., Blakey, J., Walsh, I., Richardson, M., Pegau, S., Zaneveld, J., Roesler, C., Gregg, M., MacKinnon, J., & Sosik, H. (2001). Optics, particles, stratification, and storms on the New England continental shelf. *Journal of Geophysical Research: Oceans (1978–2012), 106*(C5), 9473-9497.

Gardner, W., Mishonov, A., & Richardson, M. (2006). Global POC concentrations from in-situ and satellite data. *Deep Sea Research Part II: Topical Studies in Oceanography, 53*(5), 718-740.

Google Earth (2014). Kyuquot Sound. 50° 2'42.94"N and 127°17'47.29"W. Retrieved February 1st, 2014.

Grizzle, R. E., Greene, J. K., Luckenbach, M. W., & Coen, L. D. (2006). A new in situ method for measuring seston uptake by suspension-feeding bivalve molluscs. *Journal of Shellfish Research, 25*(2), 643-649.

Guindon, M. (2012). *Temporal and spatial dynamics of phytoplankton in an aquaculture site on the west coast of Vancouver Island during a spring diatom bloom: Remote sensing and in-situ methods.* (Unpublished Honours Thesis). University of Victoria, Victoria.

Gundersen, J. S., Gardner, W. D., Richardson, M. J., & Walsh, I. D. (1998). Effects of monsoons on the seasonal and spatial distributions of POC and chlorophyll in the Arabian Sea. *Deep-Sea Research Part II, 45*(10-11), 2103-2132.

Handå, A., Min, H., Wang, X., Broch, O. J., Reitan, K. I., Reinertsen, H., & Olsen, Y. (2012a). Incorporation of fish feed and growth of blue mussels (*mytilus edulis*) in close proximity to salmon (*salmo salar*) aquaculture: Implications for integrated multi-trophic aquaculture in Norwegian coastal waters. *Aquaculture, 356*, 328-341.

Handå, A., Ranheim, A., Olsen, A. J., Altin, D., Reitan, K. I., Olsen, Y., & Reinertsen, H. (2012b). Incorporation of salmon fish feed and feces components in mussels (*mytilus edulis*): Implications for integrated multi-trophic aquaculture in cool-temperate north Atlantic waters. *Aquaculture, 370*, 40-53.

Hannah, L., Pearce, C., & Cross, S. (2013). Growth and survival of California sea cucumbers (*parastichopus californicus*) cultivated with sablefish (*anoplopoma fimbria*) at an integrated multi-trophic aquaculture site. *Aquaculture, 406,* 34-42.

Hay, M. B., Pienitz, R., & Thomson, R. E. (2003). Distribution of diatom surface sediment assemblages within Effingham Inlet, a temperate fjord on the west coast of Vancouver island (Canada). *Marine Micropaleontology, 48*(3), 291-320.

Huot, Y., Morel, A., Twardowski, M., Stramski, D., & Reynolds, R. (2008). Particle optical backscattering along a chlorophyll gradient in the upper layer of the eastern South Pacific Ocean. *Biogeosciences, 5*(2), 495-507.

Ibarra, D. A., Cembella, A., & Grant, J. (2012). Attenuation of sunlight measured from moored radiometers to assess depletion of suspended particles caused by bivalve aquaculture. *Limnology and Oceanography-Methods, 10,* 1051-1069.

Irisarri, J., Cubillo, A. M., Fernández-Reiriz, M. J., & Labarta, U. (2013a). Growth variations within a farm of mussel (*mytilus galloprovincialis*) held near fish cages: Importance for the implementation of integrated aquaculture. *Aquaculture Research,* doi: 10.1111/are.12356

Irisarri, J., Fernández-Reiriz, M. J., Robinson, S., Cranford, P. J., & Labarta, U. (2013b). Absorption efficiency of mussels (*mytilus edulis*) and (*mytilus galloprovincialis*) cultured under integrated multi-trophic aquaculture conditions in the Bay of Fundy (Canada) and Ría Ares-Betanzos (Spain). *Aquaculture, 388,* 182-192.

Irvine, J. R., & Crawford, W. R. (2013). *State of physical, biological and selected fishery resources of pacific Canadian marine ecosystems.* (No. 032). DFO Can. Sci. Advis. Sec. Res. Doc.

Jeffrey, S., & Vesk, M. (1997). Introduction to marine phytoplankton and their pigment signatures. *Phytoplankton Pigments in Oceanography: Guidelines to Modern Methods, 10*.

Jiang, Z., Wang, G., Fang, J., & Mao, Y. (2013). Growth and food sources of pacific oyster (*crassostrea gigas*) integrated culture with sea bass (*lateolabrax japonicas*) in Ailian Bay, china. *Aquaculture International, 21*(1), 45-52.

Jones, T. O., & Iwama, G. K. (1991). Polyculture of the pacific oyster, (*crassostrea gigas*) (Thunberg), with chinook salmon (*oncorhynchus tshawytscha*). *Aquaculture, 92*, 313-322.

Krasakopoulou, E., & Karageorgis, A. P. (2005). Spatial and temporal distribution patterns of suspended particulate matter and particulate organic carbon in the Saronikos Gulf (eastern Mediterranean, Greece). *Geo-Marine Letters, 25*(6), 343-359.

Kutti, T., Ervik, A., & Hansen, P. K. (2007a). Effects of organic effluents from a salmon farm on a fjord system. I. Vertical export and dispersal processes. *Aquaculture, 262*(2), 367-381.

Kutti, T., Hansen, P. K., Ervik, A., Høisæter, T., & Johannessen, P. (2007b). Effects of organic effluents from a salmon farm on a fjord system. II. Temporal and spatial patterns in infauna community composition. *Aquaculture, 262*(2), 355-366.

Lander, T., Robinson, S. M., MacDonald, B. A., & Martin, J. D. (2012). Enhanced growth rates and condition index of blue mussels (*mytilus edulis*) held at integrated multi-trophic aquaculture sites in the Bay of Fundy. *Journal of Shellfish Research, 31*(4), 997-1007.

Lander, T., Robinson, S., MacDonald, B., & Martin, J. (2013). Characterization of the suspended organic particles released from salmon farms and their potential as a food supply for the suspension feeder, *mytilus edulis* in integrated multi-trophic aquaculture (IMTA) systems. *Aquaculture, 406*, 160-171.

Le, C., Hu, C., English, D., Cannizzaro, J., Chen, Z., Kovach, C., Anastasiou, C. J., Zhao, J., & Carder, K. L. (2013). Inherent and apparent optical properties of the complex estuarine waters of Tampa Bay: What controls light? *Estuarine, Coastal and Shelf Science, 117*, 54-69.

Lefebvre, S., Barillé, L., & Clerc, M. (2000). Pacific oyster (*crassostrea gigas*) feeding responses to a fish-farm effluent. *Aquaculture, 187*(1), 185-198.

Lewitus, A. J., Horner, R. A., Caron, D. A., Garcia-Mendoza, E., Hickey, B. M., Hunter, M., Huppert, D. D., Kudela, R. M., Langlois, G. W., & Largier, J. L. (2012). Harmful algal blooms along the North American west coast region: History, trends, causes, and impacts. *Harmful Algae, 19*, 133-159.

Lide, D. R. (2004). *CRC handbook of chemistry and physics*. CRC press.

Loisel, H., Mériaux, X., Berthon, J., & Poteau, A. (2007). Investigation of the optical backscattering to scattering ratio of marine particles in relation to their biogeochemical composition in the eastern English Channel and southern North Sea. *Limnology and Oceanography, 52*(2), 739-752.

MacDonald, B. A., Robinson, S., & Barrington, K. A. (2011). Feeding activity of mussels (*mytilus edulis*) held in the field at an integrated multi-trophic aquaculture (IMTA) site (*salmo salar*) and exposed to fish food in the laboratory. *Aquaculture, 314*(1), 244-251.

Martell, D., Duhaime, J., & Parsons, G. (Eds.). (2013). *Canadian aquaculture R&D review* (23rd ed.). Canada: Fisheries and Oceans Canada.

Martinez-Vicente, V., Land, P. E., Tilstone, G. H., Widdicombe, C., & Fishwick, J. R. (2010). Particulate scattering and backscattering related to water constituents and seasonal changes in the western English Channel. *Journal of Plankton Research, 32*(5), 603-619.

Mazzola, A., & Sarà, G. (2001). The effect of fish farming organic waste on food availability for bivalve molluscs (Gaeta gulf, central Tyrrhenian, MED): Stable carbon isotopic analysis. *Aquaculture, 192*(2), 361-379.

Mente, E., Pierce, G. J., Santos, M. B., & Neofitou, C. (2006). Effect of feed and feeding in the culture of salmonids on the marine aquatic environment: A synthesis for European aquaculture. *Aquaculture International, 14*(5), 499-522.

Millie, D. F., Schofield, O. M., Dionigi, C. P., & Johnsen, P. B. (1995). Assessing noxious phytoplankton in aquaculture systems using Bio-Optical methodologies: A review. *Journal of the World Aquaculture Society, 26*(4), 329-345.

Mobley, C. D. (1994). *Light and water: Radiative transfer in natural waters*. Academic press San Diego.

Natural Resources Canada. (2009). *Annual mean total precipitation* (Atlas of Canada 6th Edition ed.) Government of Canada.

Natural Resources Canada. (2013). Retrieved 02/01, 2014, from http://www.nrcan.gc.ca/mining-materials/certified-reference-materials/certificate-price-list/8075

Natural Resources Canada. (2013). LKDS-1 to LKSD-4 lake sediment samples. Retrieved 02/01, 2013, from http://www.nrcan.gc.ca/mining-materials/certified-reference-materials/certificate-price-list/8075

Navarrete-Mier, F., Sanz-Lázaro, C., & Marín, A. (2010). Does bivalve mollusc polyculture reduce marine fin fish farming environmental impact? *Aquaculture, 306*(1), 101-107.

Neori, A., Chopin, T., Troell, M., Buschmann, A. H., Kraemer, G. P., Halling, C., Shpigel, M., & Yarish, C. (2004). Integrated aquaculture: Rationale, evolution and state of the art emphasizing seaweed biofiltration in modern mariculture. *Aquaculture, 231*(1), 361-391.

Neukermans, G., Loisel, H., Mériaux, X., Astoreca, R., & McKee, D. (2012). In situ variability of mass-specific beam attenuation and backscattering of marine particles with respect to particle size, density, and composition. *Limnology and Oceanography, 57*(1), 124.

Obernosterer, I., Catala, P., Reinthaler, T., Herndl, G. J., & Lebaron, P. (2005). Enhanced heterotrophic activity in the surface microlayer of the Mediterranean Sea. *Aquatic Microbial Ecology, 39*(3), 293-302.

Parsons, G. J., Shumway, S. E., Kuenstner, S., & Gryska, A. (2002). Polyculture of sea scallops (*placopecten magellanicus*) suspended from salmon cages. *Aquaculture International, 10*(1), 65-77.

Peharda, M., Župan, I., Bavčević, L., Frankić, A., & Klanjšček, T. (2007). Growth and condition index of mussel *mytilus galloprovincialis* in experimental integrated aquaculture. *Aquaculture Research, 38*(16), 1714-1720.

Pope, R. M., & Fry, E. S. (1997). Absorption spectrum (380–700 nm) of pure water. II. integrating cavity measurements. *Applied Optics, 36*(33), 8710-8723.

Prussin, E. A. (2012). *Spatial Distribution of the Nutrient Plume Emanating from an Integrated Multi-Trophic Aquaculture (IMTA) Farm in British Columbia: Use of an in-Situ Kelp Bioassay to Monitor Nutrient Loading.* (Unpublished Master's Thesis). University of Victoria, Victoria.

Ras, J., Claustre, H., & Uitz, J. (2008). Spatial variability of phytoplankton pigment distributions in the subtropical South Pacific Ocean: Comparison between in situ and predicted data. *Biogeosciences, 5*(2), 353-369.

Redmond, K. J., Magnesen, T., Hansen, P. K., Strand, Ø., & Meier, S. (2010). Stable isotopes and fatty acids as tracers of the assimilation of salmon fish feed in blue mussels (*mytilus edulis*). *Aquaculture, 298*(3), 202-210.

Reid, G. (2011). Spatial modelling of integrated multi-trophic aquaculture (IMTA) shellfish. *Bulletin of the Aquaculture Association of Canada, 109*(2), 1-44.

Reid, G., Liutkus, M., Bennett, A., Robinson, S., MacDonald, B., & Page, F. (2010). Absorption efficiency of blue mussels (*mytilus edulis* and *M. trossulus*) feeding on Atlantic salmon (*salmo salar*) feed and fecal particulates: Implications for integrated multi-trophic aquaculture. *Aquaculture, 299*(1), 165-169.

Reid, G., Liutkus, M., Robinson, S., Chopin, T., Blair, T., Lander, T., Mullen, J., Page, F., & Moccia, R. (2009). A review of the biophysical properties of salmonid faeces: Implications for aquaculture waste dispersal models and integrated multi-trophic aquaculture. *Aquaculture Research, 40*(3), 257-273.

Riche, O., Johannessen, S., & Macdonald, R. (2013). Why timing matters in a coastal sea: Trends, variability and tipping points in the Strait of Georgia, Canada. *Journal of Marine Systems*, 131, 36-53. Doi: 10.1016/j.jmarsys.2013.11.003

Ridler, N., Wowchuk, M., Robinson, B., Barrington, K., Chopin, T., Robinson, S., Page, F., Reid, G., Szemerda, M., & Sewuster, J. (2007). Integrated multi− trophic aquaculture (IMTA): A potential strategic choice for farmers. *Aquaculture Economics & Management, 11*(1), 99-110.

Sarà, G., Zenone, A., & Tomasello, A. (2009). Growth of *mytilus galloprovincialis* (mollusca, bivalvia) close to fish farms: A case of integrated multi-trophic aquaculture within the Tyrrhenian Sea. *Hydrobiologia, 636*(1), 129-136.

Savoye, N., David, V., Morisseau, F., Etcheber, H., Abril, G., Billy, I., Charlier, K., Oggian, G., Derriennic, H., & Sautour, B. (2012). Origin and composition of particulate organic matter in a macrotidal turbid estuary: The Gironde estuary, France. *Estuarine, Coastal and Shelf Science, 108*, 16-28.

Schlag, A. K. (2010). Aquaculture: An emerging issue for public concern. *Journal of Risk Research, 13*(7), 829-844.

SEAVison Group. (2011). Cascadia SEAfood. Retrieved 05/01, 2014, from http://www.seavisiongroup.ca/cascadia/index.

Siegel, H., Ohde, T., Gerth, M., Lavik, G., & Leipe, T. (2007). Identification of coccolithophore blooms in the SE Atlantic Ocean off Namibia by satellites and in-situ methods. *Continental Shelf Research, 27*(2), 258-274.

Snyder, W. A., Arnone, R. A., Davis, C. O., Goode, W., Gould, R. W., Ladner, S., Lamela, G., Rhea, W. J., Stavn, R., & Sydor, M. (2008). Optical scattering and backscattering by organic and inorganic particulates in US coastal waters. *Applied Optics*, *47*(5), 666-677.

Soto, D. (2009). *Integrated mariculture: A global review*. Food and Agriculture Organization of the United Nations.

Soto, D., & Mena, G. (1999). Filter feeding by the freshwater mussel, (*diplodon chilensis*), as a biocontrol of salmon farming eutrophication. *Aquaculture, 171*(1), 65-81.

Stavn, R. H., Rick, H. J., & Falster, A. V. (2009). Correcting the errors from variable sea salt retention and water of hydration in loss on ignition analysis: Implications for studies of estuarine and coastal waters. *Estuarine, Coastal and Shelf Science, 81*(4), 575-582.

Stirling, H. P. (1995). Growth and production of mussels (*mytilus edulis*) suspended at salmon cages and shellfish farms in two Scottish sea lochs. *Aquaculture, 134*(3), 193-210.

Stramski, D., Reynolds, R., Babin, M., Kaczmarek, S., Lewis, M., Röttgers, R., Sciandra, A., Stramska, M., Twardowski, M., & Franz, B. (2008). Relationships between the surface concentration of particulate organic carbon and optical properties in the eastern South Pacific and eastern Atlantic Oceans. *Biogeosciences, 5*(1), 171-201.

Stramski, D., Boss, E., Bogucki, D., & Voss, K. J. (2004). The role of seawater constituents in light backscattering in the ocean. *Progress in Oceanography, 61*(1), 27-56.

Sullivan, J. M., Twardowski, M. S., Zaneveld, J. R. V., Moore, C. M., Barnard, A. H., Donaghay, P. L., & Rhoades, B. (2006). Hyperspectral temperature and salt dependencies of absorption by water and heavy water in the 400-750 nm spectral range. *Applied Optics, 45*(21), 5294-5309.

Sullivan, J. M., Twardowski, M. S., Donaghay, P. L., & Freeman, S. A. (2005). Use of optical scattering to discriminate particle types in coastal waters. *Applied Optics, 44*(9), 1667-1680. doi:10.1364/AO.44.001667

Sun, D., Li, Y., Wang, Q., Gao, J., Lv, H., Le, C., & Huang, C. (2009). Light scattering properties and their relation to the biogeochemical composition of turbid productive waters: A case study of Lake Taihu. *Applied Optics, 48*(11), 1979-1989.

Sutherland, T., Martin, A., & Levings, C. (2001). Characterization of suspended particulate matter surrounding a salmonid net-pen in the Broughton Archipelago, British Columbia. *ICES Journal of Marine Science: Journal Du Conseil, 58*(2), 404-410.

Taylor, B. E., Jamieson, G., & Carefoot, T. H. (1992). Mussel culture in British Columbia: The influence of salmon farms on growth of (*mytilus edulis*). *Aquaculture, 108*(1), 51-66.

Taylor, F., & Haigh, R. (1996). Spatial and temporal distributions of microplankton during the summers of 1992 1993 in Barkley Sound, British Columbia, with emphasis on harmful species. *Canadian Journal of Fisheries and Aquatic Sciences, 53*(10), 2310-2322.

Troell, M., Halling, C., Neori, A., Chopin, T., Buschmann, A., Kautsky, N., & Yarish, C. (2003). Integrated mariculture: Asking the right questions. *Aquaculture, 226*(1), 69-90.

Troell, M., & Norberg, J. (1998). Modelling output and retention of suspended solids in an integrated salmon–mussel culture. *Ecological Modelling, 110*(1), 65-77.

Tsutsumi, H., Srithongouthai, S., Inoue, A., Sato, A., & Hama, D. (2006). Seasonal fluctuations in the flux of particulate organic matter discharged from net pens for fish farming. *Fisheries Science, 72*(1), 119-127.

Twardowski, M. S., Boss, E., Macdonald, J. B., Pegau, W. S., Barnard, A. H., & Zaneveld, J. R. V. (2001). A model for estimating bulk refractive index from the optical backscattering ratio and the implications for understanding particle composition in case I and case II waters. *Journal of Geophysical Research: Oceans (1978–2012), 106*(C7), 14129-14142.

Twardowski, M. S., Sullivan, J. M., Donaghay, P. L., & Zaneveld, J. R. (1999). Microscale quantification of the absorption by dissolved and particulate material in coastal waters with an ac-9. *Journal of Atmospheric & Oceanic Technology, 16*(6), 691.

Tyrrell, T., & Merico, A. (2004). Emiliania huxleyi: Bloom observations and the conditions that induce them. *Coccolithophores* (pp. 75-97) Springer.

Wallace, J. C. (1980). Growth rates of different populations of the edible mussel, (*mytilus edulis*), in north Norway. *Aquaculture, 19*(4), 303-311.

WETLabs. (2011). *ECO triplet user's guide*. Philomath: WETLabs.

Whitmire, A. L., Pegau, W. S., Karp-Boss, L., Boss, E., & Cowles, T. J. (2010). Spectral backscattering properties of marine phytoplankton cultures. *Optics Express, 18*(14), 15073-15093.

Woźniak, S. B., Stramski, D., Stramska, M., Reynolds, R. A., Wright, V. M., Miksic, E. Y., Cichocka, M., & Cieplak, A. M. (2010). Optical variability of seawater in relation to particle concentration, composition, and size distribution in the nearshore marine environment at Imperial Beach, California. *Journal of Geophysical Research: Oceans (1978–2012), 115*(C8).

Zaneveld, J. R. V., Kitchen, J. C., & Moore, C. C. (1994). Scattering error correction of reflecting-tube absorption meters. *Ocean Optics XII,* 44-55.